UNIVERSITÉ DE NANTES
FACULTÉ DES SCIENCES ET DES TECHNIQUES

ÉCOLE DOCTORALE : SPIGA

Année 2012

Simplified and Advanced Approaches for the Probabilistic Analysis of Shallow Foundations

THÈSE DE DOCTORAT
Discipline : Génie Civil
Spécialité : Géotechnique

Présentée
et soutenue publiquement par

Ashraf AHMED

Le 28 Septembre 2012, devant le jury ci-dessous

Président	M. Roger FRANK	Professeur, Université Paris-Est
Rapporteurs	M. Alaa CHATEAUNEUF	Professeur, Université Blaise Pascal
	M. Isam SHAHROUR	Professeur, Université Lille1
Examinateurs	M. Daniel DIAS	Professeur, Université Joseph-Fourier
	M. Luc THOREL	Directeur de recherche, IFSTTAR de Nantes

Directeur de thèse : Pr. Abdul-Hamid SOUBRA

Abstract: This thesis presents simplified and advanced probabilistic analyses of shallow foundations. In the simplified probabilistic analysis, the uncertain parameters are modelled by random variables. For an obliquely loaded footing, the numerical results based on the Response Surface Method (*RSM*) and the Collocation-based Stochastic Response Surface Method (*CSRSM*) have allowed to identify the zones of failure mode predominance at both the ultimate and serviceability limit states. On the other hand, an efficient procedure was proposed to increase the number of the probabilistic outputs of the Subset Simulation (*SS*) approach with no additional time cost. In this procedure, the SS approach was combined with the *CSRSM*.

In the advanced probabilistic analysis, the uncertain parameters are modelled by random fields to take into account the soil spatial variability. In such cases, Monte Carlo Simulation (*MCS*) methodology is generally used in literature. Only the statistical moments were generally investigated in literature because of the great number of calls of the deterministic model required by this method. In this thesis, the subset simulation approach was first used as alternative to MCS methodology to compute the failure probability. This leads to a significant reduction in the number of calls of the deterministic model. Moreover, a more efficient approach called improved Subset Simulation (*iSS*) approach was developed to reduce again the number of calls of the deterministic model. The use of the iSS approach has reduced the number of calls of the deterministic model by about 50% with respect to the SS approach.
Keywords: Reliability analysis, Probabilistic analysis, Random variables, Random fields, Spatial variability, Shallow foundations, Failure probability, Ultimate and serviceability limit states.

Resumé: Cette thèse présente des approches simplifiées et avancées pour l'analyse probabiliste des fondations superficielles. Dans l'analyse probabiliste simplifiée, les paramètres incertains sont modélisés par des variables aléatoires. Pour une fondation soumise à un chargement incliné, les résultats numériques basés sur la méthode des surfaces de réponse (*RSM*) et la méthode des surfaces de réponse stochastiques (*CSRSM*) ont permis d'identifier les zones de prédominance des modes de rupture à l'état limite ultime et à l'état limite de service. D'autre part, une procédure efficace a été proposée pour augmenter le nombre des sorties probabilistes de l'approche S*ubset Simulation* (*SS*) sans appels supplémentaires au modèle déterministe. Dans cette procédure, l'approche *SS* a été combinée avec la méthode *CSRSM.*

Dans l'analyse probabiliste avancée, les paramètres incertains du sol sont modélisés par des champs aléatoires pour prendre en compte la variabilité spatiale des propriétés du sol. Dans ce cas, la méthode de simulation de Monte Carlo (*MCS*) est généralement utilisée et seuls les moments statistiques de la réponse sont étudiés en raison du grand nombre d'appels au modèle déterministe. Dans cette thèse, l'approche *SS* a d'abord été utilisée comme une méthode alternative à la méthode *MCS* pour calculer la probabilité de ruine. Ceci a conduit à une réduction significative du nombre d'appels au modèle déterministe. Ensuite, une approche plus efficace nommée *improved Subset Simulation* (*iSS*) a été développée pour réduire encore une fois le nombre d'appels au modèle déterministe. L'utilisation de l'*iSS* a réduit le nombre d'appels au modèle déterministe d'environ 50% par rapport à l'approche *SS*.
Mots clés : Analyse fiabiliste, Analyse probabilistes, Variables aléatoires, Champs aléatoires, variabilité spatiale, Fondations superficielles, Probabilité de ruine, Etat limite ultime et état limite de service.

TABLE OF CONTENTS

PART I

SIMPLIFIED PROBABILISTIC ANALYSIS OF SHALLOW FOUNDATIONS

CHAPTER 2

CHAPTER 3

CHAPTER 4

PART II

ADVANCED PROBABILISTIC ANALYSIS OF SHALLOW FOUNDATIONS

CHAPTER 5

CHAPTER 6

GENERAL INTRODUCTION

Most geotechnical analyses are traditionally based on deterministic approaches. These approaches consider representative values for the different design parameters. These values are usually the averages or the most conservative ones obtained from field or laboratory tests. In such approaches, a global safety factor is applied to take into account the soil and loading uncertainties. The choice of this factor is based on the judgment of the engineer based on his past experience. During the last years, much effort has been paid for the establishment of more reliable and efficient methods based on probabilistic (simplified and advanced) approaches. These approaches allow one to consider the propagation of the uncertainties from the input parameters (soil and/or loading parameters) to the system responses (stress, displacement, factor of safety, etc.). In the simplified probabilistic analysis, the different uncertain parameters are modeled by random variables defined by their probability density functions (PDFs). However, in the advanced probabilistic analysis, some uncertain parameters as the soil properties are modeled by random fields characterized not only by their PDFs, but also by their autocorrelation functions which represent the degree of dependence of two values of a given uncertain parameter at two different locations. These methods allow one to take into account the soil spatial variability.

The ultimate aim of this work is to study the performance of shallow foundations subjected to complex loading (horizontal and vertical loads and an overturning moment) using probabilistic approaches. The present thesis focuses on the case of obliquely loaded footings. The extension to the complex loading case and/or the seismic or dynamic loading will be the subject of future work. Both the ultimate (ULS) and the serviceability (SLS) limit states were considered in the analysis. In Part I of this thesis, the simplified probabilistic approach was used to perform the probabilistic analysis. However, in Part II, the probabilistic analysis was performed using the more advanced probabilistic approach.

Before the presentation of the different probabilistic analyses performed in this thesis (Parts I and II), a literature review is presented in chapter 1. This chapter provides (i) the different sources of uncertainties, (ii) the different methods of modelling the soil uncertain parameters, (iii) the random field discretization methods and finally (iv) the principal probabilistic methods used in literature for the uncertainty propagation.

PART I:

In Part I, the uncertain parameters were considered as random variables defined by their probability density functions. Part I consists of three chapters (chapters 2, 3 and 4).

The aim of chapters 2 and 3 is twofold: First, they aim at comparing the performance of the Response Surface Method (RSM) and the Collocation-based Stochastic Response Surface Method (CSRSM) in the framework of the probabilistic analysis of shallow foundations. Second, contrary to the existing literature which considers only the vertically loaded footings involving only one failure mode; in these chapters, the case of obliquely loaded footings that involve two failure modes was considered. In chapter 2, the RSM was used to perform the probabilistic analysis. Only the uncertainties of the soil parameters were taken into account in this chapter. However; in chapter 3, the probabilistic analysis was performed using the CSRSM. Due to the efficiency of this method to deal with greater number of random variables with respect to the RSM, the uncertainties of the soil parameters and those of the load components were taken into account simultaneously in this chapter. Chapters 2 and 3 have confirmed the superiority of the CSRSM with respect to the RSM regarding the number of calls of the deterministic model and the number of the probabilistic outputs.

The objective of Chapter 4 is to develop a new procedure which combines the subset simulation (SS) approach and the CSRSM used in chapter 3 in order to increase the number of outputs of the SS approach with no additional time cost. This procedure was illustrated through the probabilistic analysis at ULS of a strip footing subjected to a central vertical load.

PART II:

In Part II, the soil spatial variability was taken into account by modeling the soil uncertain parameters by random fields characterized by their PDFs and their autocorrelation functions. Part II consists of two chapters (chapters 5 and 6).

Contrary to the existing geotechnical literature in which the probabilistic analysis of random field problems is performed using MCS methodology, chapter 5 makes use of the SS approach. Contrary to MCS methodology, the SS approach requires a significantly reduced number of calls of the deterministic model to calculate the small failure probabilities. The efficiency of the SS approach was illustrated through the computation of the probability of exceeding a tolerable vertical displacement of a strip footing resting on a soil with a 2D spatially varying Young's modulus.

The objective of chapter 6 is to increase the efficiency of the SS approach by reducing the number of calls of the deterministic model required by this method. For this purpose, the first step of the SS approach was replaced by a conditional simulation. The efficiency of the iSS approach was illustrated through the computation of the probability of exceeding a tolerable differential settlement between two neighboring strip footings resting on a soil with a 2D spatially varying Young's modulus.

The thesis ends by a general conclusion of the principal results obtained from the analyses.

CHAPTER 1

LITERATURE REVIEW

1. Introduction

The deterministic approaches have long been used in the analysis and design of geotechnical structures. These approaches consider the soil parameters as constant inputs having conservative values. In these approaches, the uncertainties of the soil parameters are taken into account by an approximate manner using the concept of the global safety factor. This factor is based on engineering judgment. During the recent years, much effort has been paid for more rational analyses based on probabilistic approaches. Both simplified and more advanced probabilistic approaches can be found in literature. In the simplified probabilistic approaches, the uncertain parameters are modeled as random variables defined by their probability density functions (PDFs) or only by their statistical moments (i.e. mean value and standard deviation). In these approaches, the soil is considered (during each simulation) as a homogeneous material having the same value of the uncertain parameter in the entire soil domain. However; in nature, the soil parameters (shear strength parameters, elastic properties, etc.) vary spatially in both the horizontal and the vertical directions as a result of depositional and post-depositional processes. This leads to the necessity of modeling the soil parameters (during each simulation) as random fields characterized not only by their PDFs, but also by their autocorrelation functions. In this regard, more advanced probabilistic approaches were proposed in literature. In these approaches, one needs to discretize the random field into a finite number of random variables. For this purpose, several discretization methods were proposed in literature as will be shown later in this chapter.

This chapter aims at presenting the different sources of uncertainties related to the geotechnical parameters. It also presents both the simplified and advanced approaches for modelling the soil uncertainties. Then, the different methods of random field discretization are briefly described. Finally, the probabilistic methods used in this thesis to perform the probabilistic analyses are presented and discussed. The chapter ends with a conclusion.

2. Different sources of uncertainties

The geotechnical variability arises from several sources of uncertainties. According to Kulhawy (1992), the uncertainty in the design soil properties results from three main sources. These sources are:

- Inherent variability of the soil parameters
- Measurement errors
- Transformation uncertainty

The inherent soil variability results primarily from the natural geologic processes that occurred in the past and continue to modify the soil mass in-situ. The measurement error is caused by equipment, random testing effects and human errors. Collectively, these two sources (i.e. inherent variability and the measurement error) can be described as data scatter. In-situ measurements are also influenced by statistical uncertainty or sampling error that results from limited amount of information. This uncertainty can be minimized by considering more samples, but it is commonly included within the measurement error. Finally, the transformation uncertainty is introduced when the field or the laboratory measurements are transformed into the design soil properties using empirical or other correlation models. The relative contribution of these three sources to the overall uncertainty in the design soil property clearly depends on the site conditions. Therefore, the soil property statistics can only be applied to a specific set of circumstances (site conditions, measurement techniques, correlation models) for which the design soil properties were derived.

3. Modelling of uncertain soil parameters

The uncertainties of the soil parameters described in the previous section have to be taken into account in any geotechnical probabilistic analysis. Some probabilistic analyses have modelled the uncertain soil parameters using a simplified approach. In this approach, the uncertain soil parameters are modelled as random variables characterized by their PDFs or their statistical moments (i.e. mean value and standard deviation). This implies that all the realisations of a given uncertain parameter provide a homogeneous soil with a random value of this parameter that varies from one realisation to another. Notice however that the soil properties vary from point to point as a result of complex geological processes (such as sedimentation, weathering and erosion, climate, etc.) which influence their formation. This leads to the necessity of using a more advanced approach for modelling the uncertain soil parameters. In this approach, the uncertain soil parameters are modelled as random fields to take into account their spatial variability. The simplified and the more advanced approaches for modelling the uncertain soil parameters are respectively presented in the two following subsections.

3.1. Simplified approach for modelling of uncertain soil parameters

In the framework of the simplified approach of modelling the uncertain soil parameters, the variability of a given uncertain parameter is measured by the coefficicent of variation *COV* of this parameter. The coefficient of variation of a given uncertain soil parameter is defined as the ratio between its standard deviation and its mean value. Several statistical studies based on in-situ and laboratory tests have been reported in the literature to define the variability of the different soil parameters. Phoon and Kulhawy (1996) presented a number of studies based on several in-situ tests [Standard Penetration Test (SPT), Cone Penetration Test (CPT), Field Vane test (FVT), Dilatometer Test (DMT), Pressuremeter Test (PMT)] and other laboratory tests. It was shown that the variability calculated from laboratory tests is smaller than that computed from the in-situ tests. This is due to (i) the good control of measurements taken in the laboratory and (ii) the quality of the equipments in laboratory compared to that of in-situ tests.

This section aims at presenting the values of *COV* of the soil shear strength parameters and the soil elastic properties proposed in literature. Also, it aims at presenting the commonly used values of the correlation coefficent between these parameters. Concerning the type of the PDF of the different uncertain parameters; unfortunatly, there is no sufficicnt data to give a comperhensive and complete description of the type of the PDF to be used in the numerical simulations. The existing literature [e.g. Griffiths and Fenton (2001), Griffiths *et al.* (2002), Fenton and Griffiths (2002, 2003, 2005), Fenton *et al.* (2003)] tends to recommend the use of a lognormal PDF for the Young's modulus E, Poisson's ratio v and cohesion c. This recommendation is motivated by the fact that the values of these parameters are strictly positive. Concerninig the internal friction angle φ, it is recommended to adopt a beta distribtion for this parameter to limit its variation in the range of practical values.

3.1.1. Cohesion

For the undrained cohesion c_u of a clay, Cherrubini *et al*. (1993) found that the coefficient of variation of this property decreases with the increase of its mean value. They recommended a range of 12% to 45% for moderate to stiff soil.

Phoon *et al.* (1995), stated that the variability of the design soil properties depends on the quality of the measurements. Low variability of the design soil properties corresponds to good quality tests and direct laboratory or field tests. In this case, the *COV* of c_u ranges between 10% and 30%. Medium variability corresponds to indirect tests. In this case *COV* of c_u lies in a range from 30% to 50%. However, high variability corresponds to emprical correlations between the measured property and the uncertain design parameter. In this case, the *COV* of c_u ranges between 50% and 70%. Other values of $COVc_u$ proposed by other authors in literature are summerized in Table (1.1).

Table 1.1: Coefficient of variation of the soil cohesion

Author	$COVc_u$ (%)
Lumb (1972)	30 - 50 (test UC) 60 - 85 (highly variable clay)
Morse (1972)	30 - 50 (test UC)
Fredlund and Dahlman (1972)	30 - 50 (test UC)
Lee *et al*. (1983)	20 - 50 (clay) 25 - 30 (sand)
Ejezie and Harrop-Williams (1984)	28 – 96
Cherubini *et al*. (1993)	12 - 145 12 - 45 (medium to stiff clay)
Lacasse and Nadim (1996)	5 - 20 (clay – triaxial test) 10 - 30 (clay loam)
Zimbone *et al*. (1996)	43 – 46 (sandy loam) 58 – 77 (silty loam) 10 – 28 (clay)
Duncan (2000)	13 – 40

3.1.2. Angle of internal friction φ

For the internal friction angle φ, smaller values of the coefficint of variation as compared to those of the soil cohesion have been proposed in literature. Based on the results presented by Phoon *et al*. (1995), the coefficient of variation of the inetrnal friction angle ranges between 5% and 20% depending on the quality of the meaurements. For good quality tests and direct laboratory or field meaurements, the *COV* of φ ranges between 5% and 10%. For indirect meaurements, COV_{φ} lies in a range from 10% to 15%. Finally, by using emprical correlations, the COV_{φ} was found to vary between 15% and 20%. Table (1.2) presents the values of COV_{φ} proposed by several authors.

3.1.3. Young's modulus *E* and Poisson's ratio *v*

It has been shown in the literature that soils with small values of their Young’s modulus exhibit significant variability (Bauer and Pula 2000). Table (1.3) presents some values of the coefficient of variation of the Young's modulus *E* used in literature. Concerning the Poisson's ratio *v*, there is no sufficient information about its coefficient of variation. Some authors suggest that the variability of this parameter can be neglected while others proposed a very limited range of variability.

Table 1.2: Values of the coefficient of variation of the soil internal friction angle

Author	COV_{φ} (%)	Type of soil
Lumb (1966)	9	Different soil types
Baecher *et al*. (1983)	5 – 20	Tailings
Harr (1987)	7 12	Gravel Sand
Wolff (1996)	16	Silt
Lacasse and Nadim (1996)	2 – 5	Sand
Phoon and Kulhawy (1999)	5 – 11 4 – 12	Sand Clay, Silt

Table 1.3: Values of the coefficient of variation of the Young’s modulus

Author	COV_E (%)
Baecher and Christian (2003)	2 – 42
Nour *et al*. (2002)	40 – 50
Bauer and Pula (2000)	15
Phoon and Kulhawy (1999)	30

3.1.4. Coefficient of correlation *ρ*

The coefficient of correlation between two soil parameters represents the degree of dependence between these parameters. For the shear strength parameters *c* and *φ*, Lumb (1970) noted that the correlation coefficient $\rho_{c,\varphi}$ ranges from -0.7 to -0.37. Yucemen *et al*. (1973) proposed values in a range between -0.49 and -0.24, while Wolff (1985) reported that $\rho_{c,\varphi}$=-0.47. Finally, Cherubini (2000) proposed that $\rho_{c,\varphi}$=-0.61.

Concerning the correlation coefficient between the soil elastic properties *E* and *v*, this coefficient has received a little attention in literature. Bauer and Pula (2000) reported that there is a negative correlation between these parameters.

3.2. Advanced approach for modelling of uncertain soil parameters

In the advanced approach for modelling the uncertain soil parameters, the spatial variability of a given uncertain soil parameter is taken into account by modelling the uncertain parameter by a random field. In order to accurately quantify the soil spatial variability, a large number of in-situ observations is required. Generally, this is not available due to the high cost of in-situ tests. As shown in Figure (1.1), the spatial variation of a soil property can be conveniently decomposed into a smoothly varying trend function (simply estimated by fitting data using regression analysis) combined with a fluctuating component (residuals) around the trend as follows [cf. Jaksa (1995), Phoon and Kulhawy (1999) and Baecher and Christian (2003)]:

$$X(z) = t(z) + w(z) \tag{1.1}$$

in which *X(z)* is the actual soil property at the depth *z*, *t(z)* is the value of the trend at *z* and *w(z)* is the residual which represents the deviation from the trend at the depth *z*.

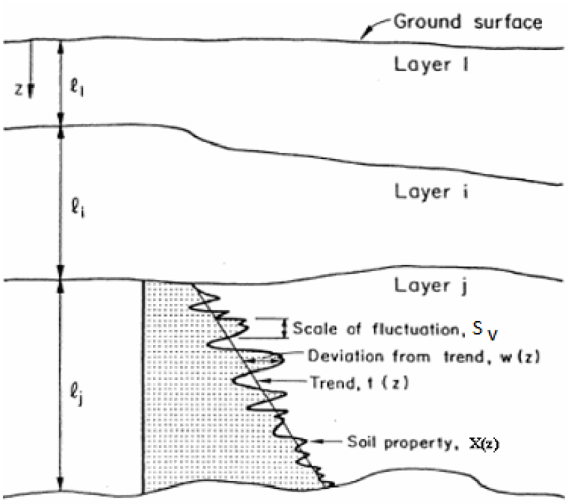

Figure 1.1: Inherent soil variability (After Phoon and Kulhawy 1999)

It should be mentioned here that the residuals are not independent. Positive residuals tend to clump together and negative residuals tend to clump together. The distance for which the residuals changes from positive to negative or from negative to positive is referred to as the scale of fluctuation (cf. the distance S_v in Figure 1.1). The dependence between residuals is measured by an autocorrelation or autocovariance function. The next subsections present a brief explanation on the autocorrelation function, autocovariance function, scale of fluctuation and autocorrelation length.

3.2.1. Autocorrelation function and autocovariance function

The correlation is the property that allows one to check if two random variables are linearly associated. The correlation between two different random variables x_1 and x_2 is measured by a correlation coefficient ρ defined as follows:

$$\rho = \frac{Cov(x_1, x_2)}{\sqrt{Var(x_1)Var(x_2)}} = \frac{1}{\sigma_{x_1}\sigma_{x_2}} E[(x_1 - \mu_{x_1})(x_2 - \mu_{x_2})] \qquad (1.2)$$

in which x_1 and x_2 might be the values of two different properties or the values of the same property at two different locations, $Cov(x_1, x_2)$ is the covariance of the two variables x_1 and x_2, $Var(x_i)$, $\sigma(x_i)$ and $\mu(x_i)$ are respectively the variance, the standard deviation and the mean value of the variable x_i $(i=1,2)$. In the case where x_1 and x_2 are two different properties, a correlation coefficient $\rho = \pm 1$ means that these two properties vary proportionally. The positive sign means that both variables increase or decrease together; however, the negative sign means that when one variable increases, the other one decreases. A correlation coefficient $\rho=0$ means that the two properties are uncorrelated.

When the correlation in Equation (1.2) is a function of the separation distance Δ, one may calculate the values of the correlations of the same property (between different locations) using the autocorrelation function defined as follows:

$$\rho_z(\Delta) = \frac{1}{Var[w(z)]} E[w(z_i)w(z_{i+1})] \tag{1.3}$$

Another alternative to the autocorrelation function is the autocovariance function defined as follows:

$$C_z(\Delta) = E[w(z_i)w(z_{i+1})] \tag{1.4}$$

In both Equations 1.3 and 1.4, $w(z_i)$ and $w(z_{i+1})$ are the residuals at two locations separated by a distance Δ and $Var[w(z)]$ is the variance of the residuals across the site. By definition, the autocorrelation at zero separation distance is $\rho_z(0)=1.0$; and it decreases with the increase in Δ.

The autocorrelation or the autocovariance function of a given soil property can be estimated from a sample of data of this property measured at different locations. Consider a sample of n observations ($x_1, \ldots, x_i, \ldots, x_n$) measured at equally spaced locations ($z_1, \ldots, z_i, \ldots, z_n$) separated by a distance Δ_j. The sample autocorrelation $\rho_z^*(\Delta_j)$ and autocovariance $C_z^*(\Delta_j)$ for a separation distance Δ_j are respectively given as follows [Jaksa (1995) and Baecher and Christian (2003)]:

$$\rho_z^*(\Delta_j) = \frac{1}{(n-1)\sigma_x^2} \sum_{i=1}^{n-1} \left[\{x(z_i) - t(z_i)\}\{x(z_{i+1}) - t(z_{i+1})\} \right] \tag{1.5}$$

$$C_z^*(\Delta_j) = \frac{1}{n-1}\sum_{i=1}^{n-1}\left[\{x(z_i) - t(z_i)\}\{x(z_{i+1}) - t(z_{i+1})\}\right] \tag{1.6}$$

where σ_x is the sample standard deviation across the site. The sample autocorrelation function $\rho_z^*(\Delta)$ and the sample autocovariance function $C_z^*(\Delta)$ are respectively obtained by (i) calculating $\rho_z^*(\Delta_j)$ and $C_z^*(\Delta_j)$ for different values of Δ_j, (ii) plotting them against Δ_j and finally, (iii) fitting the plot to a smooth function. The most commonly used autocorrelation functions were reported by Baecher and Christian (2003). They are presented in Table (1.4). In this table, l represents the so-called autocorrelation length. It is explained in some details in the following section.

Table 1.4: One-dimensional autocorrelation functions (After Baecher and Christian 2003).

Model	Equation
White noise	$\rho(\Delta) = \begin{cases} 1 \; if \; \Delta = 0 \\ 0 \; otherwise \end{cases}$
Linear	$\rho(\Delta) = \begin{cases} 1 - \left(\frac{\lvert\Delta\rvert}{l}\right) if \; \Delta \le l \\ 0 \; otherwise \end{cases}$
Exponential	$\rho(\Delta) = \exp\left(\frac{-\Delta}{l}\right)$
Squared exponential	$\rho(\Delta) = \exp^2\left(\frac{-\Delta}{l}\right)$
Power	$\rho(\Delta) = 1 + \left(\frac{\lvert\Delta\rvert^2}{l^2}\right)^{-\beta}$

The accuracy of the autocovariance and autocorrelation functions depends on the number n of observations. Referring to Jaksa (1995), the minimum number of observations has received a little effort in literature. Box and Jenkins (1970), Anderson (1976), and Davis (1986) recommended at least 50 observations. Lumb (1975) suggested that, for a full three-dimensional analysis, the minimum number of observations is of order 10^4. On the other hand, this author recommended that the best that can be achieved in practice is to study the one-dimensional variability, either vertically or horizontally, using a number of observations that ranges from 20 to 100 observations.

3.2.2. Scale of fluctuation and autocorrelation length

The scale of fluctuation or the autocorrelation length are key parameters to describe the spatial variability of a given soil property. The scale of fluctuation is defined as the distance within which the soil property shows relatively strong correlation from point to point (Jaksa 1995). Furthermore, when the soil property is plotted as a function of the distance, the scale of fluctuation is related to the distance between the intersections of the trend and the fluctuating soil property (i.e. the distance S_v in Figure 1.1). The scale of fluctuation is approximately equal to 0.8 times the average distance between the intersections of the trend and the fluctuating soil property (Vanmarcke 1977). Small values of the scale of fluctuation imply rapid fluctuation about the trend. However, high values imply a slowly varying soil property.

It should be mentioned here that the soil properties tend to be more variable in the vertical direction than in the horizontal direction. This implies that the vertical scale of fluctuation S_v of a given soil property tends to be shorter than the horizontal scale of fluctuation S_h of this property. Jaksa (1995) summarized the vertical and horizontal scales of fluctuation of the undrained shear strength published in literature. Based on this summary, S_v lies in a range of 0.13m-8.6m. However, S_h lies in a range of 46m-53m. Phoon and Kulhawy (1999) reported that S_h is more than one order of magnitude larger than S_v. According to these authors, S_v of the soil undrained shear strength ranges from 1m to 2m; however, S_h ranges from 40m to 60m.

Another statistical parameter which is related to the scale of fluctuation can be used to describe the spatial variability of the soil properties. This is the autocorrelation length l mentioned in the previous section. It is defined as the distance required for the autocorrelation function to decay from 1 to e^{-1} (0.3679). According to El-Ramly (2003), the vertical autocorrelation length ranges from 1 to 3m while the horizontal autocorrelation length is larger and it lies in a range from 10 to 40m. A literature review of typical autocorrelation lengths of different soil types and for different soil properties was given by El-Ramly (2003) and is presented in Table (1.5). Finally, it should be emphasized here that the autocorrelation function, the autocovariance function, the scale of fluctuation and the autocorrelation length are generally site specific, and often challenging due to insufficient site data and high cost of site investigations.

Table 1.5: values of the autocorrelation distances of some soil properties as given by several authors (El-Ramly 2003)

Test type	Soil property	Soil type	Autocorrelation length (m)	
			vertical	horizontal
VST	c_u(VST)	Organic soft clay	1.2	-
VST	c_u(VST)	Organic soft clay	3.1	-
VST	c_u(VST)	Sensitive clay	3.0	30.0
VST	c_u(VST)	Very soft clay	1.1	22.1
VST	c_u(VST)	Sensitive clay	2.0	-
Q_u	$c_u(Q_u)$	Chicago clay	0.4	-
Q_u	$c_u(Q_u)$	Soft clay	2.0	40.0
UU	$c_u(UU)_N$	Offshore soil	3.6	-
DSS	$c_u(DSS)_N$	Offshore soil	1.4	-
CPT	q_c	North see clay	-	30.0
CPT	q_c	Clean sand	1.6	-
CPT	q_c	North see soil	-	13.9
CPT	q_c	North see soil	-	37.5
CPT	q_c	Silty clay	1.0	-
CPT	q_c	Sensitive clay	2.0	-
CPT	q_c	Laminated clay	-	9.6
CPT	q_c	Dense sand	-	37.5

VST, vane shear test; Q_u, unconfined compressive strength test; UU, unconfined undrained triaxial test; DSS, direct shear test; CPT, cone penetration test; DMT, dilatometer test;
c_u(VST), undrained shear strength from VST; $c_u(Q_u)$, undrained shear strength from Q_u; $c_u(UU)_N$, normalized undrained shear strength from UU; $c_u(DSS)_N$, normalized undrained shear strength from DSS; q_c, CPT trip resistance;

4. Methods of discretization of random fields

In order to introduce the soil spatial variability in the analysis of geotechnical structures, the random field should be discretized into a finite number of random variables. In order to achieve this purpose, several methods of random field discretization were proposed in literature. The most commonly used methods of random field discretization in geotechnical engineering can be divided into two main groups as follows:

- **Average discretization methods**

  In these methods, the random variable related to a given element of the finite element/finite difference deterministic mesh is calculated as the average of the random field over that element [see for instance the Local Average Subdivision LAS method commonly used in geotechnical engineering as in Fenton and Griffiths (2002, 2005) and Fenton *et al.* (2003) among others].

- **Series expansion discretization methods**

  In the series expansion discretization methods, the random field is approximated by an expansion that involves deterministic and stochastic functions. The deterministic functions depend on the coordinates of the point at which the value of the random field is to be calculated. One of the commonly used series expansion methods is the Karhunen-Loève (K-L) expansion method presented by Spanos and Ghanem (1989). This method was used in chapters 5 and 6 of the present thesis to discretize the random field and it is briefly described in the next subsection.

4.1. Karhunen-Loève (K-L) expansion

Let us consider a Guassian random field *E(X, θ)* where *X* denotes the spatial coordinates and θ indicates the random nature of the random field. If μ_E is the mean of the random field, then the random field can be calculated by the K-L expansion as follows (Spanos and Ghanem 1989):

$$\mathrm{E}\,(\mathrm{X},\theta)=\mu_E+\sum_{i=1}^{\infty}\sqrt{\lambda_i}\,\phi_i(X)\,\xi_i(\theta) \tag{1.7}$$

where λ_i and ϕ_i are the eigenvalues and eigenfunctions of the autocovariance function, and $\xi_i(\theta)$ is a vector of standard uncorrelated random variables. It should be noticed here that

$\xi_i(\theta)$ are the stochastic variables that represent the random nature of the uncertain soil parameter. However, the eigenvalues and eigenfunctions λ_i and ϕ_i are the deterministic functions of the K-L expansion. They can be evaluated as the solution of the following integral equation:

$$\int_{\Omega} C(x_1, x_2)\phi_i(x_1)dx_1 = \lambda_i\phi_i(x_2) \tag{1.8}$$

This integral can be solved analytically only for few types of the autocorrelation functions. In the present thesis, an exponential autocovariance function (cf. Table 1.4) was used. For this autocovariance function, detailed closed form solution of the integral in Equation (1.8) can be found in Ghanem and Spanos (1991) and is presented in Appendix A of the present thesis.

It is to be mentioned here that for practical purposes, the expansion in Equation (1.7) is generally truncated to a given number *M* of terms as follows:

$$E(X,\theta) \approx \mu_E + \sum_{i=1}^{M} \sqrt{\lambda_i}\phi_i(X)\xi_i(\theta) \tag{1.9}$$

The choice of the number *M* of terms depends on the desired accuracy of the problem being treated. The error estimate $\varepsilon rr(X)$ after truncating the expansion to *M* terms can be calculated as follows (Sudret and Der Kiureghian 2000):

$$\varepsilon rr(X) = \sigma_E^2 - \sum_{i=1}^{M} \lambda_i\varphi_i^2(X) \tag{1.10}$$

where σ_E is the standard deviation of the random field. Finally, notice that in most geotechnical problems, the random fields are assumed to follow a log-normal PDF. This assumption is motivated by the fact that a soil parameter cannot be negative in reality. In such a case, $ln(E)$ is a normal random field with mean value $\mu_{\ln_E}$ and standard deviation $\sigma_{\ln_E}$ given as follows:

$$\sigma_{ln_E} = \sqrt{ln(1 + COV_E^2)} \tag{1.11}$$

$$\mu_{ln_E} = ln(\mu_E) - 0.5\sigma_{ln_E} \tag{1.12}$$

For a lognormal random field, Equation (1.9) becomes [Cho (2010), Cho and Park (2010)]:

$$E(X,\theta) \approx exp\left[\mu_{ln_E} + \sum_{i=1}^{M} \sqrt{\lambda_i}\phi_i(X)\xi_i(\theta)\right] \tag{1.13}$$

5. Probabilistic methods

The aim of the probabilistic methods is to propagate the uncertainties from the input parameters (e.g. c, φ, E, ν, etc.) to the system response (e.g. ultimate load, displacement, etc.) through a computational model. Each one of the existing probabilistic methods provides one or more of the following probabilistic outputs: (i) reliability index, (ii) failure probability, (iii) statistical moments (mean value μ and standard deviation σ) of the system response and (iv) the PDF of the system response with all the statistical moments (mean value, standard deviation, skewness and kurtosis). The principal probabilistic methods used in literature can be divided into three main groups according to the main probabilistic output obtained by each method as follows:

- Probabilistic methods for the computation of the reliability index
- Probabilistic methods for the computation of the failure probability
- Probabilistic methods for the computation of the statistical moments (mean value, standard deviation, etc.) of the system response

These methods are explained in the following subsections after a brief description of some basic reliability concepts.

5.1. Performance function and limit state surface

The performance function G is a function by which one can distinguish if a given set of values of the random variables leads to system failure or to system safety. The performance function can be expressed, for a given problem, in different ways. For example, for vertically loaded footings, there are two different forms of the performance function with respect to soil punching: (i) $G=(P_u/P_s)-1$ or (ii) $G=P_u-P_s$ where P_u and P_s are respectively the ultimate vertical load and the footing applied vertical load. In this example, if the random variables are the soil shear strength parameters (c and φ) and the applied load P_s is assumed to be detrministic; then, all pairs (c, φ) that make $G<0$ (i.e. $P_u<P_s$) lead to failure. However, all pairs (c, φ) that make $G>0$ (i.e. $P_u>P_s$) lead to system safety (cf. Figure 1.2).

The limit state surface of a given mechanical system is defined as the surface that joins the set of values of the random valriables (c and φ in the present case) for which failure just occurs (i.e. for which $G=0$). As shown in Figure (1.2), the limit state surface divides the space of random variables into two zones (i) a safe zone (characterized by $G>0$) for which combination of random variables (c, φ) do not lead to failure and (ii) failure zone (characterized by $G<0$) for which combinations of random variables (c, φ) lead to failure.

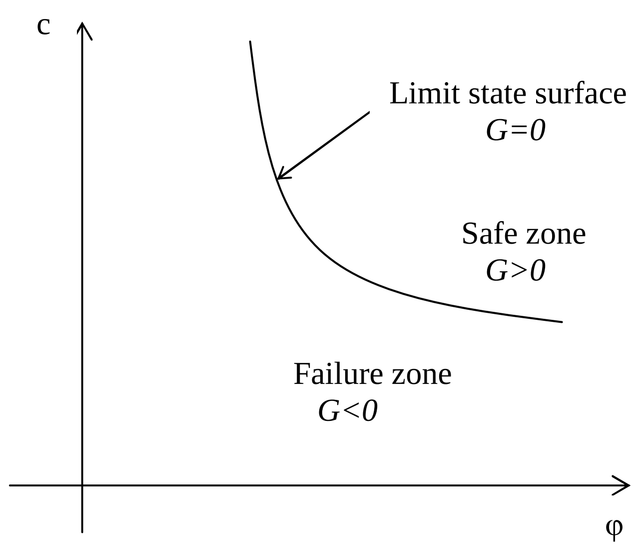

Figure 1.2: Limit state surface in the space of random variables

5.2. Probabilistic methods for the computation of the reliability index

The reliability index of a geotechnical structure provides a measure of the safety that takes into account the inherent uncertainties of the different input parameters *via* their probability density functions (PDFs). Two reliability indices are proposed in literature. These are the Cornell reliability index β_c (Cornell 1969) and the Hasofer-Lind reliability index β_{HL} (Hasofer and Lind 1974). These indices are briefly presented below.

5.2.1. Cornell reliability index β_c

This index is defined as the ratio between the mean value of the performance function *G* and its standard deviation (i.e. $\beta_C = \mu_G / \sigma_G$) where the performance function G is assumed to follow a Guassian distribution with mean μ_G and standard deviation σ_G. From this equation, it is obvious that the Cornell reliability index represents the number of standard deviations that separates the mean value of the performance function from the limit state surface G=0. The main shortcoming of the Cornell reliability index is that its value depends on the form of the performance function in case of non-linear limit state surface or in case of non-guassian random variables. Although not rigorous, β_c was frequently adopted in the past for calculating the reliability of geotechnical structures [e.g. Chowdhury and Xu (1993, 1995), Christian *et al*. (1994), Hassan and Wolff (1999), Liang *et al.* (1999), Malkawi *et al.* (2000), Bhattacharya *et al.* (2003)].

5.2.2. Hasofer-Lind reliability index β_{HL}

To overcome the inconvenience of the Cornell reliability index, another reliability index denoted β_{HL} was proposed by Hasofer and Lind (1974). This index is defined as the minimal distance that separates the limit state surface expressed in the space of standard normal uncorrelated random variables and the origin of this space (Figure 1.3). In case where the limit state surface is known analytically, β_{HL} can be easily calculated using one of the two approaches described in the two following subsections. Otherwise, the response surface method (RSM) presented hereafter is used for this computation.

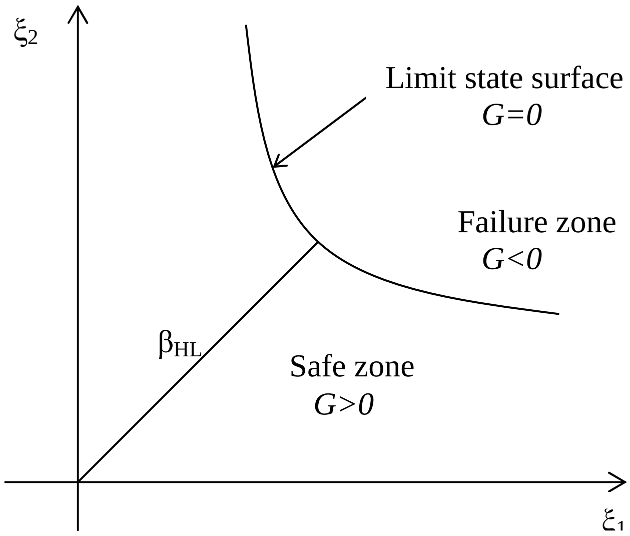

Figure 1.3: Hasofer-Lind reliability index in the standard space of random variables

5.2.2.1. Classical approach for the computation of β_{HL}

In this approach, β_{HL} is calculated by minimization of the following problem under the constraint $G=0$:

$$\beta_{HL} = \min_{G=0}\left(\sqrt{\sum_{i=1}^{n}\xi_i^2}\right) \tag{1.14}$$

where ξ_i $(i=1, 2, \ldots, n)$ are the n standard normal uncorrelated random variables corresponding to the n physical uncertain parameters. The computation of β_{HL} consists of two steps:

- In the first step, the physical (original) random variables should be transformed to the standard normal random variables. In this step, isoprobabilistic transformation is used to transform the physical random variables to standard normal random variables as follows:

$$\xi_i = \Phi^{-1}\left[F_{x_i}(x_i)\right] \tag{1.15}$$

in which, x_i is a physical random variable, F_{x_i} is the cumulative density function (CDF) of the physical random variable x_i and $\Phi^{-1}(\cdot)$ is the inverse of the CDF of the standard normal random variable. Notice that, if the original random variables are correlated, they should be transformed into uncorrelated random variables.

- In the second step, it is required to search for the minimal distance between the limit state surface and the origin of the standard space of uncorrelated random variables.

5.2.2.2. Ellipsoid approach for the computaion of β_{HL}

For normal random variables, the Hasofer-Lind reliability index β_{HL} defined in matrix formulation is given by:

$$\beta_{HL} = \min_{G=0} \sqrt{(x-\mu)^T C^{-1} (x-\mu)} \qquad (1.16)$$

in which x is the vector representing the n random variables, μ is the vector of their mean values and C is their covariance matrix. Equation (1.16) represents the equation of an ellipsoid of n dimensions. Based on this equation, Low and Tang (1997) proposed an approach to calculate β_{HL} in the original space (not in the transformed standard uncorrelated space) of random variables. In this approach, β_{HL} is calculated as the ratio between the ellipse (cf. Figure 1.4 in case of two random variables x_1 and x_2) that is tangent to the limit state surface and the unit dispersion ellipse corresponding to $\beta_{HL}=1$. To find this ratio, the unit dispersion ellipse with center at the mean values of the random variables is gradually expanded or contracted, keeping a constant aspect ratio, until touching the limit state surface $G=0$. The ratio between the ellipse that is tangent to the limit state surface and the unit dispersion ellipse is equal to β_{HL} as shown in Figure (1.4). The point of tangency (x_1^*, x_2^*) represents the most probable failure point and it is called the design point. For the particular problem of the ultimate bearing capacity presented in section 5.1, the design point (c^*, φ^*) provides the most critical values of c and φ (from a probabilistic point of view) that make the ultimate footing load P_u equal to the prescribed footing applied load P_s. This point corresponds to the closest point of the limit state surface to the origin of the standard space of random variables. Notice that c and φ are distributed according to a joint PDF and the design point is a particular point from this distribution that provides the minimal reliability of the treated problem. Notice finally that the knowledge of c^* and φ^* allows one to determine the partial safety factors corresponding to these parameters as follows: $F_c=\mu_c/c^*$ and $F_\varphi=tan(\mu_\varphi)/tan(\varphi^*)$. These factors are not constant and vary from one case to another depending on the variability of the random variables and the correlation between these variables. This is one of the important advantages of the reliability-based approach with respect to the deterministic approach which is not able to consider the real safety inherent to c and φ. Notice finally that the ellipsoid approach can be easily implemented in the Excel worksheet (see for example Youssef Abdel Massih *et al.* 2008).

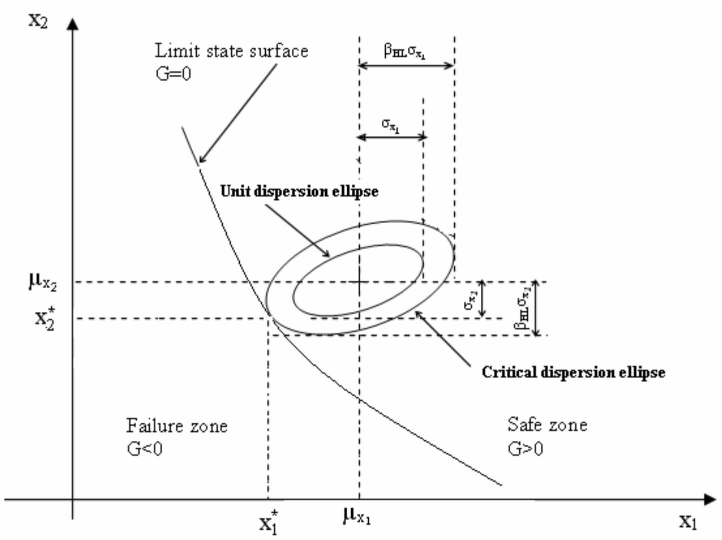

Figure 1.4: Critical and unit dispersion ellipses in the original space of random variables

5.2.2.3. Response Surface Method (RSM)

In case of complex implicit mechanical models, the Response Surface Method (RSM) comes out as a good choice to calculate β_{HL}. In this method, the response is substituted by approximate function in the neighborhood of the design point (Neves *et al.*

2008). Several algorithms were proposed in literature to aproximate the response surface using successive iterations [kim and Na (1997), Das and Zheng (2000), Tandjiria *et al.* (2000) and Duprat *et al.* (2004)]. In this thesis, the algorithm by Tandjiria *et al.* (2000) is used. This algorithm is presented in some details in chapter 2 of this thesis. The basic idea of the RSM is to approximate the system response $\Gamma(x)$ [and consequently the performance function] by an explicit function of the random variables, and to improve the approximation *via* iterations. The RSM was used by several authors [e.g. Neves *et al.* (2006), Youssef Abdel Massih and Soubra (2008) and Mollon *et al*. (2009)] and was found an efficient tool to calculate the reliability index β_{HL}. It is to be mentioned here that different types of polynomials of different orders with or without cross-terms are proposed in literature to approximate the system response or the performance function by an analytical function of the random variables.

Finally, it should be noticed that the algorithm by Tandjiria *et al.* (2000) was used in Youssef Abdel Massih (2007) to perform a reliability-based analysis of a strip footing subjected to a vertical load. In the present thesis, this algorithm was also employed in chapter 2 to perform an extensive reliability-based analysis of a circular footing subjected to an inclined load.

5.3. Probabilistic methods for the computation of the failure probability

The failure probability P_f of a mechanical system is the integral of the joint probability density function of the random variables in the failure domain. Consider a mechanical system having *n* random variables $(x_1, \ldots x_i, \ldots x_n)$. The failure probability of this system is calculated as follows:

$$P_f = \int_{G \leq 0} f(x)dx \qquad (1.17)$$

where $f(x)$ is the joint probability density function of the random variables and *G* is the performance function. The integral in Equation (1.17) represents the volume located in the failure domain (*G<0*) and limited by the joint probability density function and the limit state surface *G=0* (see Figure 1.5). In all but academic cases, the integral in Equation (1.17) cannot be computed analytically. For this reason, several numerical methods were proposed in literature to calculate P_f. A brief description of the probabilistic methods used in this thesis to calculate P_f is presented in the following subsections.

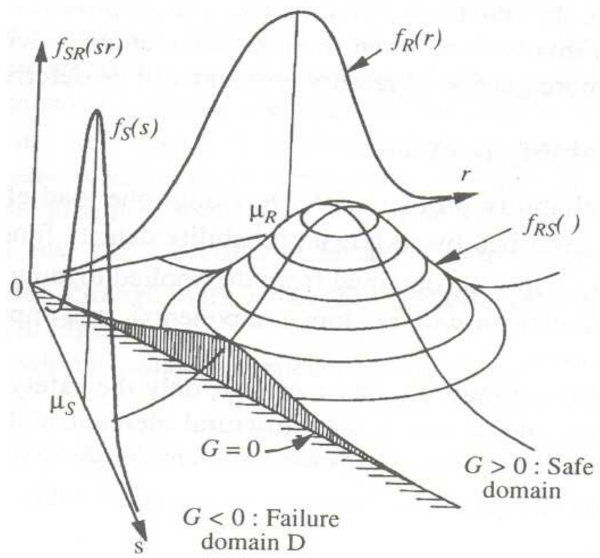

Figure 1.5: Joint probability density function and limit state surface in case of two random variables R and S (After Melchers 1999)

5.3.1. First Order Reliability Method (FORM)

The Hasofer-Lind reliability index presented previously in this chapter can be used to calculate an approximate value of the failure probability using the First Order Reliability Method (FORM) as follows:

$$P_f \approx \Phi(-\beta_{HL}) \tag{1.18}$$

where $\Phi(\cdot)$ is the cumulative density function (CDF) of a standard normal variable and β_{HL} is the Hasofer-Lind reliability index. In this method, the limit state surface is approximated by a hyperplane (first order approximation) tangent to the limit state surface at the most probable failure point called "design point". This method was used in chapter 2 of this thesis to calculate the failure probability. The main shortcoming of this method is that, in case of highly non-linear limit state surfaces, it provides a non-rigorous value of the failure probability.

5.3.2. Monte Carlo Simulation (MCS) methodology

Monte Carlo simulation (MCS) methodology is a universal method to evaluate complex integrals. Due to its high accuracy, MCS is widely used for the computation of the failure probability whatever is the degree of non-linearity of the limit state surface. It was used in this thesis as a tool to check the accuracy of less time-consuming methods that are developed for rigorous computation of small failure probabilities.

Let *I(x)* be the indicator function of the failure domain (i.e. the function that takes the value of 0 in the safe domain where G>0 and 1 otherwise). Thus, Equation (1.17) can be rewritten as follows:

$$P_f = \int_{\Omega} I(x) f(x) dx = E[I(x)] \tag{1.19}$$

in which Ω is the entire domain of random variables and $E[I(x)]$ is the expectation of the indicator $I(x)$. This expectation can be practically evaluated by generating a large number N of realizations of the random vector $\boldsymbol{x}=(x_1, \ldots, x_i, \ldots, x_n)$. For each realization j, the performance function G_j is evaluated. Then, an unbiased estimation of the failure probability is calculated as follows:

$$\tilde{P}_f = \frac{1}{N} \sum_{j=1}^{N} I_j(x) \tag{1.20}$$

where:

$$I_j(x) = \begin{cases} 1 & if \quad G_j \le 0 \\ 0 & if \quad G_j > 0 \end{cases} \tag{1.21}$$

The accuracy of the estimated failure probability can be measured by calculating its coefficient of variation as follows:

$$COV(\tilde{P}_f) = \sqrt{\frac{1-\tilde{P}_f}{N\tilde{P}_f}} \tag{1.22}$$

The smaller values of the coefficient of variation indicate more accurate values of the estimated failure probability.

In spite of being applicable whatever the complexity of the system is, MCS methodology is not practically applicable when small values of P_f are sought. This is due to the large number of realisations required to obtain an accurate value of P_f in such a case. Referring to Equation (1.22), if $P_f=10^{-4}$ and a coefficient of variation of 10% is desired, the number of realisations required to calculate P_f is about 10^6. For this reason, a more efficient method called "subset simulation" was proposed in literature to calculate the small failure probability using a reduced number of realisations compared to MCS methodology. This method is presented in the following subsection.

5.3.3. Subset simulation (SS) approach

The subset simulation (SS) approach was proposed by Au and Beck (2001) as an alternative to MCS methodology to compute the small failure probabilities. Its aim is to reduce the number of calls of the deterministic model as compared to MCS methodology. The basic idea of the SS approach is that the small failure probability in the original probability space can be expressed as a product of larger conditional failure probabilities in the conditional probability space. This method was used by several authors [Au and Beck (2003), Schuëller *et al.* (2004), Au *et al.* (2007) and Au *et al.* (2010) among others] and was found to be an efficient tool for the computation of the small failure probability. The SS approach was mainly used in literature in the cases where the uncertain parameters are modeled by random variables.

5.4. Probabilistic methods for the computation of the statistical moments of the system response

Firstly, one presents a simple approximate method that uses Taylor series expansion to provide a rough estimate of the first two statistical moments (mean value and variance) of the system response. This is followed by a more advanced and rigorous method that provides the PDF of the system response and the corresponding statistical moments.

5.4.1. First Order Second Moment (FOSM) method

This method uses Taylor series expansion to provide an approximation of the first two statistical moments, i.e. mean and variance (Haldar and Mahadevan 2000). Consider a system response Γ related to the random variables $(x_1,...x_i,...x_n)$ by a general function f where $\Gamma = f(x_1,...x_i,...x_n)$. If the mean and standard deviation of the random variables are known but the distributions of these variables are unknown, an approximate mean value of the system response and an approximate variance of this system response can be obtained. By expanding the function $f(x_1,...x_i,...x_n)$ in a Taylor series about the mean values of random variables $(\mu_{x_1},...\mu_{x_i},...\mu_{x_n})$, one obtains:

$$\Gamma = f(\mu_{x_1},...\mu_{x_i},...\mu_{x_n}) + \sum_{i=1}^{n}\left(x_i - \mu_{x_i}\right)\frac{\partial f}{\partial x_i} + \frac{1}{2}\sum_{i=1}^{n}\sum_{j=1}^{n}\left(x_i - \mu_{x_i}\right)\left(x_j - \mu_{x_j}\right)\frac{\partial^2 f}{\partial x_i \partial x_j} + ... \quad (1.23)$$

where the derivatives are evaluated at the mean values of the random variables. Truncating the series at the linear terms, the first order approximate mean value of Γ can be obtained as follows:

$$\mu_\Gamma = f(\mu_{x_1},..\mu_{x_i},..\mu_{x_n}) \quad (1.24)$$

The variance of the system response is given by the following formula:

$$Var_\Gamma = \sum_{i=1}^{n}\left(\frac{\partial f}{\partial x_i}\right)Var(x_i) + \sum_{i}^{n}\sum_{j\neq i}^{n}\frac{\partial f}{\partial x_i}\frac{\partial f}{\partial x_j}Cov(x_i, x_j) \quad (1.25)$$

This approximation of the mean and variance of the system response can be improved by including higher order terms in the Taylor series expansion.

5.4.2. Collocation-based Stochastic Response Surface Method (CSRSM)

The Collocation-based Stochastic Response Surface Method (CSRSM) called also Polynomial Chaos Expansion Method was proposed in literature and was employed by several authors [Isukapalli *et al.* (1998), Phoon and Huang (2007), Huang *et al.* (2009), Riahi *et al.* (2011), Li *et al.* (2011), Mollon *et al.* (2011), Houmadi *et al.* (2012), Mao *et al.* (2012), Soubra and Mao (2012) and Ahmed and Soubra (2012a)]. The aim of this method is to obtain the probability density function of the system response. In this method, the complex numerical model is replaced by an analytical model (meta-model). This makes it easy to compute the PDF of the system response by applying MCS methodology on the meta-model.

6. Conclusion

In this chapter, a literature review on the soil uncertainties was presented. First, the different sources of uncertainties were presented. Second, the different approaches of modeling the soil uncertain parameters were described. In this regard two approaches were presented: (i) the simplified approach in which the uncertain parameters are represented by random variables characterized by their PDFs and (ii) the advanced approach in which the uncertain parameters are represented by random fields characterized not only by their PDFs but also by their autocorrelation functions. In the framework of the simplified approach, the ranges of the coefficients of variation of the soil parameters proposed in literature were summarized. Also, the types of the PDFs of the different soil uncertain parameters were presented. Finally, the values of the coefficients of correlation ρ between soil properties proposed in literature were reported. In the framework of the advanced approach, the most commonly used autocorrelation functions proposed in literature were presented. Also, the ranges of the vertical and horizontal autocorrelation lengths were summarized. It was found that the horizontal autocorrelation length tends to be one order of magnitude higher than the vertical one.

This chapter has also presented a brief description of the commonly used methods of random field discretization in geotechnical engineering. Finally, the different probabilistic methods used in this thesis to perform the probabilistic analyses were presented and discussed. These methods were divided into three main groups according to the main obtained probabilistic output as follows:

1 – Methods for the computation of the reliability index

This group of probabilistic methods provides the reliability index by which the safety of the system is measured. This group contains three methods: (i) the classical method, (ii) the ellipsoid approach and (iii) the Response Surface Method (RSM). The first two methods are used when the limit state surface is known analytically. However, in case where the limit state surface is analytically unknown, the RSM is used to calculate the reliability index by iteratively approximating the limit state surface.

2 – Methods for the computation of the failure probability

This group of probabilistic methods provides the failure probability of a given mechanical system. This group contains three methods: (i) the First Order Reliability Method (FORM), (ii) Monte Carlo Simulation (MCS) methodology and (iii) Subset Simulation (SS) approach. The first method (i.e. FORM) provides an approximation of the failure probability based on the reliability index. This method is not rigorous in case of non-linear limit state surfaces. The second method (i.e. MCS) can be used even if the limit state surface is highly non-linear. It provides a rigorous value of the failure probability. However, it is very time-consuming especially in case of small value of the failure probability. To overcome this shortcoming, the third method (i.e. subset simulation) may be used. This method allows calculating the failure probability using a reduced number of realizations compared to MCS methodology.

3 – Methods for the computation of the statistical moments of the system response

This group includes two probabilistic methods: (i) the First Order Second Moment (FOSM) method and (ii) the Collocation-based Stochastic Response Surface Method (CSRSM). The First Order Second Moment (FOSM) is used in case where the PDFs of the random variables are unknown. This method provides only an approximate estimate of the mean value and the variance of the system response. The CSRSM provides the PDF of the system response and the corresponding statistical moments (mean value, variance, skewness and kurtosis).

PART I

SIMPLIFIED PROBABILISTIC ANALYSIS OF SHALLOW FOUNDATIONS

CHAPTER 2

RELIABILITY-BASED ANALYSIS OF OBLIQUELY LOADED FOOTINGS USING THE RESPONSE SURFACE METHOD (RSM)

1. Introduction

Previous reliability analyses on shallow foundations have focused on the case of a vertically loaded strip footing which involves a single failure mode [Bauer and Pula (2000), Cherubini (2000), Griffiths and Fenton (2001), Griffiths *et al.* (2002), Low and Phoon (2002), Fenton and Griffiths (2002, 2003), Popescu *et al.* (2005), Przewlocki (2005), Sivakumar and Srivastava (2007), Youssef Abdel Massih *et al.* (2008), Youssef Abdel Massih and Soubra (2008), Srivastava and Sivakumar (2009), Soubra and Youssef Abdel Massih (2010)]. The reliability analysis of a footing subjected to an inclined and/or an eccentric loading has received a little attention in literature. In this case, different failure modes may be involved at the ultimate limit state (ULS) such as the footing sliding, the soil punching and the footing overturning. Similar to the ULS, the serviceability limit state (SLS) may involve different unsatisfactory performance modes such as the exceeding of tolerable footing horizontal and vertical displacements and the exceeding of a tolerable footing rotation. This chapter attempts to fill this gap. It deals with the reliability analysis of a circular footing subjected to an inclined load. The motivation for this work comes principally from the offshore industry. The footings of the offshore structures should resist (in addition to the vertical weight of the structure) the horizontal loads and overturning moments arising from the environmental actions on these structures. The reliability analysis of footings under these conditions is a challenging three-dimensional (3D) problem. In this thesis, the focus was made on the case of an inclined load. The extension to the general case of complex and/or seismic or dynamic load will be the subject of a future work.

This chapter aims at providing: (i) a rigorous and unique deterministic safety measure that takes into account the two failure modes (i.e. soil punching and footing sliding) at ULS based on a deterministic approach, (ii) a rigorous and unique reliability index β_{HL} that also takes into account the two failure modes (i.e. soil punching and footing sliding) at ULS in the framework of the reliability-based analysis, (iii) the most predominant failure mode at ULS and also the most predominant unsatisfactory performance mode at SLS for the different loading configurations, and finally (iv) a parametric study showing the effect of the different governing parameters on the failure probability.

It should be mentioned that only the uncertainties of the soil parameters were considered in the reliability-based analysis. The soil shear strength parameters (c and φ) were considered as random variables at ULS and the soil elastic parameters (E and v) were considered as random variables at SLS. Notice that the system response used at ULS was the factor of safety F determined using the strength reduction method. Concerning the SLS, two system responses were used. These are the vertical and horizontal displacements of the footing center. The deterministic models used to calculate the different system responses are based on 3D numerical simulations using the Lagrangian explicit finite difference code FLAC^{3D}. Thus, the Response Surface Methodology (RSM) was used to find an approximation of the unknown limit state surfaces. The Hasofer-Lind reliability index β_{HL} was used to compute the soil-footing reliability. The First Order Reliability Method (FORM) was used to calculate the failure probability.

This chapter is organized as follows: The Response Surface Method (RSM) is first presented. This is followed by the computation of the system responses at ULS and SLS of a circular footing subjected to an inclined load. Then, a ULS deterministic analysis and both ULS and SLS reliability-based analyses of this footing are presented and discussed.

Finally, a parametric study showing the effect of the different governing parameters on the failure probability is presented and discussed. The chapter ends by a conclusion of the main findings.

2. Response Surface Method (RSM)

For the problem studied in this chapter, the response surface is not known analytically. Thus, the Response Surface Method (RSM) is used to calculate the Hasofer-Lind reliability index β_{HL}. The basic idea of the RSM is to approximate the system response $\Gamma(x)$ [and consequently the performance function *G*] by an explicit function of the random variables, and to improve the approximation *via* iterations [kim and Na (1997), Das and Zheng (2000), Tandjiria *et al.* (2000) and Duprat *et al.* (2004)]. The algorithm by Tandjiria *et al.* (2000) was used in this chapter. The expression of the system response used herein is a second order polynomial with squared terms but without cross-terms. It is given by:

$$\Gamma(x) = a_0 + \sum_{i=1}^{n} a_i.x_i + \sum_{i=1}^{n} b_i.x_i^2 \tag{2.1}$$

where x_i are the random variables, n is the number of random variables and (a_i, b_i) are unknown coefficients to be determined. Notice that the random variables x_i are characterized by their mean and standard deviation values (μ_i and σ_i). A brief explanation of the algorithm by Tandjiria *et al.* (2000) used in this chapter is given as follows:

1. Using the deterministic model, evaluate the value of the system response $\Gamma(x)$ at the point that represents the mean values μ_i of the random variables and at the $2n$ points (each at $\mu_i \pm k\sigma_i$ where k is arbitrarily chosen equal to 1 in this chapter).

2. The above $2n+1$ values of *Γ(x)* are used to solve the linear system of equations (Equation 2.1) and find the coefficients (a_i, b_i). Then, the performance function *G* can be constructed to give a tentative response surface function.
3. Calculate the tentative reliability index β_{HL} and the corresponding tentative design point x_i^* using for instance the ellipsoid approach presented in chapter 1.
4. Repeat steps 1 to 3 using each time the tentative design point x_i^* and the *2n* points (each at $x_i^* \pm k\sigma_i$) until the convergence of β_{HL}. The convergence is considered to be achieved when the absolute difference *ε* between two successive values of β_{HL} is less than a prescribed small value (e.g. $\varepsilon<10^{-1}$ in the present chapter).

Finally, the obtained β_{HL} can be used to provide an approximate value of the failure probability using the First Order Reliability Method (FORM) as follows: $P_f \approx \Phi(-\beta_{HL})$ where $\Phi(\cdot)$ is the CDF of a standard normal variable.

It should be emphasized here that in case of a large number of random variables *n*, the computation of β_{HL} becomes very time consuming. For each iteration of the RSM, the number of calls of the deterministic model required to evaluate the coefficients (a_i, b_i) is equal to $2n+1$. The number of iterations required to achieve the convergence of β_{HL} depends on the problem being treated. It ranges between 2 and 5 iterations in most geotechnical problems. Thus, the total number of calls of the deterministic model significantly increases with the increase in the number of random variables. The computation time becomes non-realistic when dealing with 3D numerical models (as is the case in the present chapter) where each call of the deterministic model is very time-expensive. Finally, it should be emphasized that the obtained limit state surface is well approximated only around the design point.

3. Computation of the system responses for the ULS and SLS analyses

The aim of this section is to present the method of computation of the system responses at ULS and SLS of a circular footing subjected to an inclined load. FLAC^{3D} software was used to calculate the different system responses. A brief overview on this software is provided in Appendix B.

For the ULS analysis, two system responses are traditionally used in the literature to check the stability of shallow footings subjected to inclined loads. These are the two individual safety factors $F_p=V_u/V$ and $F_s=H_u/H$ against soil punching and footing sliding respectively, where V_u and H_u are respectively the vertical and the horizontal ultimate loads and V and H are respectively the applied vertical and horizontal load components. These safety factors are not very rigorous because they consider only a single mode of failure (punching or sliding). They neglect the interference between the two failure modes which simultaneously exists whatever the values of the footing load components (H, V) are. A more rigorous and unique safety factor F that simultaneously takes into account the two modes of failure is proposed herein for the computation of a unique rigorous safety level of the soil-footing system. This factor is defined using the strength reduction method. In this method, the soil shear strength parameters (c, φ) are replaced by c_d and φ_d where c_d and φ_d are given by:

$$c_d = \frac{c}{F} \tag{2.2}$$

$$\varphi_d = tan^{-1}\left(\frac{tan\,\varphi}{F}\right) \tag{2.3}$$

The critical safety factor F is calculated by successively reducing c and $tan\varphi$ by an increasing tentative value of the factor F until failure occurs. The tentative value of the factor F corresponding to failure is the safety factor of the soil-footing system subjected to the loads (H, V). As may be seen later, the present definition of the safety factor allows one to simultaneously consider the two failure modes (footing sliding and soil punching) using a single simulation.

In order to calculate the safety factor F using FLAC^{3D}, a circular footing of radius R=1m that rests on a (c, φ) soil domain of radius equal to 5R and depth equal to 5R was considered in the analysis. Because of symmetry, only one half of the entire soil domain was considered (Figure 2.1). A non-uniform mesh composed of 6040 zones was used to compute the safety factor. This mesh was refined near the footing edges where high stresses and strains are developed. For the displacement boundary conditions, the bottom boundary was assumed to be fixed and the vertical cylindrical boundary was constrained in motion in the horizontal X and Y directions. Concerning the (Z, X) vertical plane of symmetry, it was constrained in motion in the perpendicular direction.

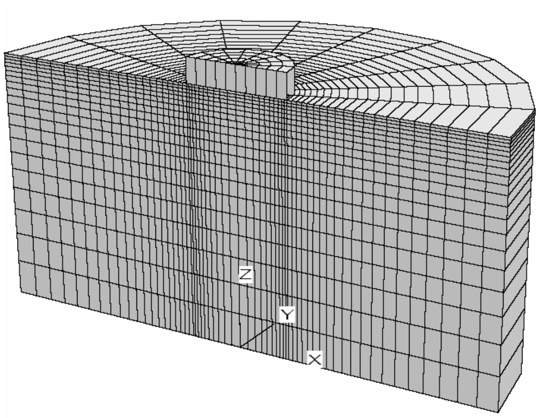

Figure 2.1: Soil domain and mesh used to simulate the soil-footing system

A conventional elastic perfectly plastic model obeying Mohr-Coulomb failure criterion was used to represent the soil behavior. Concerning the circular footing, it was modeled by an elastic perfectly plastic model obeying Mohr-Coulomb failure criterion although a linear elastic model should be used. This is because the computation of the safety factor in FLAC^{3D} (through the ‘Solve FOS’ command) cannot be achieved unless all zones of the domain (i.e. soil and foundation) are modeled by an elastic perfectly plastic model based on Mohr-Coulomb failure criterion. To overcome this inconvenience, a very large value was affected to the cohesion parameter of the foundation (see Table 2.1). Concerning the soil-footing interface, it was assumed to follow the same model as the soil with the same values of the shear strength parameters and the dilation angle. This assumption was adopted in order to simulate a perfectly rough interface between the soil and the footing. The illustrative values of the shear strength parameters (c and φ), the elastic properties (E and ν) and the dilation angle ψ of the soil, footing and interface are given in Table (2.1). The normal and the shear stiffness (K_n and K_s) of the interface are also presented in this table. Notice that K_n and K_s have no significant effect on the value of the safety factor. Notice also that at ULS, the soil Young's modulus was affected an arbitrary value of 390MPa. This value is much larger than the real value of 60MPa. This large value of the Young's modulus results in a considerable reduction in the computation time of the safety factor F and does not deteriorate the accuracy of the solution.

Table 2.1: Shear strength and elastic properties of soil, footing, and interface for the ULS analysis

Variable	Soil	Footing	Interface
c	20kPa	200GPa	20kPa
φ	30^{o}	30^{o}	30^{o}
$\psi = 2/3\ \varphi$	20^{o}	20^{o}	20^{o}
E	390MPa	25GPa	N/A
ν	0.3	0.4	N/A
K_n	N/A	N/A	1GPa
K_s	N/A	N/A	1GPa

To check the validity of the assumption of modeling the footing by an elastic perfectly plastic model with a great cohesion value, the following test was performed: First, the footing was modeled by a linear elastic model and the ultimate vertical load V_u was computed. Second, the footing was modeled by an elastic perfectly plastic model obeying Mohr-Coulomb failure criterion and the safety factor F was calculated using the computed V_u value. It was found that F is equal to one. This means that an elastic perfectly plastic behavior can be adopted for the footing to calculate the safety factor F of the soil-footing system.

Concerning the SLS analysis, two system responses were considered. These are the vertical and the horizontal footing displacements. The same mesh used for the ULS analysis is employed here to calculate the footing vertical and horizontal displacements. Similar to the ULS analysis, a conventional elastic perfectly plastic model obeying Mohr-Coulomb failure criterion was used to represent the soil behavior in the SLS analysis. This assumption was adopted here in order to take into account the possible plastification that may take place near the footing edges even under the service loads. Concerning the footing, it was assumed to follow a linear elastic model. Similar to the ULS analysis, the soil-footing interface was affected the same properties (c, φ, ψ) as the soil in order to simulate a perfectly rough interface. The illustrative values of the soil, footing, and interface properties used for the SLS analysis are given in Table (2.2).

Table 2.2: Shear strength and elastic properties of soil, footing, and interface for the SLS analysis

Variable	Soil	Footing	Interface
c	20kPa	N/A	20kPa
φ	30^{o}	N/A	30^{o}
$\psi = 2/3\ \varphi$	20^{o}	N/A	20^{o}
E	60MPa	25GPa	N/A
ν	0.3	0.4	N/A
K_n	N/A	N/A	1GPa
K_s	N/A	N/A	1GPa

In order to calculate the vertical and horizontal displacements of the footing center, geostatic stresses are first applied to the soil. Then, several cycles are run in order to achieve a steady state of static equilibrium. The obtained displacements are set to zero in order to obtain the footing displacements due to only the footing applied load. The vertical and horizontal load components are then applied to the footing center. Finally, damping of the soil-footing system was performed until reaching a steady state of static equilibrium. The obtained vertical and horizontal displacements of the footing centre are the footing displacements.

4. ULS deterministic analysis of a circular footing

The aim of this section is to use the deterministic approach for the determination of the most predominant failure mode at ULS (i.e. soil punching or footing sliding) for the different (*H, V*) loading configurations. As will be shown in the following subsection, the determination of the most predominant failure mode for the different loading configurations allows one to distinguish two zones in the (*H, V*) interaction diagram where either soil punching or footing sliding is predominant.

4.1 Failure mode predominance at ULS based on a deterministic approach

Figure (2.2) shows the (*H, V*) interaction diagram. This diagram was computed using the values of the soil parameters given in Table (2.1). Each point of the interaction diagram (except point E) is obtained by first searching a steady state of static equilibrium under the vertical load component *V*. Then, the corresponding horizontal component *H* is computed by searching a steady state of plastic flow using a prescribed horizontal velocity of 10^{-6} m/timestep. Notice that for the point corresponding to the vertical load case (Point E where *V*=5386.61kN and *H*=0kN), only a displacement control method with a vertical velocity of 10^{-6} m/timestep was used to compute the ultimate vertical load. The maximal point of the interaction diagram O' corresponds to (*V*=2660kN, *H*=744.24kN), i.e. to a load inclination α=15.6° with respect to the vertical direction.

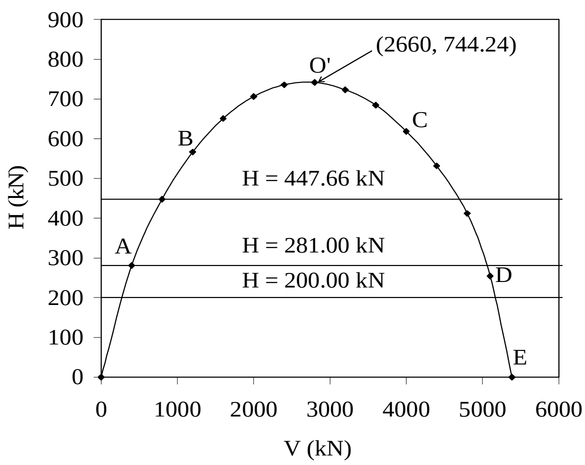

Figure 2.2: Interaction diagram (*H, V*)

The distribution of the maximum shear strain in the soil mass corresponding to different points on the interaction diagram (i.e. points A, B, O', C, D and E) are shown in Figure (2.3). This figure shows that for point A where *V* is small, the footing sliding is the most predominant while the punching mode is negligible. When increasing *V*, the punching mode increases and the sliding mode gradually decreases. For point D where *V* is very large, the soil punching is the most predominant while the footing sliding is negligible. This means that both failure modes co-exist for all loading configurations.

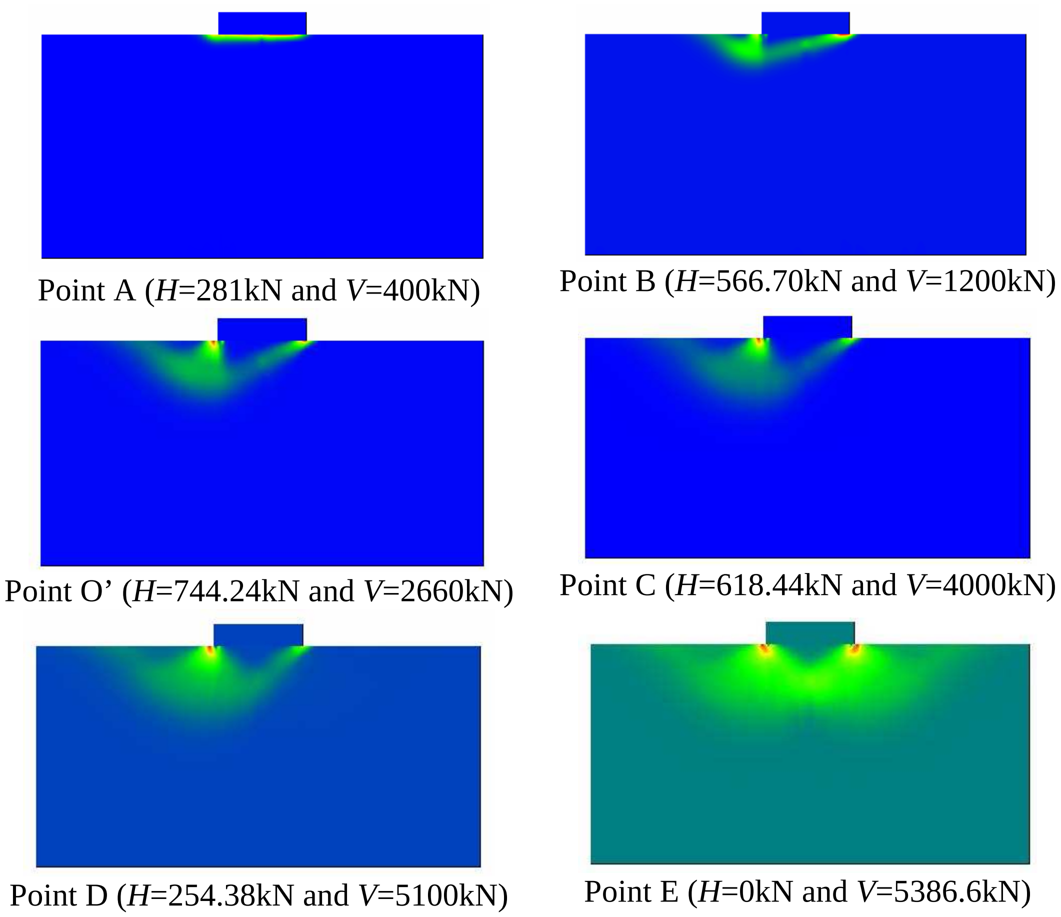

Figure 2.3: Distribution of the maximum shear strain in the soil mass for different load configurations on the interaction diagram.

The values of the safety factor corresponding to all those points (i.e. points A, B, O', C and D) were calculated. Although some points correspond to soil punching predomination and others correspond to footing sliding predomination, a unique value of the safety factor (*F*=1) was found for all these points. Also, the distribution of the maximum shear strain obtained after the computation of *F* was found the same as that obtained in Figure (2.3) when computing the failure loads. This means that the safety factor *F* can consider the simultaneous effect of the two failure modes and it provides a unique safety level whatever the predominant failure mode is.

In order to distinguish the two zones in the interaction diagram where either soil punching or footing sliding is predominant, three constant values of *H* shown in Figure (2.2) were considered to plot the safety factor *F* versus the vertical load component *V* in Figure (2.4). For the three curves shown in this figure, *F* presents a maximum value at points A_1, A_2 and A_3. These points correspond to the same ratio of *H/V* (*H/V*=0.28). This ratio is the same as that corresponding to the load configuration of the maximum point of the interaction diagram (i.e. point O') shown in Figure (2.2). Thus, points A_1, A_2, A_3 and O' belong to a straight line OO' joining the origin and the maximal point of the interaction diagram as may be seen from Figure (2.5). Each point on the line OO' provides a maximum safety factor in comparison with the other loading configurations having the same *H* value.

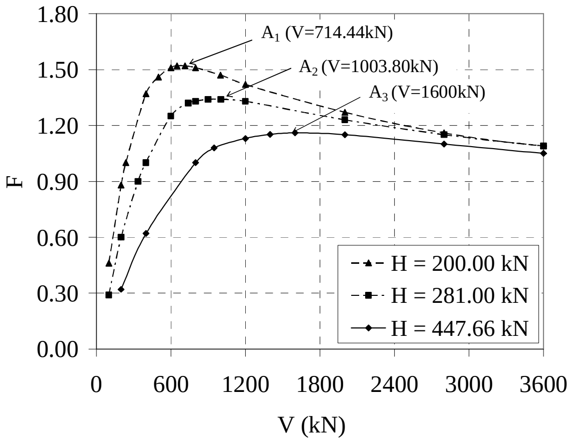

Figure 2.4: Safety factor *F* against vertical load component *V* for three values of the horizontal load component *H*

Some contour lines of the safety factor *F* are plotted in Figure (2.5) using the soil shear strength parameters $c_d=c/F$ and $\varphi_d=tan^{-1}(tan(\varphi)/F)$ for some prescribed values of *F*. It was observed that the maximum points of all these contour lines are located on the line OO' for which, all loading configurations have a ratio of H/V=0.28 [i.e. $\alpha=tan^{-1}(H/V)$ =15.6^o].

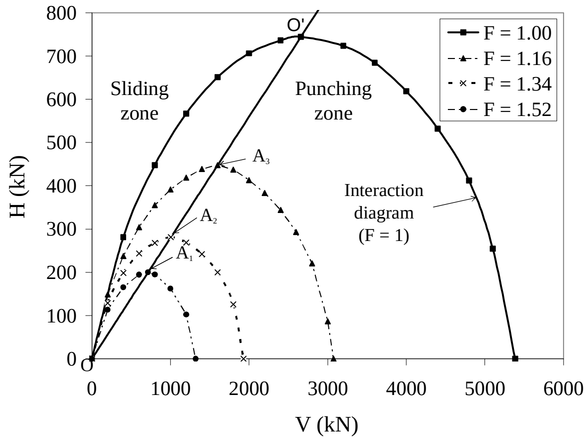

Figure 2.5: Interaction diagram (where F=1) and other contour lines of F

Line OO' can be described as the line that gives the optimal load inclination (i.e. that for which F is maximal for any prescribed value of the horizontal load component). This line may also be seen as the line that divides the (H, V) space into two zones; a zone in the left hand side of this line for which footing sliding is predominant, and another zone in the right hand side of this line for which the soil punching is predominant. This is due to the fact that at high load inclinations (i.e. for small values of V) in Figure (2.4), footing sliding is predominant and the safety factor increases with the vertical load increase. However, at small values of load inclination (i.e. for high values of V), soil punching is predominant and in this zone the safety factor decreases with the vertical load increase. To confirm these observations, the distribution of the maximum shear strain corresponding to three different values of V is plotted in Figure (2.6) for a prescribed value of H (H=447.66kN). As can be easily seen, footing sliding is predominant for small values of V while soil punching is predominant for large values of V. The case of no predominance of neither failure mode corresponds to V=1600kN where α=15.6^o. Finally, it should be emphasized that although the deterministic approach can determine the zones of predominance of the two failure modes at ULS, it is not able to determine the zones of predominance of unsatisfactory performance modes at SLS. Reliability-based approach is necessary in such a case.

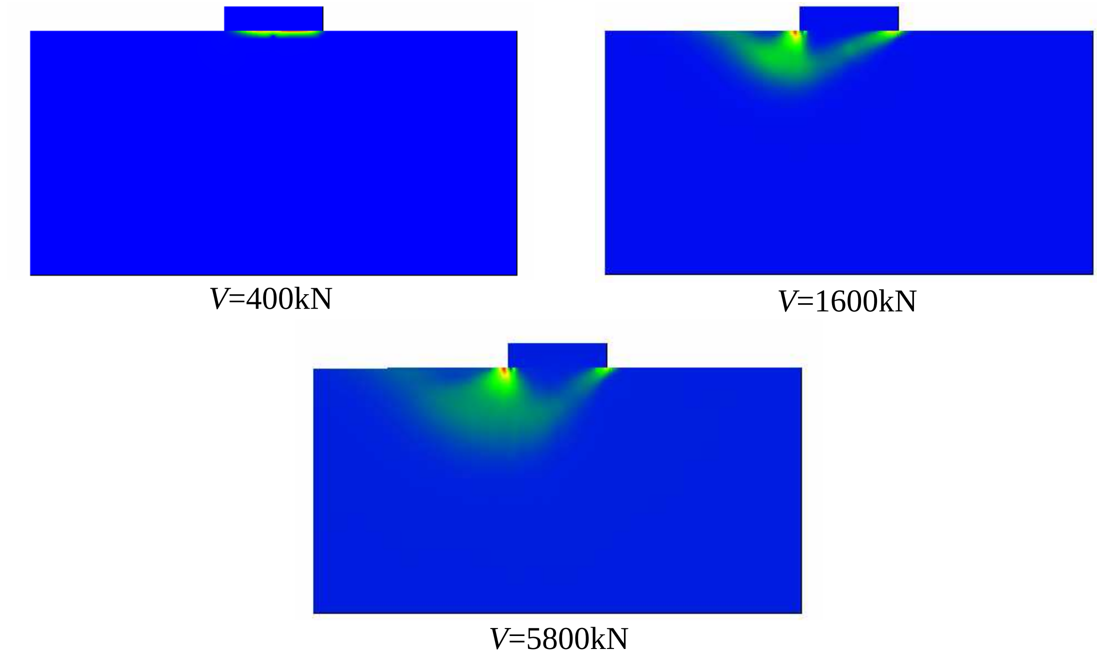

Figure 2.6: Distribution of the maximum shear strain in the soil mass for three values of the vertical load component when H=447.66kN

5. ULS and SLS reliability-based analyses of a circular footing

The determination of the zones of predominance of punching or sliding based on a deterministic analysis does not take into account the uncertainties related to the soil parameters. In this section, these uncertainties were taken into account by using a reliability-based approach. Furthermore, contrary to the deterministic approach which can handle only the ULS analysis, both the ULS and the SLS analyses are considered in the framework of the reliability-based approach. The soil shear strength parameters (c and φ) were considered as random variables at ULS; however, the soil elastic properties (E and ν) were considered as random variables at SLS. This is because the soil shear strength parameters c and φ have no significant effect on the system responses at SLS (i.e. the footing displacements) and the soil elastic parameters E and ν have no significant effect on the system response at ULS (i.e. the safety factor F). The Hasofer-Lind reliability index was adopted for the assessment of the reliability of the soil-footing system. The response surface methodology (RSM) based on the algorithm by Tandjiria *et al.* (2000) was used to compute the reliability index and the corresponding design point. The deterministic models used to calculate the system responses for both ULS and SLS analyses are those described in section 3.

The illustrative values used for the statistical moments of the different random variables are given in Table (2.3). These values correspond to those commonly encountered in practice [Cherrubini *et al.* (1993), Phoon *et al.* (1995) and Phoon and Kulhawy (1999) among others].

Table 2.3: Statistical characteristics of the different random variables

Variable	Mean value	Coefficient of variation (%)	Type of the probability density function (PDF)	
			Case of normal PDF	Case of non-normal PDF
c	20kPa	20	Normal	Log-normal
φ	30^o	10	Normal	Beta
E	60MPa	15	Normal	Log-normal
v	0.3	5	Normal	Log-normal

This table also presents the types of the probability density function (PDF) of the random variables. For each random variable, two PDF types were studied. In the first type referred to as normal PDF; c, φ, E and v were considered as normal variables. In the second type referred to as non-normal PDF; c, E and v were assumed to be log-normally distributed while φ was assumed to be bounded and a beta distribution with lower and upper bounds of 0 and 45^o respectively was adopted for this random variable. Also, both cases of correlated and uncorrelated random variables were examined. In the case of correlated random variables, a negative correlation of ρ=-0.5 was assumed between c and φ at ULS or between E and v at SLS.

After the presentation of some reliability-based results, the determination of the failure mode predominance based on a reliability-based approach will be presented.

5.1. Performance functions, reliability index and failure probability

Footings subjected to an inclined loading may be analysed at ULS as a system consisting of two different failure modes. Typically, these modes are the footing sliding and the soil punching. To calculate the failure probability of such type of footings, two performance functions with two different system responses would be required. This chapter makes use of a unique system response. This is the safety factor F defined with respect to the shear strength parameters c and $tan\varphi$. This factor was previously presented in section 3. Remember that the safety factor F is able to take into account the two failure modes simultaneously and it provides a unique safety level of the soil-footing system. Thus, it avoids the use of two reliability analyses which lead to an approximate value of the system reliability index or the system failure probability. This factor is commonly used in the slope stability analysis. It is the factor by which the available soil shear strength parameters c and $tan\varphi$ have to be reduced to bring the soil to failure. Based on this safety factor, the performance function is given as follows:

$$G_1 = F - 1 \tag{2.4}$$

For the SLS analysis, two performance functions were used. These performance functions are defined with respect to prescribed tolerable vertical and horizontal displacements of the footing centre. They are given by:

$$G_2 = \delta \mathrm{v}_{max} - \delta \mathrm{v} \tag{2.5}$$

$$G_3 = \delta u_{max} - \delta u \tag{2.6}$$

where $\delta \mathrm{v}_{max}$ and δu_{max} are respectively the tolerable vertical and horizontal displacements of the footing center and $\delta \mathrm{v}$ and δu are respectively the footing vertical and horizontal displacements due to the applied load components (V and H).

Remember here that the iterative process of the RSM ends when the absolute difference ε between two successive values of β_{HL} at two successive iterations is less than a prescribed small value (e.g. $\varepsilon<10^{-1}$ in the present chapter). Another criterion can be used to confirm the end of the iterative process of the RSM. This criterion is based on the abovementioned performance functions. Since the design point should be located on the limit state surface G=0, the value of the performance function at this point should be very close to zero. Tables (2.4a, 2.4b and 2.4c) present the successive tentative values of the reliability index and the corresponding design point as obtained at the different iterations of the RSM for the different system responses (i.e. safety factor, vertical displacement and horizontal displacement). These tables also provide the absolute value of the difference between two successive values of the reliability index and the absolute value of the performance function obtained at the different iterations.

For the safety factor F, the criterion (i.e. $\varepsilon<10^{-1}$) was reached after two iterations and the absolute value of G is equal to zero at the second iteration. Thus, only 10 deterministic numerical simulations using FLAC^{3D} were necessary for the computation of the reliability index. However, for the vertical and the horizontal displacements, the convergence criterion of β_{HL} was reached after 4 iterations and the absolute values of the performance functions were very close to zero at the fourth iteration. Thus, 20 calls of the deterministic model were necessary to calculate the reliability index in these cases.

Table 2.4a: Design point (c^*, φ^*), reliability index β_{HL}, convergence criterion ε and absolute values of the performance function at the design point as obtained at the different iterations of a RSM calculation in the case of non-normal correlated variables at ULS (V=1600kN and H=447.66kN)

Iteration	c^*	φ^*	β_{HL}	Convergence criterion ε	F	Absolute value of the performance function $G=F-1$
1	19.7820	25.7716	1.5946	-	0.99	0.01
2	19.3563	25.9493	1.5907	0.0039	1.00	0.00

Table 2.4b: Design point (E^*, v^*), reliability index β_{HL}, convergence criterion ε and absolute values of the performance function at the design point as obtained at the different iterations of a RSM calculation in the case of non-normal correlated variables at SLS (V=1600kN, H=447.66kN and δv_{max}=3cm)

Iteration	E^*x10^6	v^*	β_{HL}	Convergence criterion ε	δv (cm)	Absolute value of the performance function $G = \delta v_{max} - \delta v$
1	47.7605	0.3215	1.6560	-	2.1500	0.8500
2	32.7716	0.3179	4.0866	- 2.4306	3.1734	0.1734
3	34.8298	0.3156	3.6737	0.4129	3.0021	0.0021
4	34.8204	0.3162	3.6640	0.0097	3.0004	0.0004

Table 2.4c: Design point (E^*, v^*), reliability index β_{HL}, convergence criterion ε and absolute values of the performance function at the design point as obtained at the different iterations of a RSM calculation in the case of non-normal correlated variables at SLS (V=1600kN, H=447.66kN and δu_{max}=1.5cm)

Iteration	E^* x 10^6	v^*	β_{HL}	Convergence criterion ε	δu (cm)	Absolute value of the performance function $G = \delta u_{max} - \delta u$
1	39.3299	0.3164	2.7767	-	1.5097	0.0097
2	39.4355	0.3190	2.7423	0.0344	1.4987	0.0013
3	39.5438	0.3184	2.7254	0.0169	1.5033	0.0033
4	39.5428	0.3184	2.7243	0.0011	1.5009	0.0009

5.2. Failure modes predominance at ULS and SLS based on a reliability-based approach

For the ULS analysis, the effect of V on the failure probability P_f was shown in Figure (2.7) for three prescribed values of H. The random variables (c and φ) were considered as non-normal and correlated. In contrast to F which provides a maximum (points A_1, A_2 and A_3 in Figure 2.4), P_f presents a minimum (point B_1, B_2 and B_3 in Figure 2.7). The fact that P_f exhibits a minimum may be explained as follows: For small values of V, the footing sliding is predominant and the failure probability due to this mode is very high. As V increases, the effect of sliding decreases and that of soil punching gradually increases until both modes of failure become non-predominant and induce a minimal simultaneous effect on the failure probability. In this case, the probability of failure presents a minimum value. More increase in V leads to an increasingly failure probability. This is due to a more and more predomination of the punching failure mode; the sliding failure mode becomes negligible in this case. From Figures (2.4) and (2.7), it can be observed that for a given H value, the point of maximum safety factor and that of minimum failure probability correspond exactly to the same load inclination (α=15.6^{o}). This load inclination corresponds to the line OO' in Figure (2.5) obtained using the deterministic approach. This implies that the optimal load inclination leading to a maximal safety factor or a minimal failure probability does not depend on the soil uncertainties.

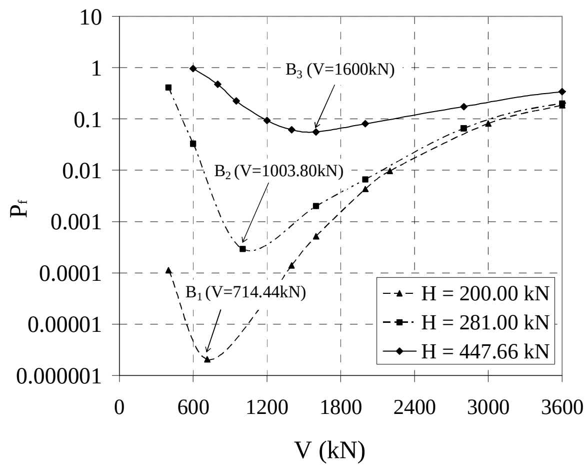

Figure 2.7: Effect of V on the failure probability P_f at ULS

In order to confirm this statement, P_f was plotted versus V for two different configurations of COV_c and COV_φ in Figure (2.8). It can be observed that for both configurations of COV_c and COV_φ, the minimum value of P_f is obtained at the same value of V. This means that the soil uncertainty has no effect on the optimal load configuration for which neither mode of failure is predominant.

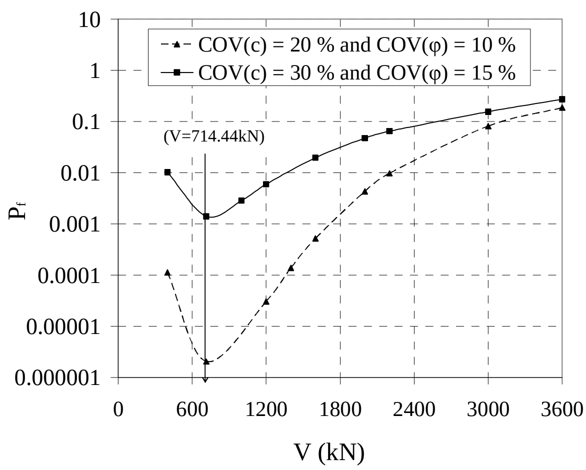

Figure 2.8: Effect of V on the P_f value at ULS for different values of COV_c and COV_φ.

As a conclusion, it can be deduced that at ULS, the optimal load inclination obtained by the deterministic approach is the same as the one obtained using the reliability-based approach which means that the optimal load inclination is independent of the soil variability. The optimal load inclination is the one for which the safety factor is maximum and the failure probability is minimum. It is also the one that separates the two zones of predominance of sliding or punching in the interaction diagram.

Concerning the SLS analysis, Figures (2.9a, 2.9b and 2.9c) present the probability P_e of exceeding a tolerable footing displacement versus the vertical applied load component V for three different values of H. In each figure, three cases are presented: (i) the probability of exceeding a tolerable vertical displacement δv_{max}=3cm, (ii) the probability of exceeding a tolerable horizontal displacement δu_{max}=1.5cm and (iii) the probability of exceeding both tolerable displacements of δv_{max}=3cm and δu_{max}=1.5cm using the equations of the system failure probability presented in Ang and Tang (1975). These equations are given in Appendix C. The random variables (E and v) were considered non-normal and uncorrelated. Figure (2.9) and Table (2.5) indicate that, for the results corresponding to the tolerable horizontal displacement, P_e presents a minimum value. This is because, at small V values, the horizontal movement of the footing is predominant. This leads to a high P_e value. As V increases, the horizontal movement decreases because of the increase in the shearing resistance at the soil-footing interface. This leads to a gradual decrease in P_e. When punching begins to predominate, one obtains an increase in P_e due to an increase in the horizontal footing displacement. For the curves of Figure (2.9) corresponding to the vertical footing displacement, P_e continuously increases with the increase of V. This is due to the increase in the vertical displacement.

The P_e values for the three cases mentioned above (i.e. probability of exceeding δv_{max}, probability of exceeding δu_{max} and the probability of exceeding both δv_{max} and δv_{max}) when H=447.66kN are provided in Table (2.5). From this table, it can be noticed that the system probability is equal to the largest probability component when the mode of exceeding δu_{max} is predominant (i.e. when V≤1600kN). It becomes larger than both components when both unsatisfactory performance modes contribute to P_e (i.e. when V >1600kN).

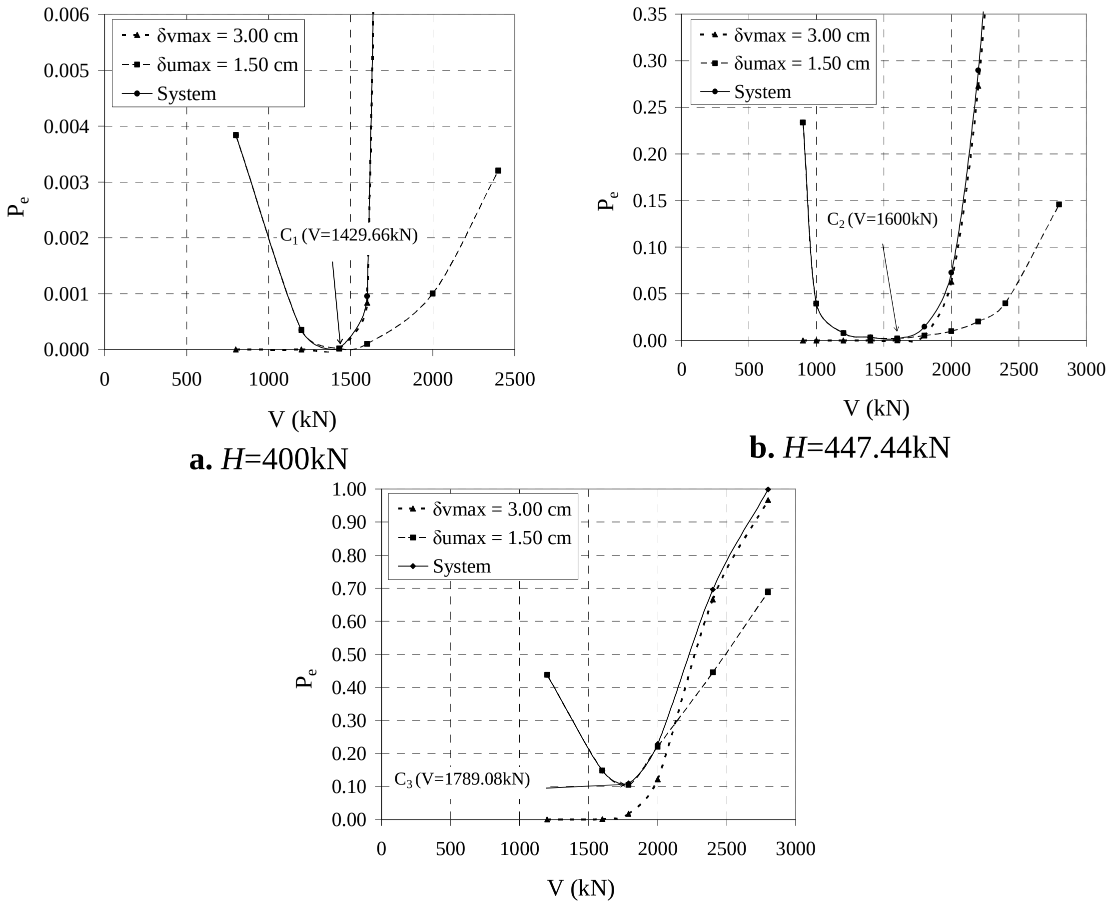

a. H=400kN

b. H=447.44kN

c. H=500kN

Figure 2.9: Effect of V on the probability P_e of exceeding tolerable vertical and horizontal displacements at SLS

It should be emphasized here that the minimum value of the system probability at SLS corresponds exactly to the same load inclination (α=15.6^o) for which the safety factor presents a maximum and the failure probability presents a minimum at ULS. This means that the load inclination which provides the minimum failure probability at ULS leads to the smallest possible movement of the foundation at SLS. It can be concluded that line

OO' (Figure 2.5) which separates the zones of predominance at ULS can also be used at SLS to distinguish the load configurations that lead to a predomination of the horizontal or the vertical footing movement. Finally, it should be emphasized that the zone of predominance of a given failure mode does not mean that the failure probability in this zone is only due to this mode. It simply means that the failure probability in this zone is mostly due to this mode and the contribution of the other mode is less significant.

Table 2.5: Effect of V on (i) probability of exceeding δv_{max}, (ii) probability of exceeding δu_{max} and (iii) system probability at SLS (H=447.66kN)

V (kN)	Probability of exceeding δv_{max} (%)	Probability of exceeding δu_{max} (%)	System probability (%)
900	$1.71\text{x}10^{-20}$	23.38	23.38
1000	$3.29\text{x}10^{-15}$	3.96	3.96
1200	$6.10\text{x}10^{-09}$	0.79	0.79
1400	$3.09\text{x}10^{-05}$	0.32	0.32
1600	0.12	0.22	0.22
1800	0.53	0.53	1.47
2000	6.29	1.01	7.28
2200	27.28	2.04	28.96
2400	63.57	4.00	64.90
2600	87.12	8.32	88.19
2800	97.12	14.57	98.13

6. Reliability-based parametric study

This section aims at investigating the effect of the load inclination α and the statistical characteristics of the soil shear strength parameters (distribution type, coefficient of variation and correlation between random variables) on the variability of the ultimate bearing capacity.

6.1. Effect of the load inclination α on the variability of the ultimate bearing capacity

Figure (2.10) shows the CDF of the ultimate bearing capacity of both vertically (α=0) and obliquely (α>0) loaded footings. The random variables (c and φ) were assumed non-normal and correlated. Figure (2.10) indicates that the variability of the ultimate bearing capacity is significant in the vertical load case (i.e. when α=0^o) where the CDF is more spread out with respect to the inclined load cases. To explain this observation, one should refer to the failure mechanisms shown in Figure (2.3). It can be observed that the size of the failure mechanism is small in the case of small values of *V* (i.e. for high load inclinations) where the footing sliding is predominant. However, its size increases with the increase of *V* (i.e. for small load inclinations) where the soil punching is predominant. The size of the failure mechanism is maximal in the vertical load case (i.e. point *E* of Figure 2.2 where *H*=0). As expected, the ultimate bearing capacity increases with the size of the failure mechanism. Therefore, when the failure mechanism is small (i.e. for an inclined load case), the variation of *c* and *φ* does not have a significant effect on the ultimate bearing capacity. However, when this mechanism is large (i.e. for a vertical load case), a small variation in *c* and *φ* results in a significant effect on the ultimate bearing capacity. Another alternative explanation may also be provided as follows: since the system response considered in this section is the ultimate bearing capacity which is intimately related to the punching failure mode, it would be expected to obtain the maximal variability when the soil punching is the most predominant (i.e. when the footing load is vertical).

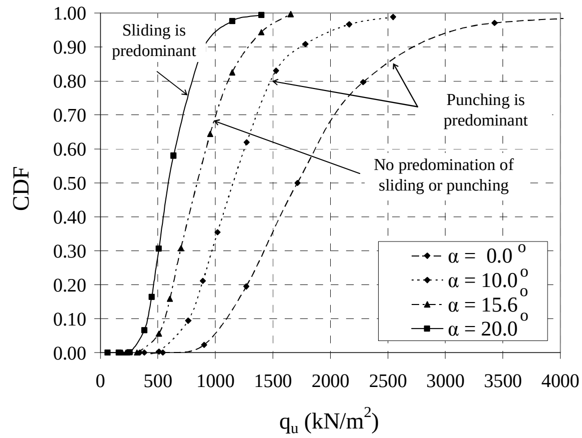

Figure 2.10: CDF of the ultimate bearing capacity q_u for different values of the load inclination α

6.2. Effect of the distribution type and the correlation between random variables on the variability of the ultimate bearing capacity

The aim of this section is to investigate the effect of the type of the PDF and the correlation between the shear strength parameters on the variability of the ultimate bearing capacity. This study was carried out when α=0 (i.e. for a vertically loaded circular footing). Both assumptions of normal and non-normal random variables were studied. Also, both correlated and uncorrelated random variables were considered in the analysis. Figure (2.11) shows that the negative correlation between the soil shear strength parameters decreases the variability of the ultimate bearing capacity (since one obtains a less spread out CDF) while the assumption of non-normal random variables very slightly decreases the variability of the ultimate bearing capacity. As a conclusion, these results indicate that the case of normal uncorrelated random variables is conservative since it provides the largest variability of the ultimate bearing capacity.

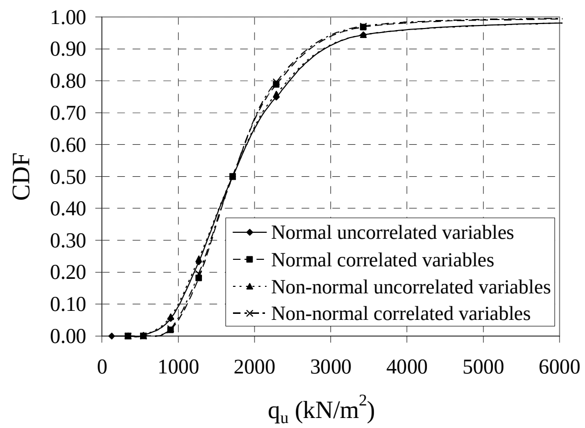

Figure 2.11: CDF of the ultimate bearing capacity q_u for different assumptions on the PDF type and the correlation when $\alpha=0^o$

6.3. Effect of the coefficient of variation of the shear strength parameters on the variability of the ultimate bearing capacity

The effect of the coefficients of variation of c and φ on the ultimate bearing capacity was investigated in Figure (2.12). The random variables were considered non-normal and correlated. This study indicates that the variability of the ultimate bearing capacity is more sensitive to the variation in the internal friction angle than to the variation in the soil cohesion. This can be easily observed from Figure (2.12) where the increase in the dispersion of the CDF of the ultimate bearing capacity due to an increase in COV_φ by 50% is larger than that due to an increase in COV_c by 100%. This reflects the important role of the angle of internal friction in the determination of the ultimate bearing capacity and consequently in footing design. Therefore, care should be taken on the rigorous determination of COV_φ in practice.

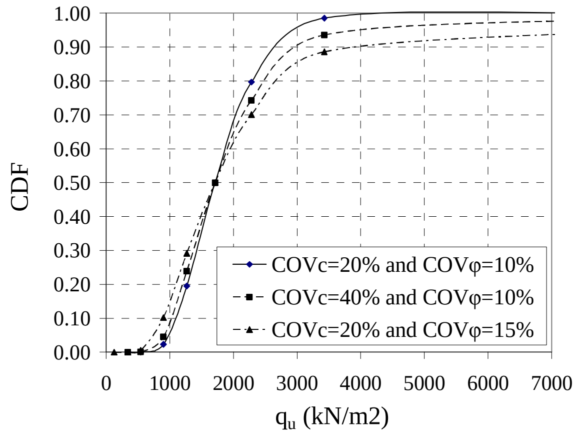

Figure 2.12: CDF of the ultimate bearing capacity q_u for different values of the coefficients of variation of the random variables when α=0°

7. Conclusion

This chapter presents a deterministic analysis at ULS and a reliability-based analysis at both ULS and SLS of a circular footing resting on a (c, φ) soil and subjected to an inclined load. Two modes of failure (soil punching and footing sliding) were considered at ULS. Also, two modes of unsatisfactory performance (exceeding of prescribed tolerable vertical and horizontal displacements of the foundation) were considered at SLS. The safety factor F defined with respect to the soil shear strength parameters c and $tan\varphi$ was used to represent the system response at ULS. On the other hand, two system responses were used at SLS. These are the footing horizontal and vertical displacements. The deterministic models used to calculate the system responses are based on 3D numerical simulations using the Lagrangian explicit finite difference code FLAC^{3D}. The soil shear strength parameters *c* and *φ* were modeled by random variables at ULS while the soil elastic properties *E* and *ν* were modeled by random variables at SLS. Hasofer-Lind reliability index was used for the computation of the reliability of the soil-footing system. The response surface methodology was used to find an approximation of the system response and the reliability index. FORM approximation was used for the computation of the failure probability.

In this chapter, the zones of predominance of the different modes at both ULS and SLS were determined. Notice that the zone of predominance of a given failure mode means that the failure probability in this zone is mostly due to this mode; however, the contribution of the other mode is less significant. The main findings of this chapter can be summarized as follows:

1- For the ULS analysis

1. The safety factor *F* defined with respect to the soil shear strength parameters *c* and *tanφ* considers the combined effect of both failure modes (soil punching and footing sliding). Notice that both failure modes co-exist whatever the loading configuration is. The safety factor *F* provides a unique and rigorous safety level of the soil-footing system. The use of this factor has the advantage of seeking the most predominant mode of failure using a deterministic approach.
2. There are several optimal loading configurations in the interaction diagram. These configurations correspond to a unique optimal load inclination and they subdivide the interaction diagram into two zones of predominance where either soil punching or footing sliding is predominant. The optimal load inclination is that for which (i) the load configurations do not exhibit predominance of neither soil punching nor footing sliding and (iii) the safety factor is maximum and the failure probability is

minimum with respect to all other load configurations having the same value of the horizontal load component.

3. The optimal loading configurations obtained by using the deterministic approach were found similar to those obtained by using the reliability-based approach. This means that the optimal load inclination does not depend on the uncertainties of the soil parameters. The optimal loading configurations are situated on the line joining the origin and the extremum of the interaction diagram.

2- For the SLS analysis

a) Contrary to the ULS analysis, the deterministic approach was not able to determine the optimal load inclination for which neither vertical nor horizontal movement is predominant at SLS. The reliability-based approach was necessary in this case. The reliability-based analysis has shown that the optimal load inclination at SLS corresponds exactly to the one obtained at ULS. This corresponds to the minimum movement of the footing center.

3- The parametric study has shown that:

a) The variability of the ultimate bearing capacity is significant for the vertical load case where only the punching failure mode is present. It becomes smaller in the inclined load case where the sliding mode is predominant.

b) The negative correlation between the shear strength parameters decreases the variability of the ultimate bearing capacity; however, the non-normality of these variables does not significantly affect this variability.

c) The variability of the ultimate bearing capacity is more sensitive to the variation of φ than that of c.

CHAPTER 3

PROBABILISTIC ANALYSIS OF OBLIQUELY LOADED FOOTINGS USING THE COLLOCATION-BASED STOCHASTIC RESPONSE SURFACE METHOD (CSRSM)

1. Introduction

In the previous chapter, the reliability-based analysis was performed using the Response Surface Method (RSM). This method is based on the approximation of the system response by a polynomial of a prescribed order. It should be emphasized here that the RSM does not provide a precise approximation of the system response except in the proximity of the design point. Thus, the RSM can be used to calculate only the reliability index and the corresponding design point for a given threshold of the system response. In the present chapter, a more efficient method called Collocation-based Stochastic Response Surface Method (CSRSM) is used. The CSRSM is based on the approximation of the system response by a polynomial chaos expansion (PCE) over a more extended zone with respect to the RSM. This method replaces the complex finite element or finite difference model by a meta-model (i.e. an analytical equation) which can be easily handled in the probabilistic analysis. It should be noticed here that the CSRSM provides a rigorous approximation of the system response in the central zone (i.e. around the mean value) if a low order PCE is used. For the remaining zones of the response surface, the approximation can be improved by increasing the PCE order. Contrary to the RSM which provides only the reliability index and the corresponding design point for a given threshold of the system response, the CSRSM allows the computation of additional probabilistic outputs. Indeed, the CSRSM permits the computation of (i) the PDF of the system response and (ii) the failure probability (for different thresholds of the system response) by applying Monte Carlo Simulation (MCS) methodology on the meta-model. Moreover, the CSRSM provides other important probabilistic outputs. These are the PCE-based Sobol indices. The PCE-based Sobol indices quantify the contribution of each random variable in the variability of the system response.

The present chapter makes use of the CSRSM to present a probabilistic analysis at both ULS and SLS of the same circular footing and the same soil characteristics studied in chapter 2. Similar to chapter 2, the system response considered at ULS is the safety factor F defined with respect to the soil shear strength parameters c and $tan\varphi$. At SLS, two system responses are used. These are the footing vertical and horizontal displacements (δv and δu). The performance functions used to calculate the failure probability are those presented in chapter 2. Also, the deterministic models used to calculate the system responses are the same models presented in chapter 2. It should be mentioned that contrary to chapter 2 in which only the uncertainties of the soil parameters were considered in the analysis; in the present chapter, the uncertainties of both the soil parameters and the load components (H and V) are taken into account at both ULS and SLS. The random variables considered at ULS are c, φ, H and V. However, the random variables considered at SLS are E, ν, H and V.

This chapter aims at presenting a global sensitivity analysis to determine the contribution of the different random variables in the variability of the system responses using the PCE-based Sobol indices. It also aims at determining the zones of predominance in the interaction diagram at both ULS and SLS taking into account the simultaneous effect of the soil and loading uncertainties. The importance of the determination of these zones arises from the fact that the variability of a given system response depends on the position of the corresponding load configuration in the interaction diagram. Finally, this chapter aims at presenting a parametric study to investigate the sensitivity of the PDFs of the different system responses to the different statistical parameters of the random variables.

This chapter is organized as follows: The Collocation-based Stochastic Response Surface Method (CSRSM) is first presented. Then, the probabilistic results are presented and discussed. The chapter ends with a conclusion of the main findings.

2. Collocation-based Stochastic Response Surface Method (CSRSM)

The basic idea of the CSRSM is to approximate a given system response by a polynomial chaos expansion (PCE) of a suitable order. In other words, the CSRSM replaces the complex numerical model by a meta-model. In order to achieve this purpose, all the uncertain parameters (which may have different PDFs) should be represented by a unique chosen PDF. Table (3.1) presents the usual PDFs and their corresponding families of orthogonal polynomials (Xiu and Karniadakis 2002).

Table 3.1: Usual probability density functions and their corresponding families of orthogonal polynomials

probability density functions	Polynomials
Gaussian	Hermite
Gamma	Laguerre
Beta	Jacobi
Uniform	Legendre

Within the framework of the CSRSM, the response of a system that involves n random variables can be expressed by a PCE as follows:

$$\Gamma_{PCE}=\sum_{i=0}^{\infty} a_i \psi_i(\xi) \approx \sum_{i=0}^{P-1} a_i \psi_i(\xi) = a_0\psi_0 + \sum_{i_1=1}^{n} a_{i_1}\psi_1\left(\xi_{i_1}\right) + \sum_{i_1=1}^{n}\sum_{i_2=1}^{i_1} a_{i_1 i_2}\psi_2\left(\xi_{i_1},\xi_{i_2}\right) + \sum_{i_1=1}^{n}\sum_{i_2=1}^{i_1}\sum_{i_3=1}^{i_2} a_{i_1 i_2 i_3}\psi_3\left(\xi_{i_1},\xi_{i_2},\xi_{i_3}\right) + \ldots \qquad (3.1)$$

where $\psi_i(\xi)$ are multi-dimensional polynomials defined as the product of one-dimensional polynomials, $\left(\xi_{i_1},\xi_{i_2},\xi_{i_3},\ldots\right)$ are independent random variables, $\left(a_0, a_{i_1}, a_{i_1 i_2}, a_{i_1 i_2 i_3},\ldots\right)$ are unknown coefficients to be evaluated and P is the size of the PCE.

The size P of the PCE (which is equal to the number of the unknown PCE coefficients) depends on the number n of random variables and the order p of the PCE. It is given as follows:

$$P = \frac{(n+p)!}{n!\ p!} \tag{3.2}$$

It should be mentioned here that in this chapter, the random variables are represented in the independent standard normal space. Thus, the suitable corresponding bases are the multidimensional Hermite polynomials as may be seen from Table (3.1). The expressions of the multi-dimensional Hermite polynomials are given as follows:

$$\psi_\alpha = \prod_{i=1}^{n} \phi_{\alpha_i}(\xi_i), \qquad \alpha_i \geq 0 \tag{3.3}$$

where $\alpha=[\alpha_1, \ldots, \alpha_n]$ is a sequence of n non-negative integers and $\phi_{\alpha_i}(\xi_i)$ are one-dimensional Hermite polynomials. More details on the one-dimensional and multidimensional Hermite polynomials are given in Appendix D.

For the determination of the PCE unknown coefficients, a non-intrusive technique (in which the deterministic model is treated as a black-box) is used. Two non-intrusive approaches have been proposed in literature: these are the projection and the regression approaches. In this thesis, the regression approach is used. In this approach, it is required to compute the system response at a set of collocation points in order to perform a fit of the PCE using the obtained system response values.

As suggested by several authors [Isukapalli *et al.* (1998), Phoon and Huang (2007) and Huang *et al.* (2009)], the collocation points can be chosen as the result of all possible combinations of the roots of the one-dimensional Hermite polynomial of order $(p+1)$ for each random variable. For example, if a PCE of order $p=2$ is used to approximate the response surface of a system with $n=2$ random variables, the roots of the one-dimensional Hermite Polynomial of order 3 are chosen for each random variable. These roots are ($-\sqrt{3}$, 0, $\sqrt{3}$) for the first random variable and ($-\sqrt{3}$, 0, $\sqrt{3}$) for the second random variable. In this case, 9 collocation points are available. These collocation points are ($-\sqrt{3}$, $-\sqrt{3}$), ($-\sqrt{3}$, 0), (-

√3, √3), (0, -√3), (0, 0), (0, √3), (√3, -√3), (√3, 0), (√3, √3). In the general case, for a PCE of order p and for n random variables, the number N of the available collocation points can be obtained using the following formula:

$$N=(p+1)^n \tag{3.4}$$

Referring to Equations (3.2 and 3.4), one can observe that the number of the available collocation points is higher than the number of the unknown coefficients. This leads to a linear system of equations whose number N of equations is greater than the number P of the unknown coefficients. The regression approach is used to solve this system. This approach is based on a least square minimization between the exact solution Γ and the approximate solution Γ_{PCE} which is based on the PCE. Accordingly, the unknown coefficients of the PCE can be computed using the following equation:

$$\boldsymbol{a} = (\boldsymbol{\Psi}^T \boldsymbol{\Psi})^{-1}.\ \boldsymbol{\Psi}^T.\ \boldsymbol{\Gamma} \tag{3.5}$$

in which $\boldsymbol{a}$ is a vector containing the PCE coefficients, $\boldsymbol{\Gamma}$ is a vector containing the system response values as calculated by the deterministic model at the different collocation points and $\boldsymbol{\Psi}$ is a matrix of size NxP whose elements are the multivariate Hermite polynomials. It is given as follows:

$$\boldsymbol{\Psi} = \begin{bmatrix} \psi_0^1(\xi) & \psi_1^1(\xi) & \psi_2^1(\xi) & \ldots\ldots\ldots\ldots\ldots \psi_{P-1}^1(\xi) \\ \psi_0^2(\xi) & \psi_1^2(\xi) & \psi_2^2(\xi) & \ldots\ldots\ldots\ldots\ldots \psi_{P-1}^2(\xi) \\ \vdots & \vdots & \vdots & \vdots \\ \vdots & \vdots & \vdots & \vdots \\ \psi_0^N(\xi) & \psi_1^N(\xi) & \psi_2^N(\xi) & \ldots\ldots\ldots\ldots\ldots \psi_{P-1}^N(\xi) \end{bmatrix} \tag{3.6}$$

Notice that in order to calculate the system response corresponding to a given collocation point, the standard normal random variables ξ_i should be expressed in the original physical space of random variables as follows:

$$x_i = F_{x_i}^{-1}\left[\Phi(\xi_i)\right] \tag{3.7}$$

in which, x_i is a physical random variable, F_{xi} is the CDF of the physical random variable and Φ is the CDF of the standard normal random variable. Notice also that if the original physical random variables are correlated, the standard normal random variables should first be correlated using the following equation:

$$\begin{bmatrix} \xi_{1c} \\ \xi_{2c} \\ . \\ . \\ . \\ \xi_{nc} \end{bmatrix} = H . \begin{bmatrix} \xi_1 \\ \xi_2 \\ . \\ . \\ . \\ \xi_n \end{bmatrix} \tag{3.8}$$

in which $\{\xi_{1c}, \xi_{2c}, ..., \xi_{nc}\}$ is the vector of correlated standard normal random variables, $\{\xi_1, \xi_2, ..., \xi_n\}$ is the vector of uncorrelated standard normal random variables and H is the Choloesky transformation of the correlation matrix of the physical random variables.

Once the PCE coefficients are determined, MCS can be applied on the obtained PCE (called meta-model) to compute both the PDF of the system response and the failure probability for different thresholds of this response. This is achieved by (i) generating a large number of realizations of the vector $(\xi_1, \xi_2, \ldots \xi_n)$ of standard normal random variables and (ii) calculating the system response corresponding to each realization by substituting the vector $(\xi_1, \xi_2, \ldots \xi_n)$ in the meta-model. It should be mentioned here that the failure probability is calculated as the ratio between the number of realizations $(\xi_1, \xi_2, \ldots \xi_n)$ for which $G \leq 0$ and the total number of realizations.

2.1. Optimal number of collocation points

As mentioned before, the number of the available collocation points significantly increases with the increase in the number of random variables and becomes very large with respect to the number of the unknown PCE coefficients. This makes it necessary to determine the optimal number of collocation points which is needed by the regression approach to solve the linear system of equations (Equation 3.5). In this regard, several empirical formulas were proposed in literature. Webster *et al.* (1996) selected a number $J=P+1$ (that are the most close to the origin of the standard space of random variables) among the N available collocation points. Isukapalli *et al.* (1998) proposed to select $J=2P$. Berveiller *et al.* (2006) suggested the use of a number J given by $J=(n-1)P$. Recently, Li *et al.* (2011) have proposed to consider different numbers of collocation points ($2P$, $3P$, $4P$, etc.). For each number of collocation points, they calculated the rank of the information matrix A where $A=(\boldsymbol{\Psi}^T \boldsymbol{\Psi})$. It was found that when the rank of the information matrix is larger than the number of the unknown coefficients (i.e. the matrix A is invertible), there is a good agreement with the results obtained when applying MCS methodology on the original deterministic model. The procedure by Li *et al.* (2011) is somewhat similar to that proposed by Sudret (2008) because both procedures are based on the concept of matrix invertibility. Notice however that the approach by Sudret (2008) leads to a smaller number of collocation points. This is because this author proposed to successively increase the information matrix A until it becomes invertible as follows: (a) the N available collocation points are ordered in a list according to increasing norm, (b) the information matrix A is constructed using the first P collocation points of the ordered list, i.e. the P collocation points that are the closest ones to the origin of the standard space of random variables and finally (c) this matrix is successively increased (by adding each time the next collocation point from the ordered list) until it becomes invertible. The different available approaches to select the necessary number of collocation points among the available ones were tested in this chapter. The approach by Sudret (2008) was found the most efficient to determine the optimal number of collocation points as will be seen later in this chapter.

2.2. Error estimates of the PCE

For a given PCE order, the accuracy of the approximation of the system response by a PCE can be measured by the error estimate. Two types of error estimates exist in literature. These are the coefficient of determination R^2 and the *leave-one-out* error Q^2 (Blatman and Sudret 2010).

Let us consider J realizations $\left\{ \xi^{(1)} = \left(\xi_1^{(1)},\ \ldots,\ \xi_n^{(1)}\right), \ldots, \xi^{(J)} = \left(\xi_1^{(J)},\ \ldots,\ \xi_n^{(J)}\right) \right\}$ of the standard normal random vector ξ, and let $\Gamma = \left\{ \Gamma\left(\xi^{(1)}\right),\ \ldots,\ \Gamma\left(\xi^{(J)}\right) \right\}$ be the corresponding values of the system response determined by deterministic calculations. The coefficient of determination R^2 is calculated as follows:

$$R^2 = 1 - \Delta_{PCE} \tag{3.9}$$

where Δ_{PCE} is given by:

$$\Delta_{PCE} = \frac{(1/J)\sum_{i=1}^{J}\left[\Gamma\left(\xi^{(i)}\right) - \Gamma_{PCE}\left(\xi^{(i)}\right)\right]^2}{Var(\Gamma)} \tag{3.10}$$

and

$$Var(\Gamma) = \frac{1}{J-1}\sum_{i=1}^{J}\left[\Gamma\left(\xi^{(i)}\right) - \bar{\Gamma}\right]^2 \tag{3.11}$$

$$\bar{\Gamma} = \frac{1}{J}\sum_{i=1}^{J}\Gamma\left(\xi^{(i)}\right) \tag{3.12}$$

Remember here that J is the number of collocation points used to evaluate the unknown coefficients of the PCE. The value $R^2 = 1$ indicates a perfect approximation of the true system response Γ, whereas $R^2 = 0$ indicates a nonlinear relationship between the true model Γ and the PCE model Γ_{PCE}.

The coefficient of determination R^2 may be a biased estimate since it does not take into account the robustness of the meta-model (i.e. its capability of correctly predicting the model response at any point which does not belong to the collocation points. As a consequence, a more reliable and rigorous error estimate, called the *leave-one-out* error estimate, was proposed by Blatman and Sudret (2010). This error estimate consists in sequentially removing a point from the J collocation points. Let $\Gamma_{\xi/i}$ be the meta-model that has been built from *(J-1)* collocation points after removing the i^{th} observation from these collocation points and let $\Delta^{i} = \Gamma(\xi^{(i)}) - \Gamma_{\xi/i}(\xi^{(i)})$ be the predicted residual between the model evaluation at point $\xi^{(i)}$ and its prediction at the same point based on $\Gamma_{\xi/i}$. The empirical error is thus given as follows:

$$\Delta^{*}_{PCE} = \frac{1}{J}\sum_{i=1}^{J}(\Delta^{i})^{2} \tag{3.13}$$

The corresponding error estimate is often denoted by Q^2 and is called *leave-one-out* error estimate. It is given as follows:

$$Q^{2} = 1 - \frac{\Delta^{*}_{PCE}}{Var(\Gamma)} \tag{3.14}$$

2.3. PCE-based Sobol indices

A Sobol index of a given input random variable is a measure by which the contribution of this input random variable to the variability of the system response can be determined. Sobol indices are generally calculated by MCS methodology (Sobol 2001). This method is very time-expensive especially when dealing with a large number of random variables. Sudret (2008) proposed an efficient approach to calculate the Sobol indices based on the coefficients of the PCE. This method is based on ranking the different terms of the PCE and gathering them into groups where each group contains only one random variable or a combination of random variables. The Sobol indices can then be calculated using the following equation:

$$SU_\alpha = \frac{\sum a_\alpha^2.E(\psi_\alpha^2)}{\sigma^2} \tag{3.15}$$

in which, α indicates that the summation is carried out for the PCE terms that contain a single random variable or a combination of random variables and σ^2 is the total variance of the system response. It is given as follows:

$$\sigma^2 = \sum_{i=1}^{P-1} a_i^2.E(\psi_i^2) \tag{3.16}$$

Some derivations related to the expressions of Sobol indices are presented in Appendix E. For more details, one can refer to Sudret (2008) and Mollon *et al.* (2011).

3. Probabilistic numerical results

This section presents the probabilistic results for the ULS and SLS analyses. It provides (i) a global sensitivity analysis using the PCE-based Sobol indices, (ii) the zones of predominance of the different failure modes in the interaction diagram and (iii) a parametric study showing the effect of the statistical characteristics of the random variables on the PDFs of the different system responses. Remember that the random variables considered at ULS are c, φ, H and V. However, the random variables considered at SLS are E, ν, H and V. The illustrative values used for the statistical characteristics of the different random variables are presented in Table (3.2). These values will be referred to hereafter as the reference values.

Table 3.2: Statistical characteristics of the different random variables

Variable	Mean value	Coefficient of variation (%)	Type of the probability density function (PDF)	
			Case of normal PDF	Case of non-normal PDF
c	20kPa	20	Normal	Log-normal
φ	30^o	10	Normal	Beta
E	60MPa	15	Normal	Log-normal
ν	0.3	5	Normal	Log-normal
H	200	40	Normal	Log-normal
V	714	10	Normal	Log-normal

Notice that a high value of the coefficient of variation of 40% was proposed for the horizontal load component *H* to represent the large uncertainties due to the wind and/or the wave loading. This value is to be compared to the value of 10% affected to the coefficient of variation of the footing vertical load component *V*. This is because *V* represents the structure weight for which the variability is small.

In this chapter, three load configurations represented by points M (*V=500kN* and *H=200kN*), N (*V=714kN* and *H=200kN*) and L (*V=3500kN* and *H=200kN*) in the interaction diagram (Figure 3.1) were considered in the following probabilistic analyses.

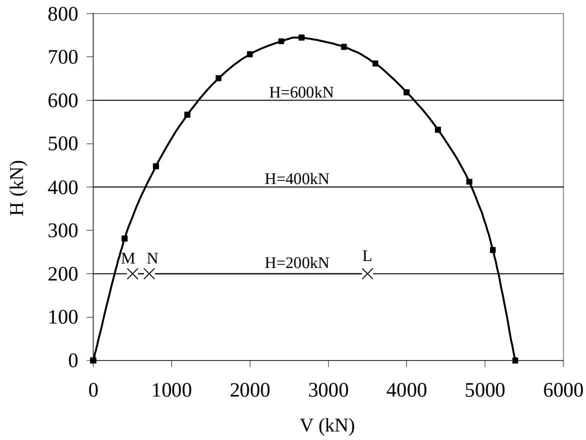

Figure 3.1: Interaction diagram

Before performing the probabilistic analysis using the CSRSM, the optimal order *p* of the PCE should be determined.

- If only the statistical moments of a given system response are sought, the PCE order is successively increased until (i) the coefficient of determination Q^2 becomes greater than a prescribed value (say 0.999) and (ii) the statistical moments converge to constant values.
- If the failure probability (by applying MCS on the meta-model) is sought, the PCE order is successively increased until (i) the coefficient of determination Q^2 becomes greater than a prescribed value (say 0.999) and (ii) the failure probability P_f converges to a constant value.

For all the subsequent ULS and SLS probabilistic analyses performed in this chapter, a third order PCE was found necessary to provide a good approximation of the system response.

It should be mentioned here that due to the large variability of the horizontal load component H, certain collocation points (among the available ones) involve a horizontal load component $H>H_u$. As a result, the system responses at SLS (i.e. footing horizontal and vertical displacements) cannot be calculated for these points. To overcome this issue, these points were removed from the list of the available collocation points. Then, the concept of matrix invertibility proposed by Sudret (2008) was applied on the remaining collocation points.

To check the efficiency of the concept of matrix invertibility proposed by Sudret (2008), a comparison between the statistical moments of the safety factor F obtained using this concept (where N=66 points) and those obtained using all the available collocation points (where N=257 points) was performed and presented in Table (3.3).

Table 3.3: Effect of the number of collocation points as suggested by different authors on the statistical moments of the safety factor

Number of collocation points	Mean value	Standard deviation	Coefficient of variation (%)	Skewness	Kurtosis
N=257 points (All available points including the origin)	1.492	0.255	17.090	0.287	0.062
N=36 points (Webster et al. 1996)	1.559	80.758	51.801	0.922	32.075
N=70 points (Isukapalli et al. 1998)	1.496	0.255	17.045	0.283	0.085
N=70 points (Li et al. 2011)	1.496	0.255	17.045	0.283	0.085
N=105 points (Berveiller *et al.* 2006)	1.487	0.253	17.014	0.277	0.073
N=66 points (Sudret 2008)	1.496	0.255	17.045	0.298	0.108

From this table, one can see that there is a good agreement with a significant reduction in the number of calls of the deterministic model (by 74.3%). The statistical moments corresponding to the different numbers of collocation points proposed empirically by the different authors are also given in this table. While some authors [Isukapalli *et al.* (1998) and Li *et al.* (2011)] provide good results, others (Webster *et al.* 1996) are unable to predict the system response. On the other hand, Berveiller et al. (2006) overestimate the number of collocation points by about 60%. As a conclusion, the rational approach proposed by Sudret (2008) will be employed for all subsequent probabilistic calculations.

3.1. Global sensitivity analysis *via* the PCE-based Sobol indices

As mentioned previously, the Sobol indices quantify the contribution of each random variable in the variability of the system response. This is of great importance because these indices help the engineer to identify the input uncertain parameters that have the greatest contribution in the variability of the system response. Moreover, they allow one to consider as deterministic the random variables that have a small contribution in the variability of the system response. This leads to a reduced computation time of the probabilistic analysis.

Table (3.4) presents the Sobol indices of the different input random variables at ULS for points M, N and L shown in Figure (3.1). For point M, one can see that the Sobol index of the horizontal load component *H* is significant (it involves more than 3/4 of the variability of the safety factor). On the contrary, the Sobol index of the vertical load component *V* is negligible. Thus, *H* has the greatest contribution in the variability of the safety factor while *V* has a negligible contribution in this variability. This may be explained by (i) the high variability of *H* and (ii) the predominance of the sliding failure mode with respect to the punching mode due to the high load inclination. Concerning *c* and *φ*, they have a small contribution in the variability of the safety factor as compared to the horizontal load component.

Table 3.4: Sobol indices for different load configurations at ULS

Random variable	Sobol indices		
	Point M	Point N	Point L
c	0.0771	0.1397	0.1605
φ	0.1214	0.2498	0.7765
V	0.0041	0.0004	0.0529
H	0.7974	0.6101	0.0101
Summation	1.00	1.00	1.00

Similarly; for point N, the Sobol index of *H* is significant and that of *V* is negligible. However, the Sobol indices of *c* and *φ* have moderate values which means that they moderately contribute to the variability of the safety factor *F*. Concerning point L, the friction angle *φ* has the greatest Sobol index. The Sobol index of the cohesion *c* is smaller but not negligible (about 16%) while the Sobol indices of *V* and *H* are very small. This result may be explained by the fact that for point L, the soil punching is likely most predominant. In this case, the parameters that mostly contribute to the variance of the response are the soil friction angle and in a lower degree the soil cohesion.

From Table (3.4), one can conclude that the variability of *V* can be neglected (i.e. *V* can be considered as a deterministic parameter) for all the load configurations. Thus, for all the subsequent ULS probabilistic calculations performed in this chapter, only *c*, *φ* and *H* will be considered as random variables. However, *V* will be considered as a deterministic parameter. This again reduces the necessary number of calls of the deterministic model from 66 to only 26. Consequently, the reduction in the number of calls of the deterministic model is equal to 90% with respect to the total initial number of 257. This strategy of reducing the number of calls of the deterministic model is recommended when dealing with a complex numerical model (as the one considered herein in the ULS analysis where the computational time for a single deterministic simulation is about 180 minutes).

For the SLS analysis, Table (3.5) presents the Sobol indices of the different random variables for both responses (*δ*v and *δu*) for the load configurations corresponding to points

M, N and L. This table indicates that the horizontal load component *H* has a negligible contribution in the variability of the vertical displacement for the three points M, N and L. However, its contribution in the variability of the horizontal displacement is very large for the three points. In contrast, the vertical load component *V* has a negligible contribution in the variability of the horizontal displacement for points M, N and L. However, it has a considerable contribution in the variability of the vertical displacement for the three points. Table (3.5) also shows that the Young's modulus *E* has a significant contribution in the variability of the vertical displacement for the three points; however, its contribution in the variability of the horizontal displacement is much smaller. Finally, Poisson ratio *v* has a very small contribution in the variability of both the vertical and the horizontal displacements for all the loading configurations.

Since both responses (δu and δv) are outcomes of a single simulation, the four input variables (i.e., *E, v, V* and *H*) will be considered as random variables in all the subsequent SLS analyses although *v* could be considered as deterministic if the deterministic model was timely-expensive. Notice that the computational time required for a single deterministic simulation (which provides both the footing vertical and horizontal displacements) was only equal to 10 minutes.

Table 3.5: Sobol indices for the different random variables at SLS

Random variable	Sobol indices					
	Point M		Point N		Point L	
	δv	δu	δv	δu	δv	δu
E	0.6297	0.0642	0.6438	0.0559	0.4609	0.0860
v	0.0199	0.0009	0.0191	0.0007	0.0155	0.0004
V	0.3263	0.0145	0.3290	0.0072	0.5232	0.0347
H	0.0241	0.9675	0.0081	0.9362	0.0004	0.8788
Summation	1.00	1.00	1.00	1.00	1.00	1.00

Finally, it should be noticed that the number of collocation points used in the SLS analysis was equal to 66 according to the concept of matrix invertibility by Sudret (2008). This number is to be compared to 257 points which is the total number of the available collocation points. This corresponds to a reduction in the number of calls of the deterministic model by 74.3%.

3.2. Failure mode predominance

This section aims at determining the most predominant failure mode at both ULS and SLS using the CSRSM probabilistic approach.

3.2.1. Failure mode predominance at ULS

In chapter 2 where only the uncertainties of soil parameters were considered, it has been shown (by using the RSM) that there is an optimal load inclination (α=15.6^o) for which the safety factor is maximum and the failure probability is minimum. This inclination is represented by the line OO' (denoted "case 1" in Figure 3.2). In this chapter, the simultaneous effect of the uncertainties of both the soil parameters and the horizontal load component on the optimal load inclination was investigated using the CSRSM. For the three values of μ_H equal to the three values of H shown in Figure 3.1, the failure probability P_f was plotted versus the vertical load component V in Figure 3.3. Remember that the failure probability is calculated by applying MCS on the meta-model. From Figure (3.3), one can observe that P_f presents a minimum value at points K_1, K_2 and K_3. These points are plotted in Figure (3.2). They are joined together by the line denoted "case 2" in this figure. This line is the one that separates the zones of predominance of the two failure modes in the case where the uncertainties of both the soil parameters and the horizontal load component are considered in the analysis.

From Figure 3.2, one can conclude that in the presence of the uncertainties of the horizontal load component, the zone of predominance of sliding slightly extends with respect to the one obtained in the case where only the soil uncertainty is considered. This means that some loading configurations which have been located in the zone of punching mode predominance (when the loading uncertainties were not taken into account) are now located in the zone of sliding mode predominance. This fact is due to the greater risk of sliding because of the great variability of the horizontal load component H in this case.

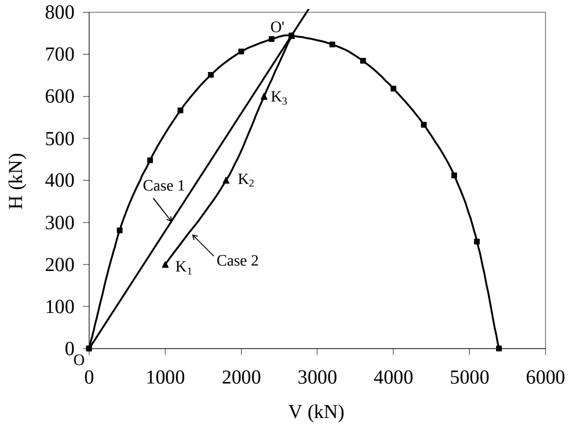

Figure 3.2: Optimal loading configurations for two cases of (i) uncertainties of soil parameters and (ii) uncertainties of soil parameters and horizontal load component

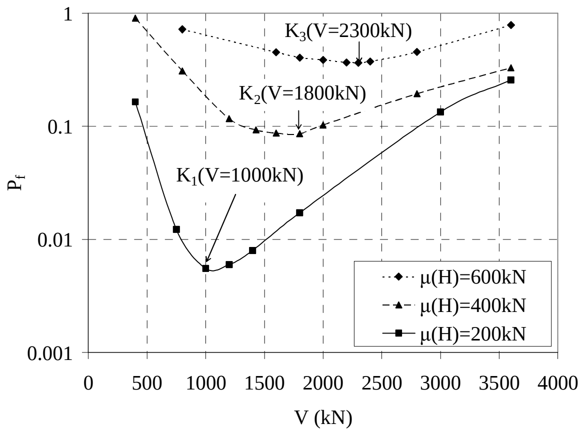

Figure 3.3: Effect of V on the failure probability P_f for three values of μ_H

Notice that the variability of the soil parameters has been shown to have no effect on the optimal load configurations (see chapter 2 of this thesis). In order to confirm this statement using CSRSM, Figure (3.4) shows the failure probability P_f against the vertical load component V when H=μ_H=200kN in the three following cases: (i) the uncertainties of only the soil parameters are considered, (ii) the uncertainty of only the horizontal load component H is considered and (iii) the uncertainties of both the soil parameters and the horizontal load component are considered. This figure also shows the safety factor F (calculated by the deterministic approach) against the vertical load component V for the same value of H. From this figure, one can observe that when considering only the uncertainties of the soil parameters, the value of V for which F presents a maximum is the same value for which P_f presents a minimum (as obtained in chapter 2 when using the RSM). However, when considering the uncertainties of both the soil parameters and the horizontal load component, the value of V for which P_f presents a minimum is different from that for which F presents a maximum. This figure also shows that when considering both the soil and the loading uncertainties, P_f presents a minimum at the same V value obtained when considering only the load uncertainty. This confirms that the soil uncertainties have no effect on the optimal load configurations and the increase in the sliding zone is due to the variability of H.

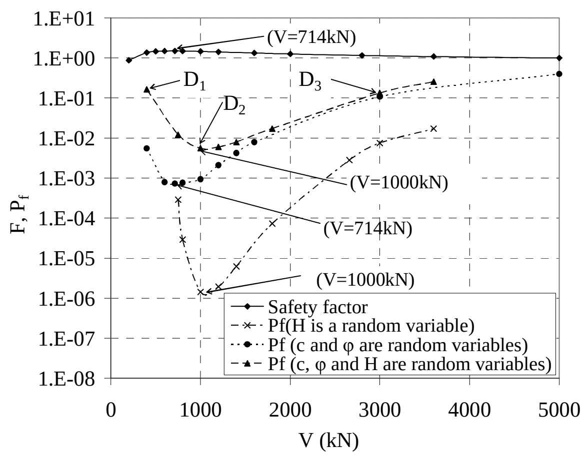

Figure 3.4: Effect of V on the safety factor F and the failure probability P_f when μ_H=*200kN*

From Figure (3.4), one can conclude that the deterministic analysis is not able to take into account the effect of the loading uncertainties on the optimal load inclination. This conclusion reflects the importance of the probabilistic approach with respect to the deterministic one in the analysis of the obliquely loaded footings.

3.2.2. Failure mode predominance at SLS

Figures (3.5a and 3.5b) present the probability P_e of exceeding a tolerable footing displacement versus the mean value of the vertical load component μ_V for two values of μ_H

(i.e. μ_H=200kN and μ_H=400kN). Notice that these two μ_H values were previously used in Figure (3.3) to determine the zones of predominance at ULS. Each one of Figures (3.5a and 3.5b) presents three cases: (i) the probability of exceeding a tolerable vertical displacement δv_{max}=3cm, (ii) the probability of exceeding a tolerable horizontal displacement δu_{max}=1.5cm and (iii) the system probability of exceeding both tolerable displacements of δv_{max}=3cm and δu_{max}=1.5cm. Figure (3.5) shows that the system probability (for the load configurations corresponding to μ_H values equal to 200kN and 400kN) presents a minimum at points K_4 and K_5.

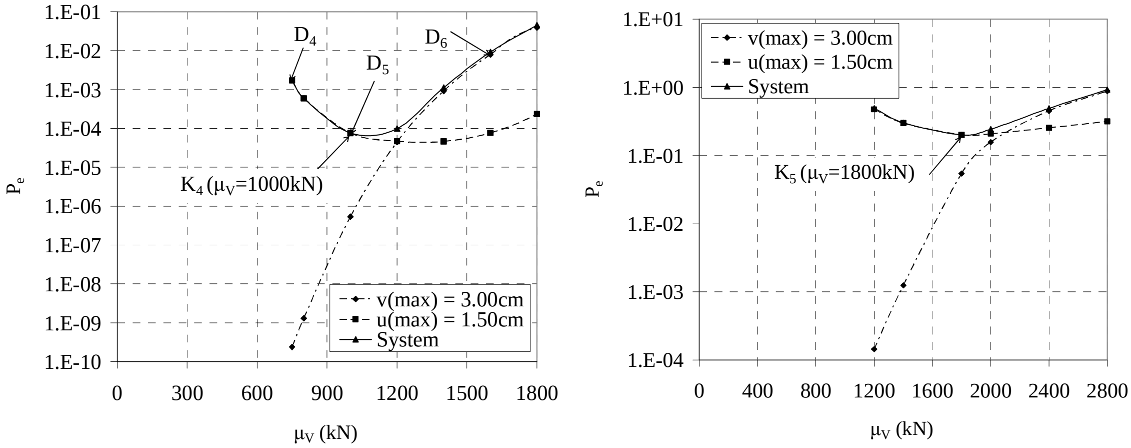

a. μ_H=200kN **b.** μ_H=400kN

Figure 3.5: Effect of μ_V on the probability P_e of exceeding tolerable vertical and horizontal footing displacements for two values of μ_H

From Figures (3.3 and 3.5), it can be observed that the μ_V values for which P_e is minimum at SLS are equal to the V values for which P_f is minimum at ULS. This means that the line denoted "case 2" in Figure (3.2) which separates the zones of predominance at ULS can also be used at SLS to distinguish the load configurations that lead to a predominance of the footing horizontal or vertical movement. This line corresponds to the configuration that lead to the minimum movement of the footing with respect to the other loading configurations having the same value of μ_H.

3.3. Effect of the most predominant failure mode on the variability of the different system responses at both ULS and SLS

As mentioned previously, the determination of the zones of predominance of the different failure modes is important. This is due to the fact that the variability of the system response corresponding to a given load configuration depends on the zone of predominance to which the load configuration belongs. In this section, the sensitivity of the PDFs of the different system responses to the most predominant failure mode was investigated and discussed.

3.3.1. Variability of the system response at ULS

Figure (3.6) shows three PDFs of the safety factor *F* for three different values of *V* when μ_H=200kN. The three values of *V* correspond respectively to points D_1, D_2 and D_3 shown in Figure (3.4). Notice that point D_1 corresponds to a load configuration where the footing sliding is predominant and point D_3 corresponds to a load configuration where the soil punching is predominant. However, point D_2 corresponds to a load configuration where neither footing sliding nor soil punching is predominant. From Figure (3.6), it can be observed that the PDF corresponding to point D_1 (which is located in the zone of sliding predominance) is more spread out than the PDF corresponding to point D_3 (which is located in the zone of punching predominance). For points D_1, D_2 and D_3, the values of the standard deviation of the safety factor are respectively equal to 0.42, 0.19 and 0.12. Notice that for point D_1 where *V* is small (zone of sliding predominance), the large variability of the safety factor is due to the large variability of *H* which has the largest weight in the variability of the safety factor in this zone (see Table 3.4). In contrast, for point D_3 where *V* is large (zone of punching predominance), the large variability of *H* has a negligible effect on the variability of the safety factor in this zone.

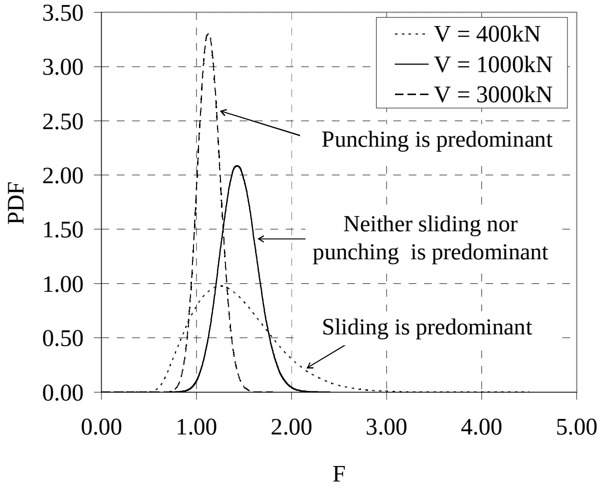

Figure 3.6: PDFs of the safety factor F for three values of V when μ_H=200kN

3.3.2. Variability of the system responses at SLS

Concerning the SLS, Figures (3.7a and 3.7b) present the PDFs of the footing horizontal and vertical displacements for three different values of μ_V when μ_H=200kN. The three μ_V values correspond respectively to points D_4, D_5 and D_6 shown in Figure (3.5a). Remember that point D_4 corresponds to a load configuration where the horizontal movement is predominant and point D_6 corresponds to a load configuration where the vertical movement is predominant. However, point D_5 corresponds to a load configuration where neither horizontal nor vertical movement is predominant.

For the footing horizontal displacement, Figure (3.7a) indicates that the PDF corresponding to point D_4 (where the horizontal movement is predominant) exhibits slightly larger variability than that corresponding to point D_6 (where the vertical movement is predominant). For points D_4, D_5 and D_6, the values of the standard deviation of the footing horizontal displacement are respectively equal to 0.0021m, 0.0019m and 0.0018m. For point D_4, the PDF is more spread out due to the large variability of H which has the greatest contribution in the variability of the footing horizontal displacement in this zone (see Table 3.5). In contrast, for point D_6, the PDF is slightly less spread out because the contribution of H decreases in this zone (see Table 3.5, point L).

For the footing vertical displacement, Figure (3.7b) shows that the PDF corresponding to point D_6 is more spread out than the PDF corresponding to point D_4. For points D_4, D_5 and D_6, the values of the standard deviation of the footing vertical displacement are respectively equal to 0.0015m, 0.002m and 0.0039m. Notice that the large variability of *H* has no effect here because *H* has a negligible contribution in the variability of the vertical footing displacement for all loading configurations (see Table 3.5). This is to be expected since the vertical footing displacement is mainly caused by *V*. Thus, the increase in the variability of this displacement from the zone of horizontal movement predominance to the zone of vertical movement predominance is due to the increase of the contribution of *V* in this variability as can be seen from Table (3.5).

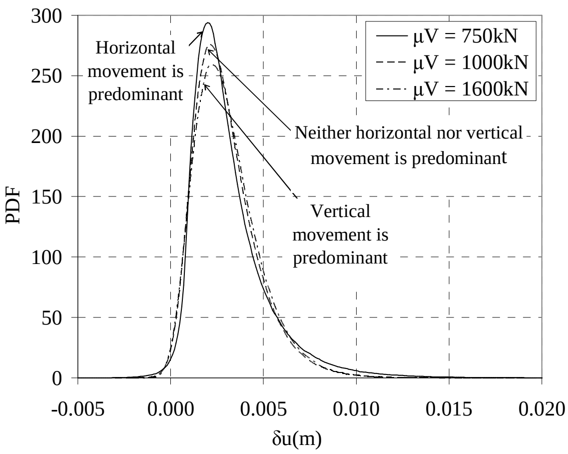

a. PDFs of the footing horizontal displacement

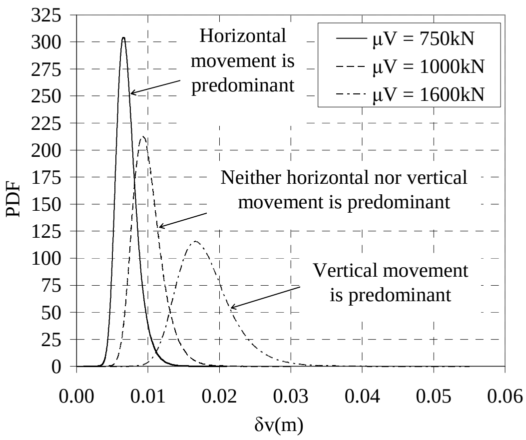

b. PDFs of the footing vertical displacement

Figure 3.7: PDFs of the footing horizontal and vertical displacements for three values of μ_V when μ_H=200kN

3.4. Parametric study

The aim of this section is to study the effect of the statistical characteristics of the random variables (coefficients of variation of the random variables, the types of the PDFs, and the correlation coefficients between random variables) on the PDFs of the system responses at ULS and SLS. This study was carried out using the load configuration corresponding to point N shown in Figure 3.1.

3.4.1. Effect of the coefficients of variation (*COVs*) of the random variables

The effect of *COVs* of the random variables on the PDFs of the three responses (i.e. the safety factor *F*, the footing horizontal displacement δu and the footing vertical displacement δv) is presented in Figures (3.7, 3.8 and 3.9) respectively. The numerical results of these figures have shown that the mean value of the different responses is not affected by the *COVs* of the random variables. Also, it was found that these mean values are those obtained deterministically using the mean values of the random variables. Thus, the variability of the system responses is better expressed herein by the coefficient of variation (not the standard deviation) since the mean values are constant.

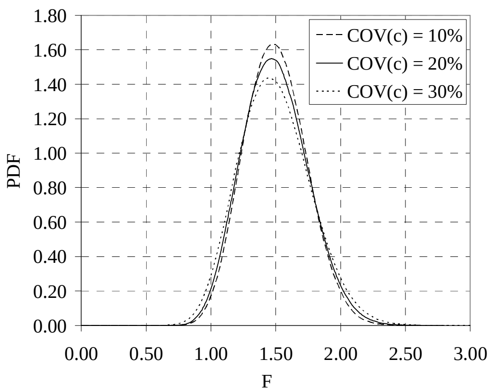

a. Impact of COV_c

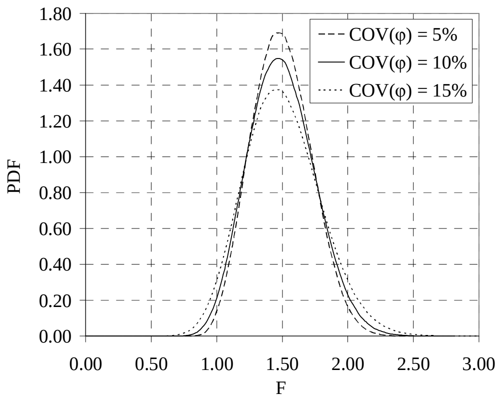

b. Impact of COV_φ

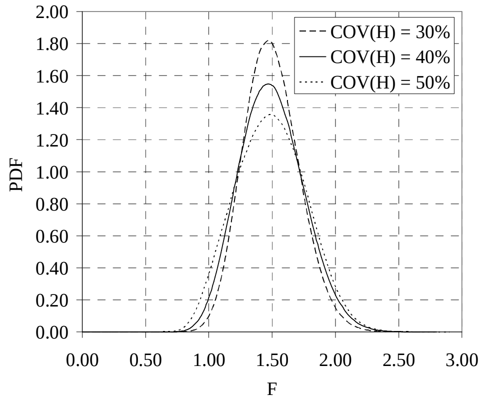

c. Impact of COV_H

Figure 3.7: Impact of *COVs* of the random variables on the PDF of the safety factor *F*

Figure (3.7) shows that the *COVs* of *c*, φ and *H* have a non-negligible effect on the variability of the safety factor. For instance, an increase in COV_c and COV_φ by 50% with respect to their reference values (cf. Table 3.2) induces an increase in *COV* of the safety factor by 9.1% and 14.8% respectively; on the other hand, an increase in COV_H by 25% with respect to its reference value (cf. Table 3.2) increases the *COV* of the safety factor by 10.6%.

The variability of the footing horizontal displacement (Figure 3.8) was found to be very sensitive to the *COV* of the horizontal load component *H* (an increase in COV_H by 25% with respect to its reference value increases the *COV* of the footing horizontal displacement by 61%), the *COV* of the remaining random variables being of negligible effect. This is because *H* has a significant contribution in the variability of the footing horizontal displacement while the other random variables (*E*, ν and *V*) have a very small contribution in the variability of this system response (see Table 3.5).

It should be noticed here that the PDFs in Figure (3.8) present negative values of δu. This is due to the large variability of *H* (COV_H=40%) which may lead to either positive or negative values of *H*. A negative value of *H* leads to a negative horizontal displacement of the footing (i.e. in the opposite direction to that corresponding to the mean value of *H*).

In contrast to the variability of the footing horizontal displacement, the variability of the footing vertical displacement is affected by the *COV* of the Young's modulus *E* and that of the vertical load component *V* (Figure 3.9). The *COV* of the Young's modulus has the greatest effect on the variability of the vertical displacement since an increase in COV_E by 33.3% with respect to its reference value increases the *COV* of the vertical displacement by 27.4%; however, an increase in COV_V by 50% with respect to its reference value increases the *COV* of this displacement by 22.1%. From these results, one can observe that the input parameters for which the *COVs* are of most significance on the variability of a system response are the same as those which have the largest contribution in the variability of this system response (as obtained using Sobol indices).

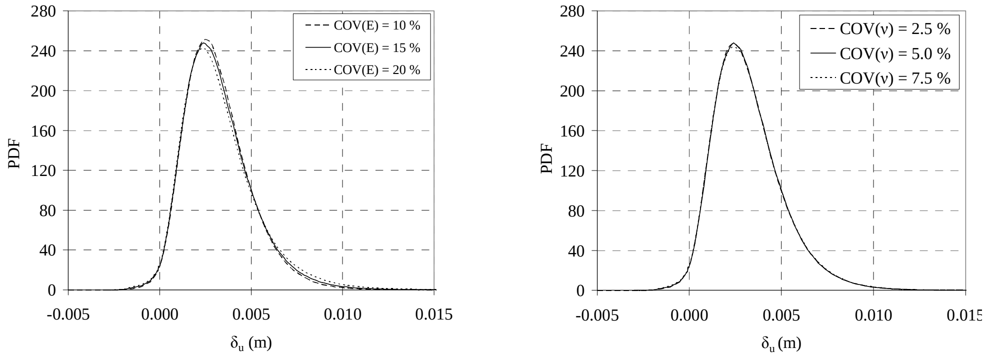

a. Impact of COV_E b. Impact of COV_ν

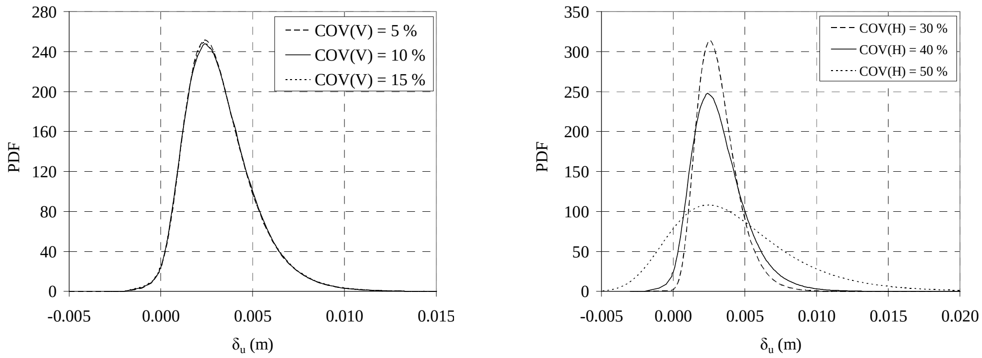

c. Impact of COV_V d. Impact of COV_H

Figure 3.8: Impact of *COVs* of the random variables on the PDF of the footing horizontal displacement δ_u

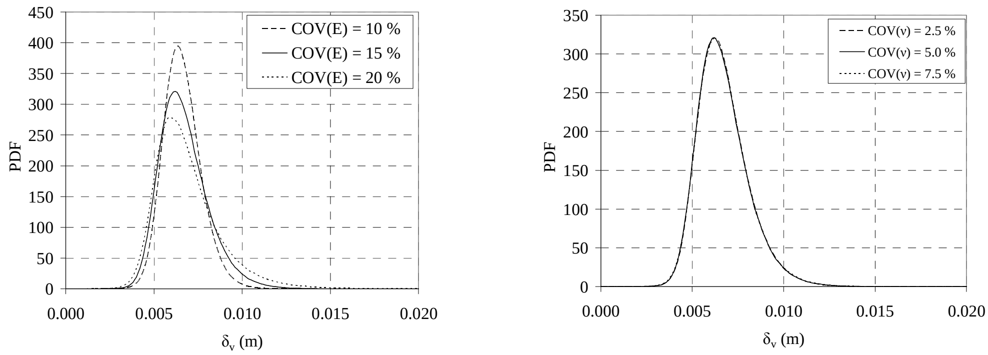

a. Impact of COV_E b. Impact of COV_ν

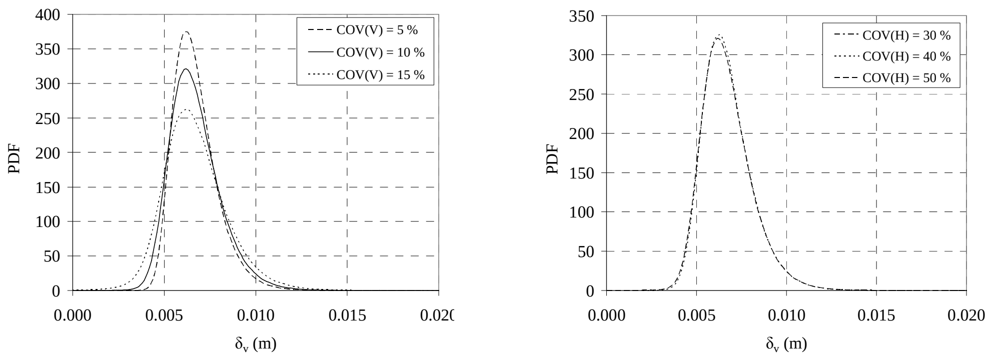

c. Impact of COV_V d. Impact of COV_H

Figure 3.9: Impact of *COVs* of the random variables on the PDF of the footing vertical displacement δv

The effect of *COVs* of the random variables on Sobol indices was shown in Table (3.6) in the case of ULS. This table shows that the increase in the *COV* of a certain random variable increases its Sobol index and decreases the Sobol indices of the other variables. This means that the increase in the coefficient of variation of a certain random variable increases its weight in the variability of the system response and decreases the weights of the other random variables. The same trend was observed in the SLS analyses (Tables 3.7 and 3.8).

Table 3.6: Effect of the coefficients of variation of the random variables (c, φ, H) on Sobol indices at ULS where the system response is F

Sobol index	Reference case (COV_c=20%, COV_φ=10% and COV_H=40%)	COV_c		COV_φ		COV_H	
		10%	30%	5%	15%	30%	50%
$S(c)$	0.1434	0.0389	0.2775	0.1765	0.1072	0.1860	0.1156
$S(\varphi)$	0.2531	0.2817	0.2132	0.0776	0.4355	0.3313	0.2026
$S(H)$	0.6035	0.6794	0.5093	0.7459	0.4573	0.4827	0.6818
Summation	1.00	1.00	1.00	1.00	1.00	1.00	1.00

Table 3.7: Effect of the coefficients of variation of the random variables (E, v, V, H) on Sobol indices at SLS where the system response is δv

Sobol indices	**Reference case (COV_E=15%, COV_v=5%, COV_V=10% and COV_H=40%)**	COV_E		COV_v		COV_V		COV_H	
		10%	20%	2.5%	7.5%	5%	15%	30%	50%
$S(E)$	0.6438	0.4221	0.7872	0.6550	0.6266	0.8559	0.4497	0.6591	0.6405
$S(v)$	0.0191	0.0275	0.0101	0.0046	0.0412	0.0263	0.0129	0.0194	0.0072
$S(V)$	0.3290	0.5379	0.1983	0.3320	0.3250	0.1092	0.5349	0.3195	0.2910
$S(H)$	0.0081	0.0125	0.0044	0.0084	0.0072	0.0086	0.0025	0.0020	0.0613
Summation	1.00	1.00	1.00	1.00	1.00	1.00	1.00	1.00	1.00

Table 3.8: Effect of the coefficients of variation of the random variables (*E, v, V, H*) on Sobol indices at SLS where the system response is δu

Sobol indices	**Reference case (*COV_E=15%, COV_v=5%, COV_V=10%* and *COV_H=40%*)**	*COV_E*		*COV_v*		*COV_V*		*COV_H*	
		10%	20%	2.5%	7.5%	5%	15%	30%	50%
S(E)	0.0559	0.0238	0.1084	0.0561	0.0555	0.0626	0.0375	0.1265	0.0532
S(v)	0.0007	0.0008	0.0006	0.0001	0.0029	0.0008	0.0004	0.0017	0.0004
S(V)	0.0072	0.0074	0.0067	0.0073	0.0069	0.0013	0.0261	0.0089	0.0068
S(H)	0.9362	0.9680	0.8843	0.9365	0.9347	0.9353	0.9360	0.8629	0.9396
Summation	1.00	1.00	1.00	1.00	1.00	1.00	1.00	1.00	1.00

3.4.2. Effect of the correlation and the distribution type of the random variables

This section aims at investigating the effect of the distribution type of the input random variables and the correlation between random variables on the statistical moments of the system responses at both ULS and SLS. Two cases of normal and non-normal random variables were considered at ULS and SLS. Also, two cases of uncorrelated $\left(\rho_{c,\varphi} = 0,\ \rho_{E,\nu} = 0\right)$ or correlated $\left(\rho_{c,\varphi} = -0.5,\ \rho_{E,\nu} = -0.5\right)$ random variables were also considered at ULS and SLS. Tables (3.9, 3.10 and 3.11) show the effect of the correlation and the distribution type of the random variables on the statistical moments of the safety factor, the footing vertical displacement and the footing horizontal displacement. These tables indicate that the mean values of the three system responses are very slightly affected by both the correlation and the distribution type of the random variables. These tables also show that the coefficients of variation of these responses decrease when the random variables are negatively correlated.

The non-normality of the random variables seems to have a significant effect on the coefficient of variation of a system response only for the footing horizontal displacement. This may be explained by the large variability of *H* and the significant weight of *H* in the variability of the footing horizontal displacement (see the difference between the normal and log-normal distributions of *H* for *COV=40%* on Figure 3.10). Similarly to the coefficients of variation of the system responses, the skweness and kurtosis are slightly affected by the negative correlation and they are sensitive to the distribution type of the random variables especially for the footing horizontal displacement. The same explanation given above remains valid in this case.

Table 3.9: Effect of the PDF type of the random variables (c, φ, H) and the correlation coefficient $\rho_{c,\varphi}$ on the statistical moments of the safety factor

Distribution type and correlation	Mean	Standard deviation	Coefficient of variation (%)	Skewness	Kurtosis
Normal uncorrelated variables	1.495	0.251	16.789	0.245	-0.095
Normal correlated variables	1.493	0.226	15.126	0.152	-0.279
Non-normal uncorrelated variables	1.500	0.247	16.466	-0.131	0.131
Non-normal correlated variables	1.501	0.221	14.747	-0.402	0.373

Table 3.10: Effect of the probability distribution type of the random variables (E, v, H, V) and the correlation coefficient $\rho_{E,v}$ on the statistical moments of the footing vertical displacement

Distribution type and correlation	Mean (m)	Standard deviation (m)	Coefficient of variation (%)	Skewness	Kurtosis
Normal uncorrelated variables	$7x10^{-3}$	$1.38x10^{-3}$	19.691	0.880	1.573
Normal correlated variables	$7x10^{-3}$	$1.30x10^{-3}$	18.571	0.773	1.414
Non-normal uncorrelated variables	$7x10^{-3}$	$1.39x10^{-3}$	19.898	0.621	0.669
Non-normal correlated variables	$7x10^{-3}$	$1.29x10^{-3}$	18.516	0.565	0.543

Table 3.11: Effect of the probability distribution type of the random variables (E, v, H, V) and the correlation coefficient $\rho_{E,v}$ on the statistical moments of the footing horizontal displacement

Distribution type and correlation	Mean (m)	Standard deviation (m)	Coefficient of variation (%)	Skewness	Kurtosis
Normal uncorrelated variables	$3x10^{-3}$	$1.85x10^{-3}$	57.40	1.030	1.957
Normal correlated variables	$3x10^{-3}$	$1.84x10^{-3}$	57.20	1.020	1.870
Non-normal uncorrelated variables	$3x10^{-3}$	$2.17x10^{-3}$	67.10	2.598	11.707
Non-normal correlated variables	$3x10^{-3}$	$2.16x10^{-3}$	66.50	2.543	11.048

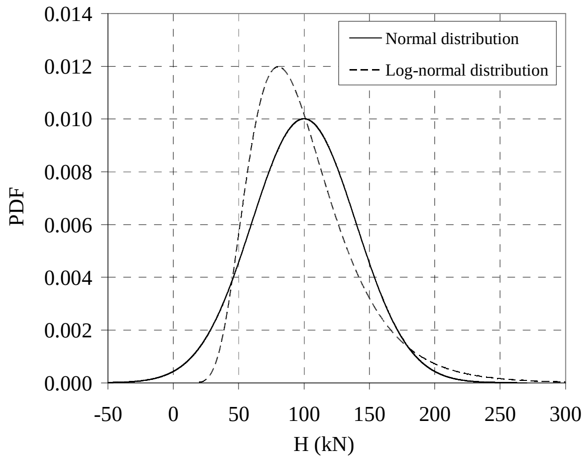

Figure 3.10: Comparison between normal and log-normal distribution of *H*.

Finally, it should be noticed that the coefficient of variation of the footing horizontal displacement is considerably larger than that of the footing vertical displacement for the same uncertainties of the input parameters (see Tables 3.10 and 3.11). This means that the footing horizontal displacement is a key parameter that should be carefully considered in design since it is very sensitive to the input uncertain parameters.

4. Conclusion

This chapter presents a probabilistic analysis at both ULS and SLS of the same circular footing considered in chapter 2. In this chapter, a more efficient method called the Collocation-based Stochastic Response Surface Method (CSRSM) was used. The use of this method allowed the evaluation of the contribution of each random variable in the variability of the different system responses using the PCE-based Sobol indices. Contrary to chapter 2 in which only the soil uncertainty was considered, in the present chapter both the soil and loading uncertainties were taken into account in the analysis. The simultaneous effect of these uncertainties on the optimal loading configurations at both ULS and SLS was investigated. In addition, the effect of the type of the most predominant failure mode on the variability of the different system responses was presented. Finally, a parametric study showing the effect of the statistical parameters of the random variables on the PDFs of the different system responses was presented and discussed.

The general conclusions of this chapter can be summarized as follows:

1 - For the ULS analysis

a) A global sensitivity analysis using the PCE-based Sobol indices has shown that the vertical load component *V* has a negligible weight in the variability of the safety factor and it can be considered as deterministic.

b) The optimal loading configurations obtained by using the deterministic analysis were found similar to those obtained by using the probabilistic approach when considering only the soil uncertainties. This means that the optimal load inclination does not depend on the uncertainties of the soil parameters. In this case, the optimal loading configurations are situated on the line joining the origin and the extremum of the interaction diagram.

c) Although the deterministic approach was able to determine the zones of predominance of sliding and punching when considering only the soil uncertainties, it was not able to determine these zones when considering the uncertainty of the horizontal load component. The probabilistic approach was necessary in this case.

d) The uncertainty of the horizontal load component *H* was found to slightly extend the zone of sliding predominance in the interaction diagram with respect to that obtained by the deterministic approach. This means that contrary to the variability of the soil properties, the variability of the load components affects the optimal load configurations.

e) The safety factor *F* was found to exhibit more variability for the load configurations corresponding to the zone of sliding predominance.

2 - For the SLS analysis

a) A global sensitivity analysis using the PCE-based Sobol indices has shown that the variability of the footing horizontal displacement is mainly due to the horizontal load component. On the other hand, the variability of the footing vertical displacement was mainly due to the Young's modulus and the vertical load component; the Young's modulus being of larger weight.

b) The zones of predominance of horizontal or vertical soil movement at SLS were found the same as the zones of predominance of footing sliding or soil punching at ULS.

c) The footing vertical displacement was found to exhibit larger variability for the load configurations corresponding to the zone of predominance of the vertical soil movement. However, the footing horizontal displacement was found to exhibit larger variability for loading configurations corresponding to the zone of predominance of the horizontal soil movement.

3 - Parametric study

a) The increase of the coefficient of variation *COV* of a given random variable increases the variability of the system response. The random variables for which the *COV* has a significant effect on the variability of a given system response are those (obtained using Sobol indices) which have the largest contribution in the variability of this system response.

b) The increase in *COV* of a given variable increases its Sobol index and decreases the Sobol indices of the other random variables. This means that the increase in *COV* of a certain random variable increases its weight in the variability of the system response and decreases the weights of the other random variables.

c) The negative correlation between the random variables has a slight effect on the coefficient of variation, skewness and kurtosis of the different system responses.

d) The non-normality of the random variables has a negligible effect on the variability of the safety factor and the vertical footing displacement. However, it has a significant effect on the variability of the footing horizontal displacement.

e) For the same uncertainties of the input parameters, the coefficient of variation of the footing horizontal displacement is considerably larger than that of the footing vertical displacement. This means that the footing horizontal displacement is a key parameter that should be carefully considered in design since it is very sensitive to the input uncertain parameters.

CHAPTER 4

COMBINED USE OF THE COLLOCATION-BASED STOCHASTIC RESPONSE SURFACE METHOD AND THE SUBSET SIMULATION APPROACH FOR THE PROBABILISTIC ANALYSIS OF FOOTINGS

1. Introduction

The probabilistic approaches used in the previous chapters (i.e. RSM and CSRSM) are based on the approximation of the system response by an analytical equation. It should be emphasized here that when dealing with highly nonlinear response surfaces, these methods lead to inaccurate solutions if one uses low order polynomials and they become very time-expensive when using a polynomial of higher order. The time cost becomes of great concern in case of a large number of random variables because of the proliferation of the number of unknown coefficients of the response surface and consequently of the number of calls of the deterministic model. On the other hand, Monte Carlo Simulation (MCS) methodology is well-known to be a rigorous and robust tool to calculate the failure probability P_f even when dealing with highly nonlinear response surfaces. The accuracy of MCS methodology does not depend on the shape of the response surface but it depends on the number of simulations. It should be noticed that MCS becomes very time-consuming when computing a small failure probability. This is due to the large number of calls of the deterministic model required in such a case. As alternative to MCS methodology, the Subset Simulation (SS) approach was proposed by Au and Beck (2001) to calculate the small failure probability using a much smaller number of calls of the deterministic model. In this approach, the failure probability is expressed as a product of conditional probabilities of some chosen intermediate failure events. Thus, the problem of evaluating a small failure probability in the original probability space is replaced by a sequence of more frequent events in the conditional probability space.

Notice that the SS approach is efficient in computing the failure probability, but it does not provide any information about the probability density function (PDF) of the system response (i.e. it does not allow one to perform an uncertainty propagation from the input variables to the system output). Also, it does not provide any information about the contribution of each input uncertain parameter in the variability of the system response (i.e., it does not allow one to perform a global sensitivity analysis). In addition, the SS approach does not allow one to calculate the design point (the most probable failure point) which has an important practical implication since it can be used to calculate the partial safety factor corresponding to each input random variable. To overcome the above mentioned shortcomings, the SS approach is combined herein with the CSRSM. First, a classical subset simulation computation is performed to calculate the failure probability. Then, the values of the system response obtained during this computation are used in a CSRSM analysis with no additional cost to obtain the other outputs cited above (i.e. uncertainty propagation, global sensitivity analysis and reliability-based analysis and design).

Since the aim here is to show the efficiency of the proposed procedure of combining the SS approach with the CSRSM, a simple problem was chosen to illustrate this procedure. In this problem a probabilistic analysis at the ultimate limit state (ULS) of a strip footing resting on a (c, φ) soil and subjected to an axial vertical load P_a was performed. A deterministic model (with small computation time) based on the upper-bound theorem of the limit analysis theory was used to calculate the system response. The small computation time of this model allows the validation of the proposed procedure by comparison of its results with those given by MCS methodology applied on the original deterministic model. In this chapter, the soil shear strength parameters c and φ are considered as random variables. The system response considered in the analysis is the ultimate bearing capacity q_u.

The present chapter is organized as follows: The subset simulation approach is first presented. Then, the extension of the SS approach to perform uncertainty propagation and a global sensitivity analysis is described. This is followed by the probabilistic analysis of a strip footing at ULS to illustrate the efficiency of the proposed procedure. The chapter ends with a conclusion of the main results.

2. Subset Simulation (SS) approach

The basic idea of the subset simulation approach is that the small failure probability can be expressed as a product of larger conditional failure probabilities. Consider a failure region F defined by the condition $G<0$ where G is the performance function and let $(s_1, \ldots, s_k, \ldots, s_{Nt})$ be a sample of N_t realisations of a vector **'s'** composed of M random variables. It is possible to define a sequence of nested failure regions $F_1, \ldots, F_j, \ldots, F_m$ of decreasing size where $F_1 \supset \ldots \supset F_j \supset \ldots \supset F_m = F$ (Figure 4.1). An intermediate failure region F_j can be defined by $G<C_j$ where C_j is an intermediate failure threshold whose value is larger than zero. Thus, there is a decreasing sequence of positive failure thresholds $C_1, \ldots, C_j, \ldots, C_m$ corresponding respectively to $F_1, \ldots, F_j, \ldots, F_m$ where $C_1 > \ldots > C_j > \ldots > C_m = 0$. In the SS approach, the space of uncertain parameters is divided into a number m of levels with equal number N_s of realizations $(s_1, \ldots, s_k, \ldots, s_{Ns})$. An intermediate level j contains a safe region and a failure region defined with respect to a given failure threshold C_j. The conditional failure probability corresponding to this intermediate level j is calculated as follows:

$$P(F_j | F_{j-1}) = \frac{1}{N_s} \sum_{k=1}^{Ns} I_{F_j}(s_k) \tag{4.1}$$

where $I_{F_j}(s_k)=1$ if $s_k \in F_j$ and $I_{F_j}(s_k)=0$ otherwise. Notice that in the SS approach, the first N_s realizations are generated using MCS methodology according a target PDF P_t. The next N_s realizations of each subsequent level are obtained using Markov chain method based on

Metropolis-Hastings (M-H) algorithm (explained in Appendix F) according to a proposal PDF P_p.

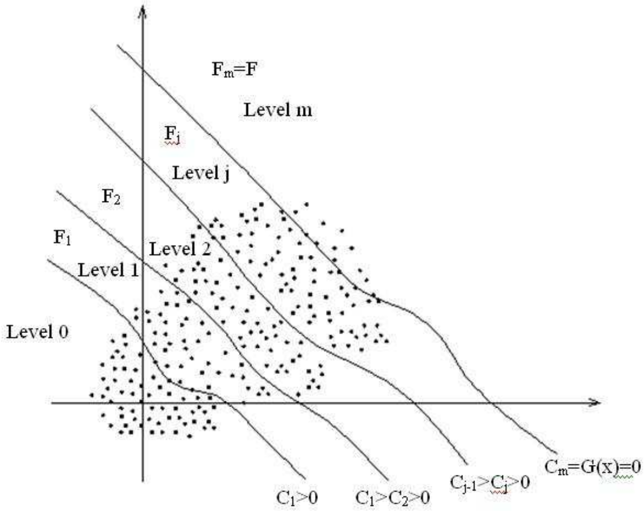

Figure 4.1: Nested Failure domain

The failure probability $P(F)=P(F_m)$ of the failure region F can be calculated from the sequence of conditional failure probabilities as follows:

$$P(F)=P(F_m)=P(F_m/F_{m-1})\text{x}P(F_{m-1}/F_{m-2})\text{x}P(F_{m-2}/F_{m-3})\text{x} \ldots \text{x}P(F_2/F_1)\text{x}P(F_1) \quad (4.2)$$

This equation can be regarded as a system consisting of m components (related to the m failure regions $F_1, \ldots, F_j,\ldots, F_m$) connected in parallel. Consequently, the failure probability of the failure region F is the intersection of all conditional failure probabilities of the failure regions $F_1, \ldots, F_j,\ldots, F_m$. Thus, the failure probability $P(F)$ is:

$$P(F)=P(\cap_{j=1}^{m} F_j) \quad (4.3)$$

where

$$P(\cap_{j=1}^{m} F_j)=P(F_m \left| \cap_{j=1}^{m-1} F_j \right.) x P(\cap_{j=1}^{m-1} F_j)=P(F_m \left| F_{m-1} \right.) x P(\cap_{j=1}^{m-1} F_j)=\ldots=P(F_1)\prod_{j=2}^{m} P(F_j \left| F_{j-1} \right.) \quad (4.4)$$

It should be noticed here that the computation of the failure probability $P(F)$ is determined using alternatively one of the following two procedures. The first procedure consists in prescribing a sequence of $C_1, \ldots, C_j,\ldots, C_m$ so that $C_1>\ldots>C_j>\ldots> C_m=0$ and then, calculating the different values of $P(F_j/F_{j-1})$ at the different levels using Equation

(4.1). The second procedure consists in first prescribing a constant conditional failure probability $P(F_j/F_{j-1})$ for the different levels and then, in calculating the different C_j values corresponding to these levels. The value of C_j of level j is the one for which the ratio between the number of realizations for which $G<C_j$ and the number of realizations N_s of this level (which is identical for the different levels), is equal to the prescribed value $P(F_j/F_{j-1})$. In this thesis and in Ahmed and Soubra (2012a), the second procedure is used. Notice that, for simplicity in notations, the constant conditional failure probability $P(F_j/F_{j-1})$ will be referred to as p_0 lateron. The algorithm of the SS approach can be described by the following steps:

1- Generate a realization of the vector **'s'** of M random variables by MCS according to the target PDF P_t.

2- Using the deterministic model, calculate the system response corresponding to this realization.

3- Repeat steps 1 and 2 until obtaining a prescribed number N_s of realizations of the vector **'s'** and the corresponding system response values. Then, evaluate the corresponding values of the performance function to obtain the vector $G_0 = \{ G_0^1,...,G_0^k,...,G_0^{Ns} \}$. Notice that the values of the performance function of the different realizations are arranged in an increasing order in the vector G_0. Notice also that the subscripts '0' refer to the first level (level 0) of the subset simulation.

4- Prescribe a constant conditional failure probability p_0 for all the failure regions F_j $(j=1,\ldots, m)$ and evaluate the first failure threshold C_1 which corresponds to the failure region F_1 where C_1 is equal to the $[(N_s x p_0)+1]^{th}$ value in the increasing list of elements of the vector G_0. This ensures that the value of $P(F_1)$ will be equal to the prescribed p_0 value.

5- Among the N_s realizations, there are $[N_s x p_0]$ ones whose values of the performance function are less than C_1 (i.e. they are located in the failure region F_1). These realizations are used as 'mother realizations' to generate additional $[(1-p_0)N_s]$ realizations of the vector ***'s'*** using Markov chain method based on Metropolis-Hastings algorithm (see Appendix F). These new realizations are located in the second level (level 1 in Figure 4.1).

6- The values of the performance function corresponding to the realizations obtained from the preceding step are listed in an increasing order and are gathered in the vector of performance function values $G_1 = \{ G_1^1,...,G_1^k,...,G_1^{Ns} \}$.

7- Evaluate the second failure threshold C_2 as the $[(N_s x p_0)+1]^{th}$ value in the increasing list of the vector G_1.

8- Repeat steps 5-7 to evaluate the failure thresholds $C_3, C_4, \dots, C_m$ corresponding to the failure regions $F_3, F_4, \dots, F_m$. Notice that contrary to all other thresholds, the last failure threshold C_m is negative. Thus, C_m is set to zero and the conditional failure probability of the last level $[P(F_m/F_{m-1})]$ is calculated as follows:

$$P(F_m \left| F_{m-1} \right.) = \frac{1}{N_s} \sum_{k=1}^{Ns} I_{F_m}(s_k) \tag{4.5}$$

where $I_{F_m}(s_k)=1$ if the performance function $G(s_k)$ is negative and $I_{F_m}(s_k)=0$ otherwise.

9- The failure probability $P(F)$ is evaluated according to Equation (4.2).

3. Extension of the SS approach for uncertainty propagation and global sensitivity analysis

This chapter is devoted to employ the SS approach to compute not only the failure probability but also the PDF of the system response and the corresponding statistical moments without an additional cost. This aim can be achieved by combining the SS approach with CSRSM.

It should be remembered here that in CSRSM, the unknown PCE coefficients are determined by using the values of the system response calculated at several collocation points. Although the roots of the one-dimensional Hermite polynomials are generally used for the determination of the collocation points [Isukapalli *et al.* (1998), Isukapalli (1999), Phoon and Huang (2007), Huang *et al.* (2009), Li *et al.* (2011), Mollon *et al.* (2011)], this technique is not mandatory. In this study, the combination between the SS approach and the CSRSM is carried out by using the values of the system response obtained by the SS approach for the determination of the PCE coefficients in the CSRSM. Thus, the computation of the PCE coefficients requires no additional calls of the deterministic model.

Once the PCE coefficients are determined, the MCS methodology is applied on the obtained PCE. This allows one to obtain the PDF of the system response. It should be emphasized here that in addition to computing the PDF of the system response, the proposed procedure has four other advantages:

1. The computed PCE coefficients can be used to perform a global sensitivity analysis based on the PCE-based Sobol indices described in the preceding chapter.
2. Contrary to the SS approach, the procedure proposed in this study allows the computation of the failure probability for all the values of the applied footing pressure that are greater than the one considered in the SS analysis without the need to repeat the deterministic calculations (i.e. without an additional cost). This is because the limit state surfaces corresponding to larger values of the applied footing pressure are closer to the origin of the standard space of random variables and thus, they are included in the sampling zone of the SS methodology as will be seen later.
3. The obtained PCE allows one to perform a reliability-based analysis or a reliability-based design (RBD). For the reliability-based analysis, the Hasofer-Lind reliability index and the corresponding design point can be easily determined since the PCE is

obtained in the standard uncorrelated space of the random variables. This is done by searching the point which is located on the limit state surface and has the minimum norm in the standard space of random variables. The design point is of great importance since it provides information about the partial safety factors of the different random variables. Concerning the RBD, the obtained PCE makes it easy to compute the dimension of the structure corresponding to a target reliability index.

4. The obtained PCE allows one to undertake a probabilistic parametric study to show the effect of the different characteristics of the random variables (e.g. coefficient of variation *COV*, coefficient of correlation $\rho_{c,\varphi}$ and the non-normality) on the PDF of the system response.

4. Probabilistic analysis of strip footings

In this section, the efficiency of the proposed procedure to compute the outputs cited above is illustrated through an example problem. In this example, a probabilistic analysis of a shallow strip footing of breadth b=2m resting on a (c, φ) soil and subjected to an axial vertical load P_a=650kN/m (i.e. an applied uniform vertical pressure q_a=325kN/m^2) is performed. The analysis is carried out at the ultimate limit state. The system response is the ultimate bearing capacity q_u. The uncertain parameters considered in the analysis are the soil shear strength parameters c and φ. Two types of the probability density functions are considered for these random variables (normal and non-normal as shown in Table 4.1). In the case of non-normal random variables, the soil cohesion was assumed to follow a log-normal probability density function. However, the soil friction angle was assumed to be bounded and to follow a beta probability density function with lower and upper bounds of 0 and 45^o respectively. Also, two cases of uncorrelated (i.e. $\rho_{c,\varphi}$=0) or correlated (i.e. $\rho_{c,\varphi}$=-0.5) random variables were also considered in the analysis. The illustrative values used for the statistical parameters of these random variables are those commonly encountered in practice [Phoon and Kulhawy (1999) and Wolff (1985) among others] and they are presented in Table (4.1). These values will be referred to hereafter as the reference values.

Table 4.1: Statistical characteristics of the random variables

Random variable	Mean	Coefficient of variation (%)	Type of the probability density function (PDF)	
			Case of normal PDFs	Case of non-normal PDFs
c	20kPa	20	Normal	Log-normal
φ	30^{o}	10	Normal	Beta

The performance function used to calculate the failure probability is defined as follows:

$$G = (q_u/q_a) - 1 \tag{4.6}$$

The ultimate bearing capacity q_u is calculated using the deterministic model presented by Soubra (1999). This model is based on the upper-bound approach of limit analysis. It will be briefly presented in the following subsection.

4.1. Deterministic model

The deterministic model is based on the upper-bound theorem of the limit analysis theory using a kinematically admissible failure mechanism. The approach is simple and self-consistent and it obtains rigorous upper-bound solutions in the framework of the limit analysis theory. The failure mechanism used for the computation is a translational symmetrical multiblock mechanism (Figure 4.2).

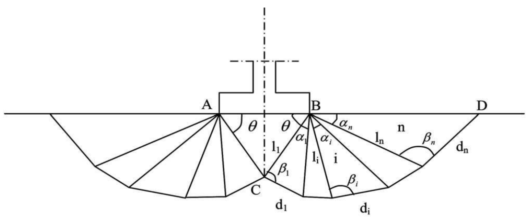

Figure 4.2: Failure mechanism for the ultimate bearing capacity analysis

The bearing capacity is obtained by equating the total rate of work of the external forces to the total rate of energy dissipation along the lines of velocity discontinuities. The ultimate bearing capacity (in the absence of a surcharge loading on the ground surface) is given as follows:

$$q_u = \frac{1}{2}\gamma b N_\gamma + c N_c \tag{4.7}$$

in which b is the footing breadth, γ and c are the soil unit weight and cohesion and N_γ and N_c are the bearing capacity factors due to the soil weight and cohesion, respectively. The coefficients N_γ and N_c are functions of the soil friction angle φ and the geometrical parameters of the failure mechanism shown in Figure (4.2). The ultimate bearing capacity of the foundation is obtained by minimization of Equation (4.7) with respect to the mechanism's geometrical parameters. For further details on the failure mechanism, the reader can refer to Soubra (1999). It should be mentioned here that although the results given by this approach are upper-bound solutions, they are the smallest ones against the available results given by rigid block mechanisms. Notice also that the computation time of the ultimate bearing capacity is equal to about 0.2 minutes. The small computation time of this model allows the validation of the proposed procedure by comparison of its results with the results given by MCS methodology applied on the original deterministic model as will be shown in the next section. Finally, notice that the deterministic ultimate bearing capacity (i.e. the ultimate bearing capacity obtained using the mean values of c and φ given in Table 4.1) is equal to 1071.72kN/m^2. Thus, for the adopted q_a value (q_a=325kN/m^2), the punching safety factor $F_p=q_u/q_a$ is equal to 3.3.

4.2. Validation of the proposed procedure by comparison with MCS methodology

This section is devoted to the validation of the proposed procedure by comparison of its results with those given by MCS methodology applied on the original deterministic model. The comparison involves the values of the failure probability together with the probability density function (PDF) and the statistical moments (mean, coefficient of variation, skewness and kurtosis) of the system response.

It should be mentioned here that, in order to calculate the failure probability by the SS approach, a Gaussian PDF was used as a target probability density function P_t (i.e. it was used to generate the N_s realizations for the first level of the SS approach). Concerning the proposal probability density function P_p (which is used to generate the realizations of levels 1, …, j, …, m), any PDF which can be operated easily can be used as a proposal PDF since its type does not affect the efficiency of the SS approach (Au and Beck 2001). In this study, a uniform PDF was used. The conditional failure probability p_0 was chosen to be equal to 0.1. Notice that the value of p_0 affects the number m of levels required to reach the limit state surface G=0. However, it has a very small effect on the total number of realizations N_t (which is a multiple of the number of levels i.e. N_t=mxN_s) required to reach this limit state surface. If p_0 is large, the sequence of failure thresholds C_1, …, C_j, …, C_m will decrease slowly and a large number of levels will be required to reach the limit state surface. In this case, a small number N_s of realizations per level will give a prescribed high accuracy of the $P(F)$ computation. On the contrary, if p_0 is small, the sequence of failure thresholds will reach the limit state surface quickly and a small number of levels will be required. In this case, a large number N_s of realizations per level will be required to attain the same prescribed high accuracy of the $P(F)$ computation. As a conclusion, an arbitrary value of p_0 can be considered for the probabilistic analysis with a small effect on the computational time. Notice finally that the modified Metropolis-Hastings algorithm proposed by Santoso *et al*. (2011) was used in this study to generate next realizations from existing ones for the levels (1,2, 3, …, m) of subset simulation (see Appendix F).

Remember that the PCE order plays a key role in the accuracy of the approximation by a PCE. The optimal PCE order was defined in this chapter as the minimal order that leads to (i) a coefficient of determination Q^2 greater than a prescribed value (say 0.9999) and (ii) the convergence of the failure probability and the statistical moments of the system response. The numerical results have shown that a third order PCE is necessary to satisfy the abovementioned conditions. Thus, this PCE order will be used in all subsequent probabilistic calculations performed in this chapter.

4.2.1. Validation in terms of failure probability P_f

To ensure a rigorous computation of the failure probability by the SS approach, the number of realizations N_s to be used per level of SS approach must be sufficient to provide a small value of the coefficient of variation COV_{Pf} of this failure probability. Figure (4.3) shows the variation of COV_{Pf} computed by SS approach with the number of realizations N_s to be used per level. For more details on the computation of COV_{Pf} by SS approach, one can refer to Au and Beck (2003). Figure (4.3) shows that COV_{Pf} decreases (i.e. the accuracy of the calculation increases) with the increase of N_s. It attains a small value (about 10%) when N_s=10,000 realizations per level. Consequently, 10,000 realizations were considered at each level to calculate P_f by the SS approach. The corresponding P_f value was found equal to $3.15\text{x}10^{-4}$. Notice that 4 levels of SS approach were necessary to calculate this failure probability and thus, the total number of realizations required by the SS approach is N_t=10,000+(3x9,000)=37,000 realizations. It should be emphasized here that the high number of realizations (i.e. 37,000 realizations) is due to the small value of COV_{Pf} adopted in the computation. For practical purposes, a higher value of COV_{Pf} would be acceptable and thus, a smaller number of realizations would be required. For instance, if N_s=1,000 realizations, COV_{Pf} would be equal to 31.5% and P_f would be equal to $2.56\text{x}10^{-4}$. This means that for COV_{Pf}=31.5%, the number of realizations is reduced by 90% with respect to the one corresponding to $COV_{Pf}\approx$10%; however, the difference in the P_f value is only 18.7%.

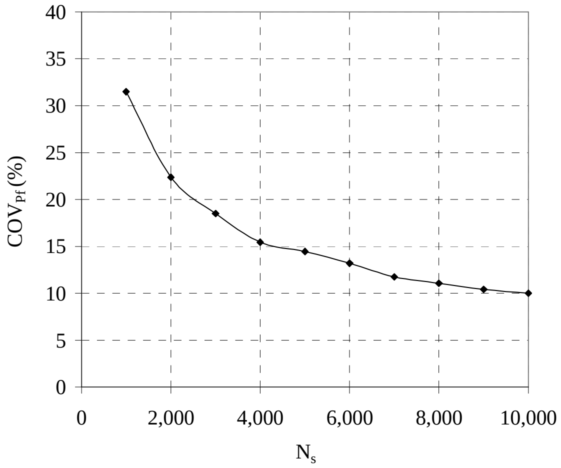

Figure 4.3: Coefficient of variation of P_f (calculated by SS approach) versus the number of realizations N_s used per level

The P_f value computed above (i.e. P_f=3.15x10^{-4}) is to be compared with the value of P_f=3.22x10^{-4} computed by applying MCS methodology on the original deterministic model. One can observe that the two values are very close. Notice that 360,000 realizations were used to calculate the failure probability by applying MCS on the original deterministic model to attain the same COV_{Pf} as that of SS (i.e. about 10% as may be seen from Figure 4.4). This means that for the same accuracy, the number of calls of the deterministic model required by MCS to calculate P_f is reduced by 89.7% by using the SS approach.

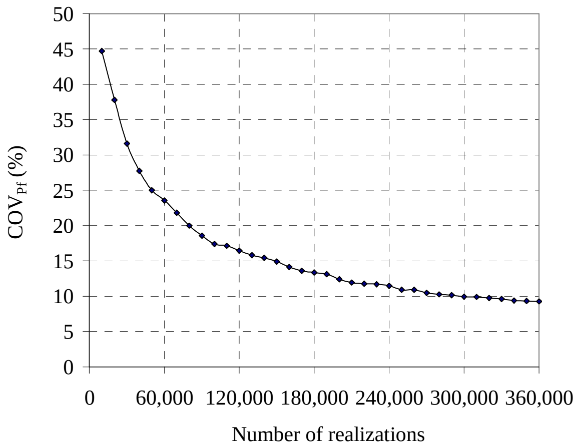

Figure 4.4: Coefficient of variation of P_f (calculated by applying MCS on the original deterministic model) versus the number of realizations

It should be noticed here that contrary to MCS methodology which can be used to compute the failure probabilities corresponding to different values of q_a without repeating the deterministic calculations, the SS approach allows one to calculate the failure probability corresponding to only one q_a value. If the failure probability corresponding to another q_a value is required, one needs to repeat all the deterministic calculations. The combination of SS approach and the CSRSM overcomes this shortcoming. This means that once a single SS computation (corresponding to a given q_a value) is performed, it can be used to accurately calculate the failure probability corresponding to any q_a value larger than the original one. The accuracy of this computation is ensured by the fact that all the limit state surfaces corresponding to larger q_a values are included in the sampling zone of the SS approach (see Figure 4.5).

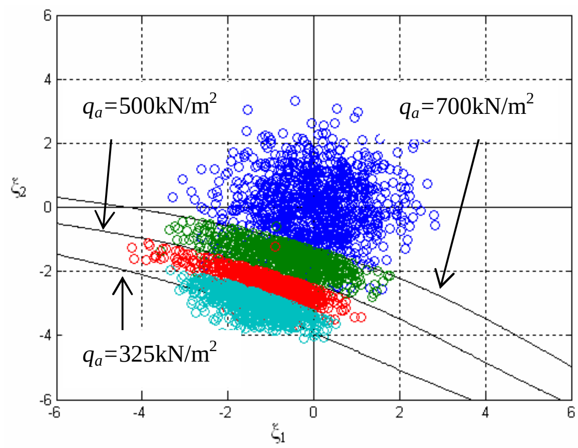

Figure 4.5: Limit state surfaces corresponding to different values of q_a plotted in the standard space of random variables

Table (4.2) presents a comparison between the failure probabilities computed by the proposed procedure (using a single SS computation) and those calculated by MCS methodology applied on the original deterministic model for different q_a values. This table shows a good agreement between the two methods with a maximal difference of 11.53%. This indicates that contrary to the SS approach, the procedure proposed in this study allows the computation of the failure probability for the values of the footing pressure that are greater than the one considered in the SS analysis.

Table 4.2: Comparison between the failure probability computed by applying MCS on the original deterministic model and that calculated by applying MCS on the meta-model for different values of the footing applied pressure q_a

q_a (kN/m^2)	Failure probability	
	MCS applied on the original deterministic model	MCS applied on the meta-model
325	3.22×10^{-4}	3.15×10^{-4}
350	6.42×10^{-4}	5.68×10^{-4}
375	1.22×10^{-3}	1.10×10^{-3}
400	2.34×10^{-3}	2.10×10^{-3}
425	3.90×10^{-3}	3.70×10^{-3}
450	6.41×10^{-3}	6.16×10^{-3}
475	9.81×10^{-3}	9.70×10^{-3}
500	1.46×10^{-2}	1.44×10^{-2}
525	2.07×10^{-2}	2.07×10^{-2}
550	2.83×10^{-2}	2.88×10^{-2}
575	3.77×10^{-2}	3.86×10^{-2}
600	4.88×10^{-2}	4.93×10^{-2}
625	6.17×10^{-2}	6.28×10^{-2}
650	7.66×10^{-2}	7.73×10^{-2}
675	9.36×10^{-2}	9.42×10^{-2}
700	1.11×10^{-1}	1.12×10^{-1}

4.2.2. Validation in terms of probability density function (PDF)

Once the PCE coefficients are determined, the uncertainty propagation can be performed. The PDF, CDF and the statistical moments of the system response can be easily determined by applying MCS methodology on the obtained PCE (meta-model). In order to validate these results, they were compared in Figures (4.6a, 4.6b) and Table (4.3) with those obtained by applying MCS on the original deterministic model using (as before) 360,000 realizations. These results show that there is a good agreement between the proposed procedure and the classical MCS methodology applied on the original deterministic model for both the central part and the tail of the distribution of the PDF of the system response. As a conclusion, the proposed procedure allows one to rigorously determine not only the failure probability but also the statistical moments of the system response with no additional calls of the deterministic model.

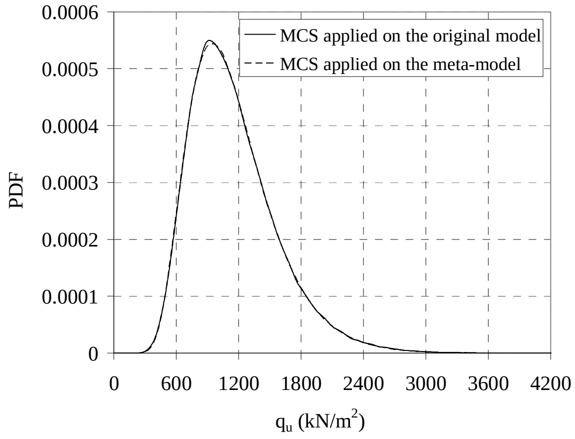

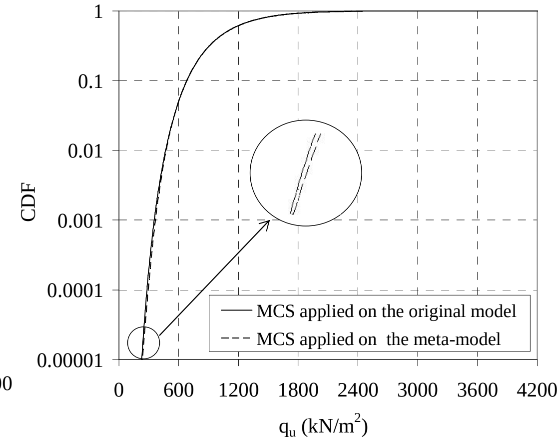

Figure 4.6: Comparison between the PDF and CDF of the ultimate bearing capacity computed by applying MCS on the original deterministic model and those computed by applying MCS on the meta-model

Table 4.3: Comparison between the statistical moments of the ultimate bearing capacity computed by applying MCS on the original deterministic model and those computed by applying MCS on the meta-model

	Mean (kN/m^2)	Standard deviation (kN/m^2)	Coefficient of variation (%)	Skewness	Kurtosis
MCS applied on the original deterministic model	1150.50	419.50	36.46	1.06	1.82
MCS applied on the meta-model	1150.60	418.30	36.35	1.05	1.78

4.3. Global sensitivity analysis *via* PCE-based Sobol indices

As mentioned previously, Sobol indices provide a measure of the contribution of each random variable to the variability of the system response. The Sobol indices of the soil cohesion SU_c and the soil friction angle SU_φ were calculated and were found equal to 0.1025 and 0.8975 respectively. This means that, for the statistical moments of the input uncertain parameters considered in this paper, the soil friction angle has a significant weight in the variability of the ultimate bearing capacity. However, the soil cohesion has a relatively small weight in the variability of this response. This conclusion is in conformity with that found in chapter 3 using the CSRSM.

4.4. Reliability index, design point and partial safety factors

As mentioned in chapter 1, the Hasofer-Lind reliability index β_{HL} is a mean by which the safety of a given geotechnical system is measured. It represents the minimum distance between the origin and the limit state surface G=0 in the standard space of uncorrelated random variables. In this chapter, the computation of β_{HL} is performed by using the PCE. The point (c^*, φ^*) resulting from the minimization is called the design point. It is the most probable failure point corresponding to a given q_a value.

Table (4.4) presents the reliability index, the design point and the corresponding partial safety factors ($F_c = \mu_c / c^*$, $F_\varphi = \tan(\mu_\varphi) / \tan\varphi^*$) for different q_a values. This table also presents the punching safety factor $F_p=q_u/q_a$ where q_u is the deterministic ultimate bearing capacity (q_u=1071.72kN/m^2). Notice that all the results presented in Table (4.4) are obtained using only one SS computation (when q_a=325kN/m^2). These results are accurate since they correspond to q_a values larger than 325kN/m^2 which means that the corresponding limit state surfaces are included in the sampling zone. This is ensured by the fact that the distance between the origin and the farthest collocation point in the standard space of random variables is d_{max}=5.04. This distance is larger than all values of β_{HL} presented in this table. From Table (4.4), one can observe that the increase in q_a increases the values of c^* and φ^* at the design point. However, the reliability index and the partial safety factors F_c and F_φ decrease with the increase in q_a. This is to be expected since the increase in the footing pressure decreases the footing safety and thus provides smaller resistance factors. Notice that for the punching safety factor F_p=3 which is generally used in practice, the corresponding partial safety factors F_c and F_φ are respectively 1.34 and 1.44. These values are somewhat close to those provided by Eurocode 7 where F_c and F_φ are respectively equal to 1.4 and 1.25. Finally, it should be emphasized that these results could not be obtained using the SS approach since this method does not provide an analytical expression of the system response (or the limit state surface). They are obtained with the use of the SS approach combined with the polynomial chaos expansion methodology.

Table 4.4: Punching safety factor, reliability index, design point and partial safety factors for different values of the footing applied pressure q_a

q_a(kN/m^2)	$F_p=q_u/q_a$	β_{HL}	c^*(kN/m^2)	φ^*(^{o})	F_c	F_φ
325	3.30	3.48	14.51	20.04	1.38	1.58
350	3.06	3.25	14.88	20.67	1.35	1.53
357.24	3.00	3.19	14.98	20.84	1.34	1.51
375	2.86	3.04	15.23	21.26	1.31	1.48
400	2.68	2.84	15.56	21.81	1.29	1.44
425	2.52	2.65	15.86	22.35	1.26	1.40
450	2.38	2.48	16.14	22.84	1.24	1.37
475	2.26	2.31	16.39	23.31	1.22	1.34
500	2.14	2.16	16.63	23.76	1.20	1.31
525	2.04	2.01	16.85	24.18	1.19	1.29
550	1.95	1.88	17.06	24.58	1.17	1.26
575	1.86	1.75	17.25	24.96	1.16	1.24
600	1.79	1.62	17.43	25.33	1.15	1.22
625	1.71	1.51	17.59	25.67	1.14	1.20
650	1.65	1.39	17.75	26.00	1.13	1.18
675	1.59	1.29	17.90	26.32	1.12	1.17
700	1.53	1.19	18.05	26.63	1.12	1.15

4.5. Reliability-based analysis and design

Figure (4.7) presents two fragility curves in the normal and semi-log scales. These curves provide the variation of the failure probability with the allowable footing pressure q_a where $q_a=P_u/(bxF_p)$ when the random variables are non-normal and uncorrelated (the punching safety factor F_p was taken equal to 3 in this study). These curves can be used to perform either a reliability-based design or a reliability-based analysis. Concerning the RBD, if for example a strip footing is required to support a service load of 500kN with a prescribed failure probability of 10^{-3}, from Figure (4.7b), the allowable footing pressure is equal to q_a=125kN/m^2. Consequently, the required footing breadth for a service load of 500kN/m is $b=P_a/q_a$=500/125=4m. For the reliability-based analysis, Figure (4.7b) provides the failure probability of a strip footing subjected to a given service load. For instance, if a footing of breadth b=2m is subjected to a service load of P_a=250kN/m (i.e. subjected to an allowable pressure of q_a=250/2=125kN/m^2), the corresponding failure probability is equal to 10^{-3}.

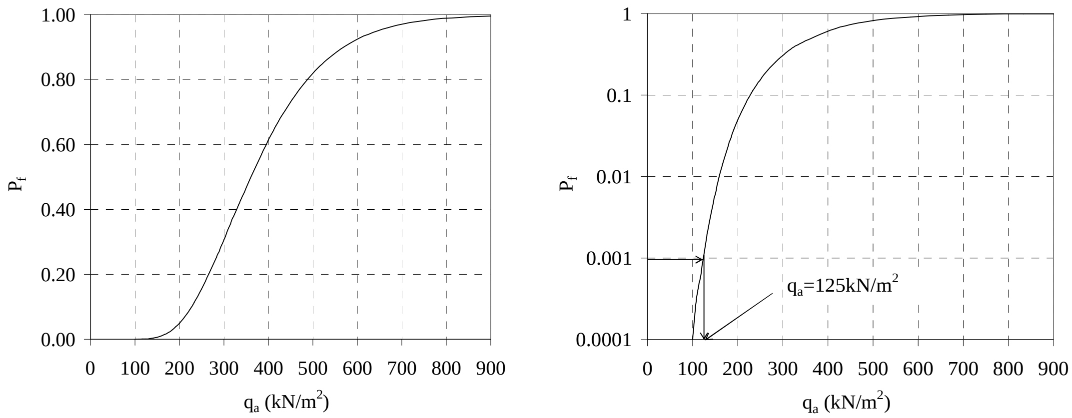

a. normal scale   b. semi-log scale

Figure 4.7: Fragility curve in the case of uncorrelated non-normal random variables using a) normal scale and b) semi-log scale

Finally notice that only one SS calculation was performed to compute the fragility curves in Figure (4.7). This calculation corresponds to the smallest value of q_a. However; for larger q_a values, MCS methodology was applied on the obtained PCE to calculate the failure probability with no additional deterministic calculations. This demonstrates once again the interest of the extension of the SS approach.

4.6. Parametric study

The aim of this section is to investigate the effect of the statistical characteristics (coefficient of variation *COV*, coefficient of correlation ρ and the type of the probability density function) of the random variables on the system response (ultimate bearing capacity).

4.6.1. Effect of the coefficients of variation (*COVs*) of the random variables

This section presents the effect of COV_c and COV_φ on (i) the PDF of the system response and the corresponding statistical moments and (ii) the Sobol indices SU_c and SU_φ.

Notice that, in order to investigate the effect of *COV* of a certain random variable, its *COV* is increased or decreased by 50% with respect to its reference value; however, the *COV* of the other random variable remains constant.

Figures (4.8a and 4.8b) present respectively the effect of COV_c and COV_φ on the PDF of the system response. The corresponding values of the statistical moments are given in Table 4.5. This table also provides the effect of COV_c and COV_φ on the Sobol indices.

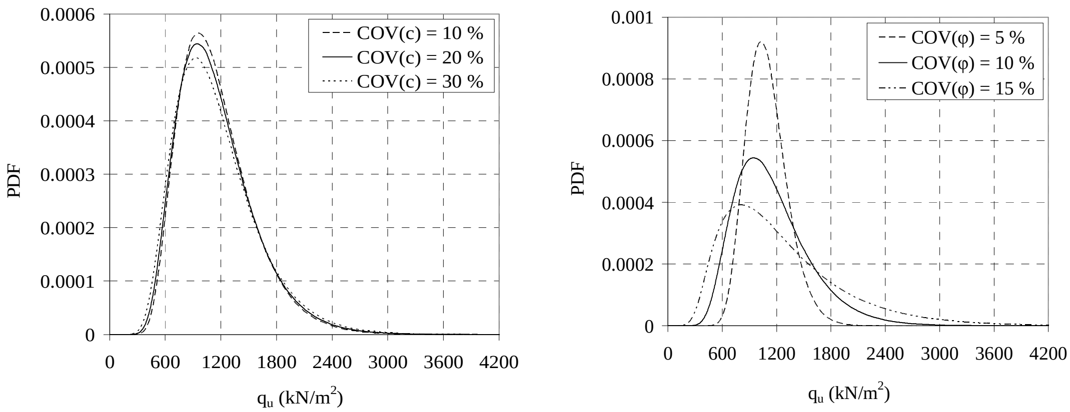

a. effect of COV_c **b.** effect of COV_φ

Figure 4.8: Effect of the coefficient of variation of random variables on the PDF of the ultimate bearing capacity

From these results, one can observe that COV_c has a negligible effect on the mean value, skewness and kurtosis of the system response; however, it has a small effect on the variability of this response. For instance, an increase in COV_c by 50% with respect to its reference value increases the *COV* of the system response by only 6.9%. Concerning COV_φ, it was found to have a significant effect on the mean value, skewness and kurtosis of the system response. Also, similar to the results obtained in chapter 2, the variability of the system response was found to be very sensitive to the variability of the soil friction angle (an increase in COV_φ by 50% with respect to its reference value increases the *COV* of the system response by 48.9%). One may observe that the random variable for which the *COV* is of a significant influence on the variability of the system response (i.e. φ) is the one that has the greater value of Sobol index. Remember here that φ has a Sobol index of 0.8975 while c has a Sobol index of 0.1025 for the reference case studied before. Finally, Table (4.5) shows that the increase in *COV* of a given random variable increases its Sobol index (i.e. its weight in the variability of the system response) and decreases the Sobol index of the other random variable. This means that the increase in the *COV* of a certain parameter increases its weight in the variability of the system response and decreases the weight of the other parameter in the variability of this response. These observations agree well with the results obtained in chapter 3 of this thesis.

Table 4.5: Effect of the coefficients of variation of the soil cohesion (COV_c) and the soil friction angle (COV_φ) on the statistical moments of the ultimate bearing capacity and on Sobol indices

COV(%)		Mean Value of q_u (kN/m^2)	Standard deviation of q_u (kN/m^2)	Coefficient of variation of q_u (%)	Skewness of q_u	Kurtosis of q_u	Sobol indices	
							SU_c	SU_φ
COV_c (%)	10	1151.05	402.21	34.94	1.04	1.75	0.0278	0.9722
	20	1150.60	418.30	36.35	1.05	1.78	0.1025	0.8975
	30	1149.08	446.52	38.86	1.10	1.98	0.2030	0.7970
COV_φ (%)	5	1091.51	225.00	20.61	0.56	0.56	0.3320	0.6680
	10	1150.60	418.30	36.35	1.05	1.78	0.1025	0.8975
	15	1256.11	680.05	54.14	1.51	3.66	0.0431	0.9569

4.6.2. Effect of the correlation and the distribution type of the random variables

Figure (4.9) shows the effect of the correlation and the non-normality of the random variables on the PDF of the ultimate bearing capacity and Table (4.6) shows the corresponding statistical moments. These results indicate that the mean value is very slightly affected by both the correlation and the non-normality of the random variables. The results also indicate that both assumptions of non-normal variables and negative correlation between these variables slightly decrease the variability of the system response. For instance, the assumption of non-normal random variables decreases the *COV* of the system response by 1.9% and 4.7% respectively for correlated and uncorrelated random variables. On the other hand, the negative correlation decreases the *COV* of the system response by 4.5% and 1.8% respectively for the cases of normal and non-normal random variables. Concerning the skewness and kurtosis, , they were found to decrease with both the negative correlation and the assumption of non-normal random variables. As a conclusion, these results indicate that the case of normal uncorrelated random variables is conservative since it provides the largest variability of the ultimate bearing capacity. This conclusion is in conformity with that obtained in chapter 2 of this thesis.

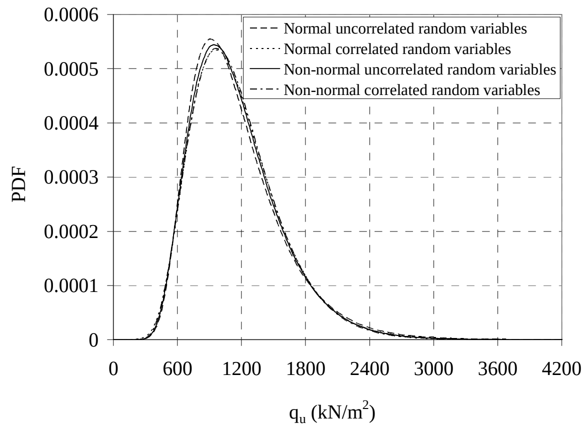

Figure 4.9: Effect of the correlation between random variables and the type of the probability density function of these variables on the PDF of the ultimate bearing capacity

Table 4.6: Effect of the correlation between the random variables and the type of the probability density function of these variables on the statistical moments of the ultimate bearing capacity

Type of the probability density function and correlation	Mean valueof q_u (kN/m^2)	Standard deviation of q_u (kN/m^2)	Coefficient of variation of q_u (%)	Skewness	Kurtosis
Normal uncorrelated variables	1150.51	438.75	38.14	1.28	2.69
Normal correlated variables	1151.09	419.11	36.41	0.96	1.58
Non-normal uncorrelated variables	1150.60	418.30	36.35	1.07	1.78
Non-normal correlated variables	1150.53	410.85	35.71	0.96	1.43

5. Conclusion

This chapter presents an efficient procedure that allows one to increase the number of the probabilistic outputs of the SS approach with no additional time cost. In this procedure, the SS approach was combined with the Collocation-based stochastic response surface method (CSRSM). The combination was carried out by using the different realisations of random variables generated by the SS approach (for which the system response values are already computed by the SS approach) as collocation points in the CSRSM. This procedure was illustrated through the probabilistic analysis at ULS of a strip footing resting on a (c, φ) soil and subjected to a vertical load P_a. The shear strength parameters c and φ were modeled by random variables. The ultimate bearing capacity q_u was used to represent the system response. In addition to the failure probability computed by the SS approach, the proposed procedure provided the PDF of the ultimate bearing capacity with no additional calls of the deterministic model. Moreover, it provided the Sobol indices to evaluate the contribution of each random variable to the variability of the ultimate bearing capacity. Finally, the failure probabilities corresponding to P_a values greater than the original one used in the SS computation were easily calculated. The main results obtained from the numerical example can be summarized as follows:

1- The PDF of the ultimate bearing capacity and its corresponding statistical moments, as determined by the proposed procedure, have shown a good agreement with those obtained by applying MCS methodology on the original deterministic model.

2- The failure probabilities computed by the proposed procedure and corresponding to q_a values larger than the original one used to perform a SS computation agree well with those computed by applying MCS methodology on the original deterministic model.

3- The global sensitivity analysis based on the PCE-based Sobol indices has shown that the soil friction angle has a significant weight in the variability of the ultimate bearing capacity (S_φ=0.8975); however, the soil cohesion has a relatively small weight in the variability of this response (S_c=0.1025). This conclusion is valid for the values of the soil uncertainties considered in this thesis which are the ones frequently encountered in practice for a (c, φ) soil.

4- The increase in the footing pressure q_a increases the values of c and φ at the design point. However, the reliability index β_{HL} and the partial safety factors F_c and F_φ decrease with the increase in the footing pressure. This is to be expected since the increase in the footing pressure decreases the safety of the soil-footing system.

5- A fragility curve which can be used to perform either a reliability analysis or a reliability based design of the strip footings was presented. Concerning the reliability analysis, this curve provides the failure probability of a strip footing subjected to a given service load. For the reliability-based design, it allows one to calculate the footing breadth required to support a given service load for a target failure probability.

6- A parametric study has shown that:

a) The increase in COV_φ considerably increases the variability of the system response; however, the increase of COV_c has a small effect on this variability.

b) The random variable for which the *COV* is of a significant influence on the variability of the system response (i.e. φ) is the one that has the greater value of Sobol index.

c) The increase in *COV* of a given random variable increases its Sobol index and decreases the Sobol index of the other random variable. This means that the increase in the COV of a certain parameter increases its weight in the variability of the system response and decreases the weight of the other parameter.

d) The variability of the system response was found to decrease with the assumption of non-normal variables with respect to the case of normal variables. This variability also decreases when considering negative correlation between random variables as compared to the case of uncorrelated variables.

PART II

ADVANCED PROBABILISTIC ANALYSIS OF SHALLOW FOUNDATIONS

CHAPTER 5

PROBABILISTIC ANALYSIS OF FOOTINGS RESTING ON A SPATIALLY VARYING SOIL USING SUBSET SIMULATION (SS) APPROACH

1. Introduction

The probabilistic analysis of geotechnical structures presenting spatial variability in the soil properties is generally performed using Monte Carlo simulation (MCS) methodology. This methodology is not suitable for the computation of a small failure probability because it becomes very time-expensive in such a case due to the large number of simulations required to calculate the failure probability. For this reason, only the mean value and the standard deviation of the system response were extensively investigated in literature. Au and Beck (2001) proposed the subset simulation (SS) approach as an alternative to MCS methodology to calculate the small failure probabilities. Except Au *et al*. (2010) and Santoso *et al*. (2011) who applied the SS approach to one-dimensional (1D) random field problems, the SS method was mainly applied in literature to problems where the uncertain parameters are modeled by random variables.

In the present chapter, the subset simulation method is employed to perform a probabilistic analysis at the serviceability limit state (SLS) of a rigid strip footing resting on a soil with a two-dimensional (2D) spatially varying Young's modulus and subjected to an axial vertical load (P_s). Notice that most previous studies that considered the soil spatial variability have modeled the uncertain parameters by isotropic random fields [e.g. Fenton and Griffiths (2003), Popescu *et al*. (2005), Griffiths *et al*. (2006), Sivakumar *et al*. (2006) and Soubra *et al*. (2008) at ULS and Fenton and Griffiths (2002, 2005) and Fenton *et al*. (2003) at SLS]. However, due to the layered nature of soils, their parameters generally exhibit a larger autocorrelation length in the horizontal direction compared to that in the vertical direction. Thus, the Young's modulus is considered herein as an anisotropic random field. The Karhunen-Loeve (K-L) expansion is used to discretize the random field. The deterministic model employed for the computation of the system response is based on numerical simulations using the commercial software FLAC^{3D}. It should be emphasized here that the soil spatial variability causes uneven footing displacement. Due to its high rigidity, the footing undergoes a linear vertical displacement. Thus, the average value of the footing vertical displacement is considered herein to represent the system response. This average is equal to the vertical displacement at the footing center.

After the presentation of the method of computation of the failure probability by the SS approach in the case of a random field problem, the probabilistic analysis of a strip footing resting on a spatially varying soil and the corresponding results are presented and discussed. The chapter ends with a conclusion.

2. Method of computation of the failure probability by the SS approach in case of a spatially varying soil property

As mentioned previously, this chapter aims at employing the SS methodology for the computation of the failure probability in the case of a spatially varying soil property modeled by a random field. The random field was discretized in this chapter using the K-L expansion. In order to calculate the failure probability, a link between the SS approach and the K-L expansion was performed. It should be emphasized here that the K-L expansion includes two types of parameters (deterministic and stochastic) as follows:

$$E(X,\theta) \approx \mu_E + \sum_{i=1}^{M} \sqrt{\lambda_i}\phi_i(X)\xi_i(\theta) \tag{5.1}$$

The deterministic parameters are the eigenvalues and eigenfunctions λ_i and ϕ_i of the covariance function. The role of these parameters is to ensure the correlation between the values of the random field at the different points in the space. On the other hand, the stochastic parameters are represented by the vector of the standard normal random variables $\{\xi_i\}_{i=1,\ldots,M}$. The role of these parameters is to ensure the random nature of the uncertain parameter. The link between the SS approach and the K-L expansion was performed through the vector $\{\xi_i\}_{i=1,\ldots,M}$. This ensures that the subset simulation technique does not affect the correlation structure of the random field.

The basic idea of the link is that for a given random field realisation obtained by K-L expansion, the vector $\{\xi_i\}_{i=1,\ldots,M}$ represents a sample 's' of the subset simulation method for which the system response is calculated in two steps. The first step is to substitute the vector $\{\xi_i\}_{i=1,\ldots,M}$ in the K-L expansion to calculate the values of the random field at the centers of the different elements of the deterministic mesh according to their coordinates. The second step is to use the deterministic model to calculate the corresponding system response. The algorithm of the subset simulation approach in case of a spatially varying soil property is an extension of the algorithm presented in the previous chapter. It can be described as follows:

1. Choose the number M of terms of K-L expansion. This number must be sufficient to accurately represent the target random field.
2. Generate a vector of (M) standard normal random variables $\{\xi_1, \ldots, \xi_i, \ldots, \xi_M\}$ by direct Monte Carlo simulation.
3. Substitute the vector $\{\xi_1, \ldots, \xi_i, \ldots, \xi_M\}$ in the K-L expansion to obtain the first realisation of the random field. Then, use the deterministic model to calculate the corresponding system response.
4. Repeat steps 2 and 3 until obtaining a prescribed number N_s of realisations of the random field and their corresponding values of the system response. Then, evaluate the

corresponding values of the performance function to obtain the vector G_0 where $G_0 = \{G_0^1, ..., G_0^k, ..., G_0^{Ns}\}$. Notice that the values of the performance function of the different realizations are arranged in an increasing order in the vector G_0. Notice also that the subscripts '0' refer to the first level (level 0) of the subset simulation approach.

5. Prescribe a constant intermediate conditional failure probability p_0 for all the failure regions F_j (j=1, 2, …, m) and evaluate the first failure threshold C_1 which corresponds to the failure region F_1 where C_1 is equal to the $[(N_s \text{x} p_0)+1]^{th}$ value in the increasing list of elements of the vector G_0. This ensures that the value of $P(F_1)$ will be equal to the prescribed p_0 value.
6. Among the N_s realisations, there are $[N_s \text{x} p_0]$ ones whose values of the performance function are less than C_1 (i.e. they are located in the failure region F_1). The corresponding vectors of standard normal random variables $\{\xi_1, …, \xi_i, ..., \xi_M\}$ of these realisations are used as 'mother vectors' to generate additional $[(1-p_0)N_s]$ vectors of standard normal random variables $\{\xi_1, …, \xi_i, ..., \xi_M\}$ using Markov chain method based on Metropolis-Hastings algorithm. These new vectors are substituted in the K-L expansion to obtain the random field realisations of level 1.
7. The values of the performance function corresponding to the realisations of level 1 are listed in an increasing order and are gathered in the vector of performance function values $G_1 = \{G_1^1, ..., G_1^k, ..., G_1^{Ns}\}$.
8. Evaluate the second failure threshold C_2 as the $[(N_s \text{x} p_0)+1]^{th}$ value in the increasing list of the vector G_1.
9. Repeat steps 6-8 to evaluate the failure thresholds C_3, C_4, …, C_m corresponding to the failure regions F_3, F_4, …, F_m. Notice that contrary to all other thresholds, the last failure threshold C_m is negative. Thus, C_m is set to zero and the conditional failure probability of the last level $P(F_m/F_{m-1})$ is calculated as:

$$P(F_m|F_{m-1}) = \frac{1}{N_s}\sum_{k=1}^{Ns} I_{F_m}(s_k) \qquad (5.2)$$

where $I_{F_m}=1$ if the performance function $G(s_k)$ is negative and $I_{F_m}=0$ otherwise.

10. Finally, the failure probability $P(F)$ is evaluated as follows:

$$P(F) = P(F_1) x \prod_{j=2}^{m} P(F_j|F_{j-1}) \qquad (5.3)$$

It should be mentioned that, a normal PDF was used herein as a target probability density function P_t. However, a uniform PDF was used as a proposal probability density function P_p. The intermediate failure probability p_0 of a given level j (j=1, 2, …,m) was chosen equal to 0.1. It should also be mentioned that the modified Metropolis-Hastings algorithm proposed by Santoso *et al*. (2011) was used in this chapter. Remember that this algorithm is presented in Appendix F. The next section is devoted to the presentation of the probabilistic analysis of strip footings resting on a spatially varying soil using the subset simulation approach.

3. Probabilistic analysis of strip footings

The probabilistic analysis of shallow foundations resting on a spatially varying soil has been extensively considered in literature [e.g. Fenton and Griffiths (2003), Pula and Shahrour (2003), Popescu *et al*. (2005), Griffiths *et al*. (2006), Sivakumar *et al*. (2006) and Soubra *et al*. (2008) at ULS and Fenton and Griffiths (2002, 2005) and Fenton *et al*. (2003) at SLS]. These authors have used MCS methodology to perform the probabilistic analysis. In these studies, the mean value and the standard deviation of the system response were extensively investigated. This was not the case for the failure probability because MCS methodology requires a large number of calls of the deterministic model to accurately calculate a small failure probability.

This chapter presents a probabilistic analysis at SLS of a strip footing resting on a spatially varying soil using the SS approach. The objective is the computation of the probability P_e of exceeding a tolerable vertical displacement under a prescribed footing load. A footing of breadth b=2m that is subjected to a central vertical load P_a=1000kN/m (i.e. an applied uniform vertical pressure q_a=500kN/m^2) was considered in the analysis. The Young's modulus was modeled by a random field and it was assumed to follow a log-normal probability density function. The mean value and the coefficient of variation of the Young's modulus were respectively μ_E=60MPa and COV_E=15%. An exponential covariance function was used in this study to represent the correlation structure of the random field. The random field was discretized using K-L expansion. Although an isotropic random field is often assumed in literature [e.g. Fenton and Griffiths (2002, 2005), Fenton *et al*. (2003)], the vertical autocorrelation length tends to be shorter than the horizontal one due to the geological soil formation process for most natural soil deposits (Cho and Park 2010). A common ratio of about 1 to 10 for these autocorrelation lengths can be used (Baecher and Christian 2003). Notice however that in this chapter, other values of this ratio were studied and analyzed in order to explore some interesting features related to the autocorrelation lengths.

The performance function used to calculate the probability P_e of exceeding a tolerable vertical displacement was defined as follows:

$$G=\delta v_{max}-\delta v \qquad (5.4)$$

where δv_{max} is a prescribed tolerable vertical displacement of the footing center and δv is the vertical displacement of the footing center due to the applied pressure q_a.

3.1. Deterministic model

The deterministic model used to calculate the footing vertical displacement δv was based on the commercial numerical code FLAC^{3D}. For this calculation, a footing of width *b* that rests on a soil domain of width *B* and depth *H* was considered in the analysis (Figure 5.1). In contrast to the case of random variables where only one-half of the soil domain (and consequently one-half of the footing) shown in Figure (5.1) may be considered in the analysis, the entire soil domain shown in Figure (5.1) was considered herein. This is because the random field creates non-symmetrical soil movement. An optimal non-uniform but symmetrical mesh composed of 750 zones was employed. The mesh was refined near the footing edges where high stress gradient may occur. For the displacement boundary conditions, the bottom boundary was assumed to be fixed and the vertical boundaries were constrained in motion in the horizontal directions. Although an SLS analysis is considered herein, the soil behavior was modeled by a conventional elastic-perfectly plastic model based on Mohr-Coulomb failure criterion in order to take into account the possible plastification that may occur near the edges of the foundation even under the service loads. On the other hand, the strip footing was modeled by a linear elastic model. It is connected to the soil *via* interface elements. The values of the different parameters of the soil, footing and interface are given in Table (5.1).

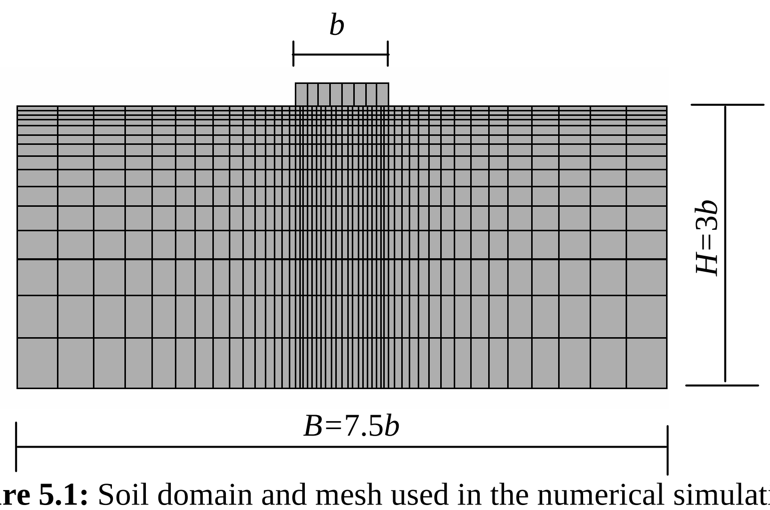

Figure 5.1: Soil domain and mesh used in the numerical simulations

In order to calculate the footing vertical displacement for a given random field realisation, (i) the vertical and horizontal coordinates of the center of each element of the mesh were calculated; then, the K-L expansion was used to calculate the value of the Young's modulus at the center of each element, (ii) geostatic stresses were applied to the soil, (iii) the obtained displacements were set to zero in order to obtain the footing displacement due to only the footing applied pressure and finally, (iv) the uniform vertical pressure was applied to the footing and the vertical displacement at the footing centre due to this pressure was calculated.

Table 5.1: Shear Strength and Elastic Properties of Soil, Footing, and Interface

Variable	Soil	Footing	Interface
C	20kPa	N/A	20kPa
φ	30^o	N/A	30^o
ψ=2/3 φ	20^o	N/A	20^o
E	60MPa	25GPa	N/A
ν	0.3	0.4	N/A
K_n	N/A	N/A	1GPa
K_s	N/A	N/A	1GPa

3.2. Probabilistic numerical results

This section aims at presenting the probabilistic numerical results. It is organized as follows: (i) the minimal number M of terms of K-L expansion corresponding to a prescribed accuracy was determined, (ii) the optimal number of realisations N_s per level of the SS approach was selected, (iii) a parametric study to investigate the effect of the horizontal and vertical autocorrelation lengths of the random field and its coefficient of variation on P_e was presented and discussed and finally, (iv) reliability-based design and analysis of strip footings based on some fragility curves were presented and discussed.

It should be mentioned that all subsequent probabilistic results are presented based on non-dimensional horizontal and vertical autocorrelation lengths $L_{ln\,x}$, $L_{ln\,y}$ where $L_{ln\,x}=l_{ln\,x}/b$ and $L_{ln\,y}=l_{ln\,y}/b$. In these expressions, $l_{ln\,x}$ and $l_{ln\,y}$ are respectively the horizontal and vertical lengths over which the values of the log-elastic modulus are highly correlated. The non-dimensionality of $L_{ln\,x}$ and $L_{ln\,y}$ was found to be valid only when the ratio between the depth H of the soil domain and the footing width b (i.e. H/b) is constant (H/b=3 in the present case). Concerning the breadth B of the soil domain, it was found to have no effect on the P_e value.

3.2.1. Optimal size of K-L expansion

As is well-known, the accuracy of the approximated random field depends on the size of the K-L expansion (i.e. the number of terms M). Figure (5.2) presents the error estimate of the approximated random field for the most critical configurations of $L_{ln\,x}$ and $L_{ln\,y}$ used in this chapter, i.e. for those requiring greater number of terms in the K-L expansion. These configurations correspond to [($L_{ln\,x}$=5 and $L_{ln\,y}$=0.25) and ($L_{ln\,x}$=2.5 and $L_{ln\,y}$=0.5)] in case of anisotropic random field and [($L_{ln\,x}$=$L_{ln\,y}$=0.5) and ($L_{ln\,x}$=$L_{ln\,y}$=1.5)] in case of isotropic random field.

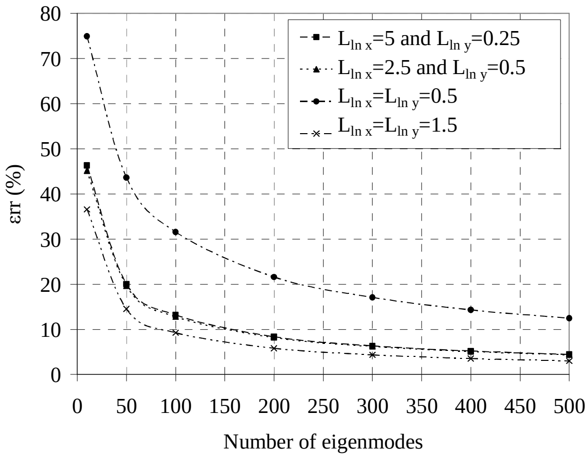

Figure 5.2: Error estimate versus the number of eigenmodes for different values of $L_{ln\,x}$ and $L_{ln\,y}$ when H/b=3

Figure (5.2) indicates that the error estimate decreases with the increase in the number of terms of the K-L expansion. From this figure, for M=100 terms, the error estimate is less than 13% for the previously mentioned cases except for the case of $L_{ln\,x}$=$L_{ln\,y}$=0.5 where $M \approx 500$ terms are required to obtain such a small error. Notice that the configurations used herein correspond to $L_{ln\,x}$ and $L_{ln\,y}$ values equal to or greater than the aforementioned configurations. As a conclusion, the number of terms of the K-L expansion will be set to M=100 terms for all the probabilistic calculations presented in this chapter except for the case of the isotropic random field when $L_{ln\,x}$ and $L_{ln\,y}$ are less than 1.5 where M will be set equal to 500 terms. This ensures that for all the configurations considered in this chapter, the error will be less than 13%.

3.2.2. Selection of the optimal number of realisations N_s per level of SS approach

The number of realisations N_s to be used per level of the SS approach should be sufficient to accurately calculate the P_e value. This number should be greater than 100 to provide a small bias in the calculated P_e value (Honjo 2008). In order to determine the optimal number of realisations N_s to be used per level, different values of N_s (50, 100, 150, 200 and 250 realisations) were considered to calculate P_e. A random field with $L_{ln\,x}$=5 and $L_{ln\,y}$=0.5 (called hereafter the reference case) was considered herein. Notice that the failure thresholds C_j of the different levels of the subset simulation were calculated and presented in Table (5.2) for the abovementioned values of N_s. This table indicates that the failure threshold decreases with the successive levels until reaching a negative value at the last level which means that the realisations generated by the subset simulation successfully progress towards the limit state surface G=0. Table (5.3) presents the P_e values and the corresponding values of the coefficient of variation for the different number of realizations N_s. As expected, the coefficient of variation of P_e decreases with the increase in the number of realizations N_s.

Table 5.2: Evolution of the failure threshold C_j with the different levels j of the SS approach and with the number of realisations N_s per level

Failure threshold C_j for each level j	Number of realisations N_s per level				
	50	100	150	200	250
C_1	0.0086	0.0077	0.0080	0.0076	0.0076
C_2	0.0058	0.0048	0.0050	0.0041	0.0040
C_3	0.0044	0.0015	0.0019	0.0011	0.0011
C_4	0.0017	-0.0019	-0.0007	-0.0020	-0.0018
C_5	-0.0015	-	-	-	-

Table 5.3: Values of P_e and COV_{Pe} versus the number N_s of realizations per level

	Number of realisations N_s per level				
	50	100	150	200	250
P_ex(10^{-4})	0.34	4.60	2.07	3.78	3.77
COV_{Pe}	0.92	0.71	0.60	0.51	0.38

For each N_s value, P_e computed by SS approach was compared to that obtained by MCS methodology using N=20,000 realisations. The comparison was carried out in Figure (5.3) at the different levels, i.e. at the different failure threshold C_j of the SS approach. Notice that for a given N_s value, the computation of P_e at a given level j of the SS approach is performed by using Equation (5.3) with the appropriate number of levels. On the other hand, in order to calculate P_e at this level by MCS methodology, the performance function is set equal to the corresponding failure threshold C_j. In this case, the failure region is defined by $G \leq C_j$ and the safety region is defined by $G > C_j$. Thus, the value of P_e at a given level j can be calculated as follows:

$$P(F_j) = \frac{1}{N}\sum_{k=1}^{N} I_{F_j}(G_k) \tag{5.5}$$

where G_k is the value of the performance function corresponding to the kth realisation of MCS with $I_F = 1$ if $G_k < C_j$ and $I_F = 0$ otherwise.

Figure (5.3a) shows that for the case where N_s=50 realisations, P_e calculated by the SS approach is different from that computed by MCS methodology for the different levels of the SS approach. This observation is in conformity with the recommendation by Honjo (2008) who suggested that the N_s value should be at least equal to 100. The difference between the P_e values calculated by the SS approach and those computed by MCS becomes smaller for larger N_s values (Figures 5.3b, 5.3c, 5.3d and 5.3e). For the cases where $N_s \geq 200$ realisations (Figures 5.3d and 5.3e), the failure probabilities calculated by subset simulation were found to be very close to those computed by MCS methodology for the different levels of the SS approach. Consequently, N_s=200 realisations will be considered in the subsequent probabilistic calculations. In this case, the final P_e value (i.e. $P(F_m)$) which corresponds to C=0 was equal to 3.78x10^{-4}. This value is to be compared to the value of 3.8x10^{-4} given by MCS. It should be mentioned here that, since p_0 was chosen to be equal to 0.1, 4 levels of subset simulation were found necessary to reach the limit state surface G=0 as may be seen from Table (5.2). Therefore, when N_s=200 realisations, a total number of realisations N_t=200+180x3=740 realisations were required to calculate the final P_e value. In this case, the COV of P_e computed by SS is equal to 0.51. Notice that if the same value of COV (i.e. 0.51) is desired by MCS to calculate P_e, the number of realisations would be equal to 12,000. This means that, for the same accuracy, the SS approach reduces the number of realisations by 93.8%. On the other hand, if one uses MCS with the same number of realisations (i.e. 740 realisations), the value of COV of P_e would be equal to 1.89. This means that for the same computational effort, the SS approach provides a smaller value of COV_{Pe} than MCS.

Although the computation time of the 20,000 realisations by MCS is significant (about 70 days), this number of realisations remains insufficient to assure an accurate P_e value with a small value of COV_{Pe}. The COV_{Pe} for 20,000 realisations by MCS was found about 0.4. As an alternative approach, one may determine the optimal N_s value by comparing the P_e values given by subset simulation for increasing N_s values. The N_s value beyond which P_e converges (i.e. slightly varies with the increase of N_s) is the optimal N_s value. In the present analysis, it was found that P_e converges when N_s=200 realisations. This is because the final P_e values (corresponding to C=0) are respectively equal to 3.78x10^{-4} and 3.81x10^{-4} for N_s=200 and 250 realisations. The corresponding values of COV_{Pe} are equal to 0.51 and 0.43 which indicates (as expected) that the COV_{Pe} decreases with the increase in the number of realisations. As a conclusion, this alternative procedure is recommended to determine the optimal N_s value for the probabilistic analysis based on the SS approach.

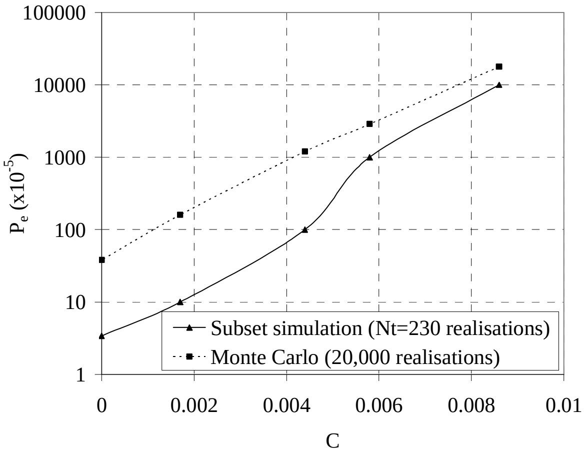

a. N_s=50 realisations per level

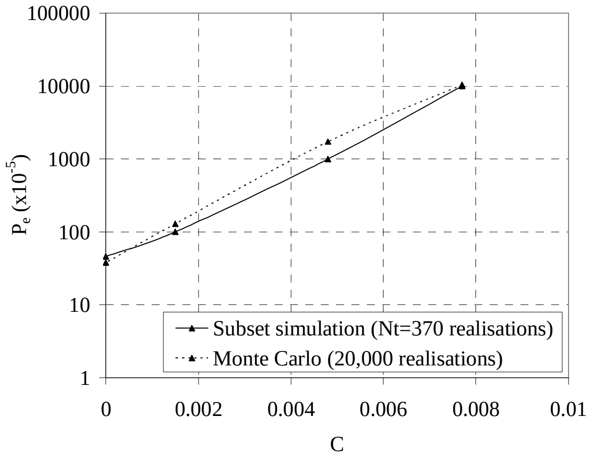

b. N_s=100 realisations per level

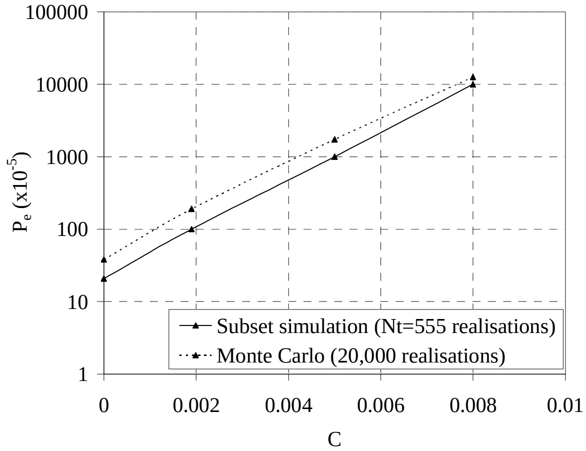

c. N_s=150 realisations per level

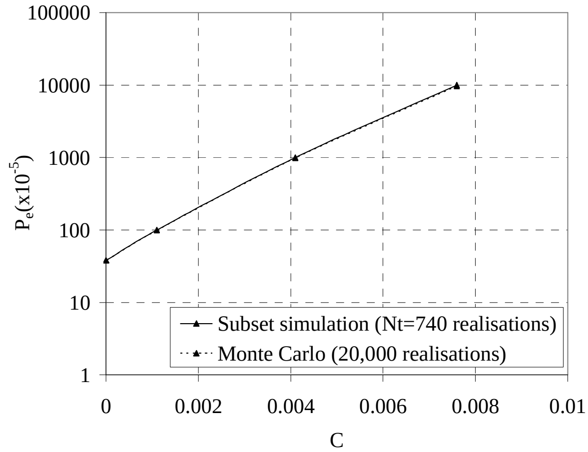

d. N_s=200 realisations per level

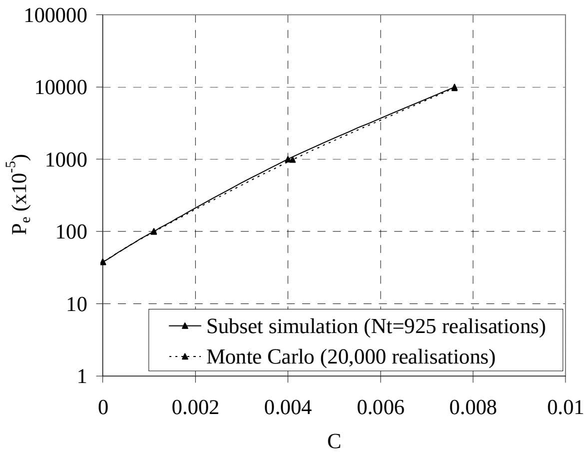

e. N_s=250 realisations per level

Figure 5.3: Comparison between the P_e values obtained by subset simulation and those obtained by MCS for five values of N_s ($\delta v_{max}/b$=2x10^{-2} and q_a=500kN/m^2)

3.2.3. Parametric study

In this section, a parametric study is performed to investigate the effect of the soil variability (coefficient of variation and autocorrelation lengths of the Young's modulus) on the P_e value.

Figure (5.4) shows the effect of the autocorrelation length on P_e in the case of an isotropic random field. This figure also shows (for the same value of the coefficient of variation) the value of P_e corresponding to the case of a homogeneous soil. In this case, P_e was calculated based on the assumption that, for a given realisation, each element of the deterministic grid was affected the same random value of the Young's modulus (i.e. the Young's modulus was modeled as a random variable and not as a random field). Figure (5.4) indicates that the increase in the autocorrelation length ($L_{ln\ x}= L_{ln\ y}$) increases the P_e value. However, the rate of increase gets smaller for the large values of the autocorrelation lengths (when $L_{ln\ x}=L_{ln\ y}>50$) to attain an asymptote corresponding to the case of a homogeneous soil (see Figure 5.5a). Remember that in the case of a homogeneous soil, the Young's modulus is randomly chosen (for each realisation) from a PDF and thus, it may vary in a wide range which results in some realisations with small value of the Young's modulus. These realisations lead to high values of the footing vertical displacement and thus, they lead to a high probability to exceed the tolerable footing vertical displacement. On the other hand, for small values of the autocorrelation length, one obtains a soil heterogeneity which results in a variety of values of the Young's modulus in the entire soil domain (Figure 5.5b). In this case, the soil under the footing contains some zones with high values of the Young's modulus and other zones with small values of the Young's modulus (i.e. a mixture of stiff zones and soft zones). Due to the high footing rigidity, the footing displacement is resisted by the stiff soil zones under it; the soft soil zones under the footing being of little effect in this case. This leads to a small value of the footing vertical displacement and consequently to a small probability of exceeding the prescribed tolerable footing vertical displacement. This phenomenon is most significant for the very small values of the autocorrelation length.

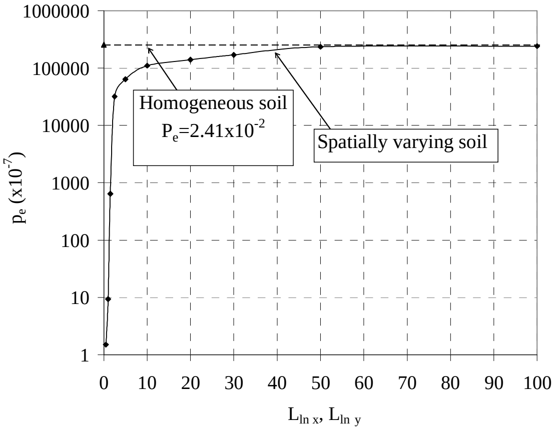

Figure 5.4: Effect of the autocorrelation length on P_e in case of an isotropic random field ($\delta v_{max}/b$=2x10^{-2} and q_a=500kN/m^2)

As a conclusion, for a given value of the coefficient of variation, modeling the Young's modulus as a random variable rather than a random field is conservative (Fenton and Griffiths 2002, 2005). This is because the settlement predicted when assuming a homogeneous soil may be much larger than that of a real soil for which the parameters vary spatially.

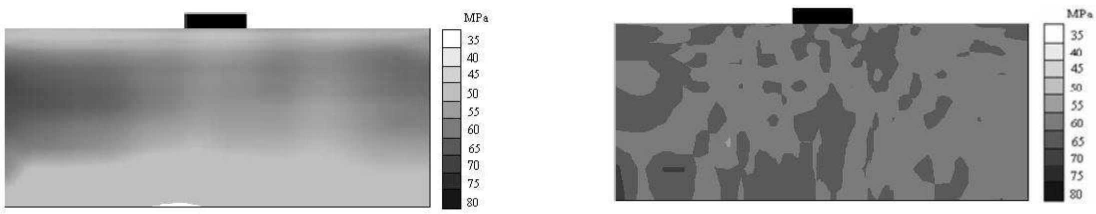

a. $L_{ln\ x}$=$L_{ln\ y}$=100 b. $L_{ln\ x}$=$L_{ln\ y}$=0.1

Figure 5.5: Grey-scale representation of the random field for two values of the autocorrelation length in case of an isotropic random field

In order to investigate the effect of the anisotropy of the random field, P_e was computed and plotted versus the non-dimensional horizontal and vertical autocorrelation lengths ($L_{ln\ x}$ and $L_{ln\ y}$) in Figures (5.6 and 5.7) respectively. Both figures show that P_e presents a maximum value at a certain ratio of $L_{ln\ x}$ to $L_{ln\ y}$. This observation can be explained as follows:

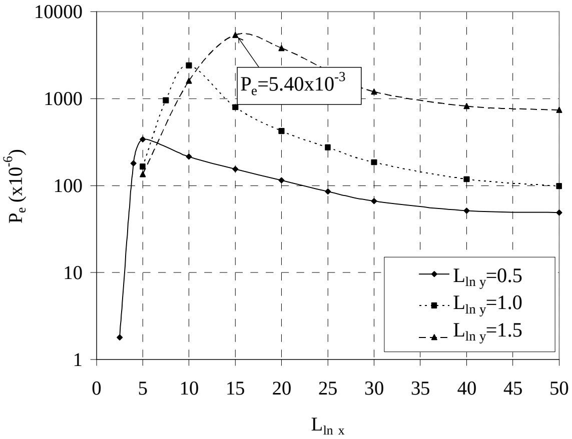

Figure 5.6: Effect of the horizontal autocorrelation length on P_e for different values of $L_{ln\ y}$ ($\delta v_{max}/b$=2x10^{-2} and q_a=500kN/m^2)

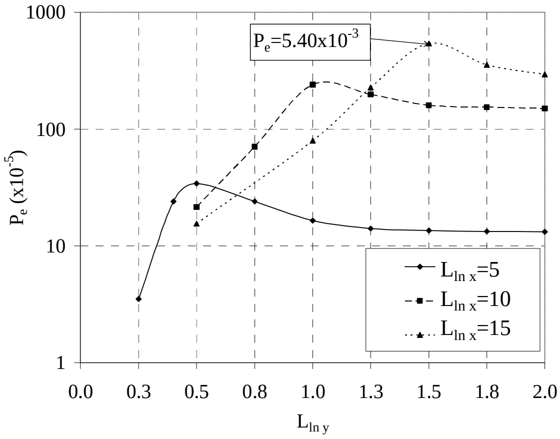

Figure 5.7: Effect of the vertical autocorrelation length on P_e for different values of $L_{ln\ x}$ ($\delta v_{max}/b$=2x10^{-2} and q_a=500kN/m^2)

Referring to Figure (5.6), the very small value of $L_{ln\ x}$ creates a vertical multilayer composed of thin sub-layers each of which may have either a high or a small value of the Young's modulus (Figure 5.8a). This variety of sub-layers leads to a small footing displacement and consequently to a small probability to exceed the tolerable displacement. The small footing displacement occurs because the rigid footing is resisted by the sub-layers having high values of Young's modulus beneath it; the sub-layers having small values of Young's modulus being of little effect in this case. On the other hand, when $L_{ln\ x}$ is very large, one obtains a horizontal multilayer for which each sub-layer may have either a high or a small value of the Young's modulus (Figure 5.8b). Notice that the P_e value seems to tend to the value corresponding to a one-dimensional random filed as $L_{ln\ x}$ gets larger and approaches infinity. To check this statement, the P_e value corresponding to the one-dimensional vertical random field and that corresponding to a very large value of $L_{ln\ x}$

(i.e. $L_{ln\ x}$=5000) were calculated for the three cases considered in Figure (5.6) (i.e. for $L_{ln\ y}$=0.5, 1 and 1.5) and were presented in Table (5.4) together with the other cases corresponding to the 2D random field. These results confirm that P_e tends to the value corresponding to the one-dimensional case as $L_{ln\ x}$ gets larger and approaches infinity and this value is smaller than the other values corresponding to the 2D random field.

a. $L_{ln\ x}$=0.1 and $L_{ln\ y}$=1.5

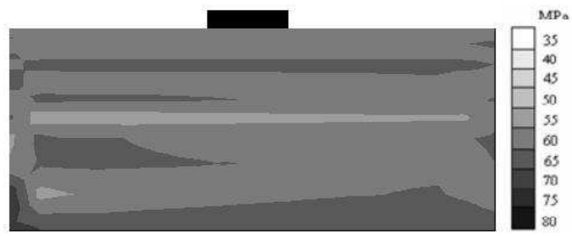

b. $L_{ln\ x}$=5000 and $L_{ln\ y}$=0.1

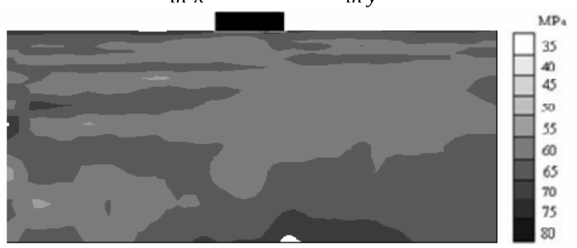

c. $L_{ln\ x}$=1.5 and $L_{ln\ y}$=0.1

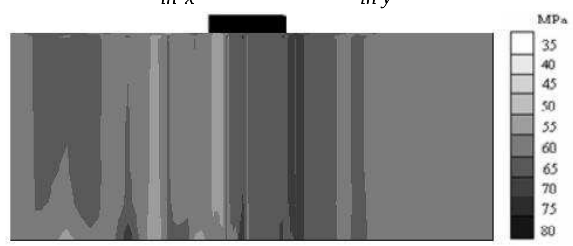

d. $L_{ln\ x}$=0.1 and $L_{ln\ y}$=5000

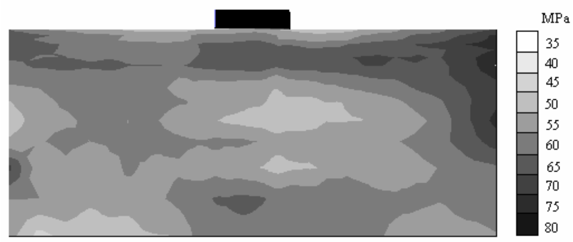

e. $L_{ln\ x}$=5 and $L_{ln\ y}$=0.5

Figure 5.8: Grey-scale representation of the random field for different values of the autocorrelation lengths in case of an anisotropic random field

The reason why the case of 1D random field presents a smaller P_e value with respect to the case of the 2D random field is that the uniform strong horizontal layers along the entire soil domain (because of the perfect correlation between the values of the Young's modulus in the horizontal direction) lead to smaller footing displacement and thus provide smaller values of P_e. Finally, for medium values of $L_{ln\ x}$, the soil contains a number of stiff zones adjacent to a number of soft zones whose areas are less extended in both the horizontal and the vertical directions compared to those corresponding to the case of small and high values of $L_{ln\,x}$ (Figure 5.8e). This leads to a larger footing displacement. As a result, P_e reaches its maximum value for these intermediate values of $L_{ln\,x}$.

Table 5.4: Effect of $L_{ln\,x}$ on P_e for different values of $L_{ln\,y}$

$L_{ln\,x}$	P_e		
	$L_{ln\,y}$=0.5	$L_{ln\,y}$=1.0	$L_{ln\,y}$=1.5
2.50	1.80×10^{-6}	-	-
4.00	1.79×10^{-4}	-	-
5.00	3.41×10^{-4}	1.65×10^{-4}	1.35×10^{-4}
10.00	2.15×10^{-4}	24.0×10^{-4}	1.60×10^{-3}
15.00	1.55×10^{-4}	7.95×10^{-4}	5.40×10^{-3}
20.00	1.15×10^{-4}	4.23×10^{-4}	3.80×10^{-3}
25.00	8.55×10^{-5}	2.75×10^{-4}	2.10×10^{-3}
30.00	6.65×10^{-5}	1.85×10^{-4}	1.20×10^{-3}
40.00	5.15×10^{-5}	1.19×10^{-4}	8.20×10^{-4}
50.00	4.90×10^{-5}	9.88×10^{-5}	7.40×10^{-4}
5000.00	3.20×10^{-5}	5.85×10^{-5}	3.65×10^{-4}
One-dimensional	2.45×10^{-5}	4.75×10^{-5}	2.45×10^{-4}

Referring to Figure (5.7), when $L_{ln\,y}$ is very small, one obtains a horizontal multilayer composed of thin sub-layers (Figure 5.8c). On the other hand, the large value of $L_{ln\,y}$ creates a vertical multilayer and makes the random field tend to the case of one-dimensional horizontal random field (Figure 5.8d). For medium values of $L_{ln\,y}$, the soil is composed of some zones with high values of Young’s modulus and other zones with small values of Young’s modulus (Figure 5.8e). For the three cases of small, intermediate or high values of $L_{ln\,y}$, the same explanation given before for Figure (5.6) remains valid herein.

As a conclusion, the soil configuration gradually changes from a vertical to a horizontal multilayer as $L_{ln\,x}$ increases. Similarly, the soil configuration gradually changes from a horizontal to a vertical multilayer as $L_{ln\,y}$ increases. The footing vertical displacement is the largest for medium values of $L_{ln\,x}$ or $L_{ln\,y}$ where the soil movement may occur more easily. Consequently, P_e presents a maximum value in this case.

Notice that the ratio of $L_{ln\,x}/L_{ln\,y}$ for which P_e is maximum depends on the values of the soil and footing parameters (i.e. μ_E, ν, b). For the case studied herein, this ratio is equal to 10. Notice finally that for the same ratio of $L_{ln\,x}/L_{ln\,y}$ but greater values of $L_{ln\,x}$ and $L_{ln\,y}$, the maximum value of P_e was found to be higher (Figures 5.6 and 5.7). This is due to the simultaneous increase of the autocorrelation lengths in both the vertical and the horizontal directions which makes the P_e tend to the value corresponding to the case of the random homogeneous soil that does not exhibit spatial variability. In this case, the P_e value is equal to $2.41\text{x}10^{-2}$ (Figure 5.4). This value is greater by more than one order of magnitude with respect to the maximum value of P_e given in Figures (5.6 and 5.7) which is equal to $5.4\text{x}10^{-3}$. This clearly illustrates, once again, the benefit of considering the soil spatial variability in the analysis.

The numerical results of Figures (5.6 and 5.7) also indicate that P_e is more sensitive to the vertical autocorrelation length. This is because the rate of change in P_e (i.e. rate of increase or decrease) when increasing the vertical autocorrelation length by a certain percentage is larger than that when increasing the horizontal autocorrelation length by the same percentage. For example, the increase in the vertical autocorrelation length by 100% with respect to the reference case (i.e. $L_{ln\,x}$=5 and $L_{ln\,y}$=0.5) decreases the value of P_e by 51.6%. However, the increase in the horizontal autocorrelation length by 100% with respect to the reference case decreases the value of P_e by only 36.9%.

The effect of the coefficient of variation of the Young's modulus on P_e was presented in Figure (5.9). This figure indicates that, for both cases of isotropic and anisotropic random fields, the increase in the coefficient of variation of the Young's modulus from

10% to 15% significantly increases the value of P_e. The increase is greater than one order of magnitude for both cases of isotropic and anisotropic autocorrelation lengths. This means that careful experimental investigations concerning the variability of this parameter are necessary to lead to reliable results.

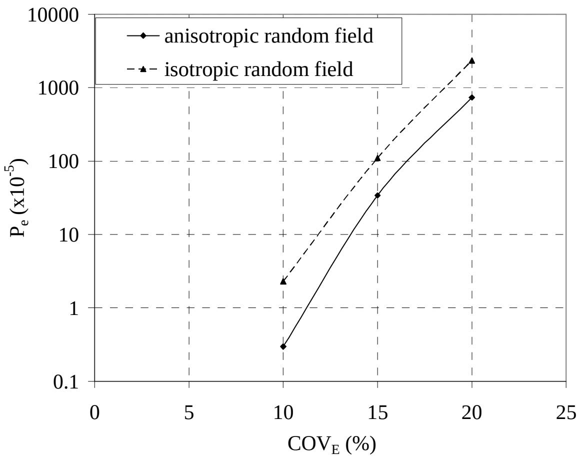

Figure 5.9: Effect of COV_E on the P_e value in case of (i) anisotropic random field with $L_{ln\,x}$=5 and $L_{ln\,y}$=0.5 and (ii) isotropic random field with $L_{ln\,x}$=$L_{ln\,y}$=5

3.2.4. Reliability-based design and analysis of strip footings

The probability that a certain level of damage (tolerable vertical displacement) will be exceeded under a given applied footing pressure can be expressed in the form of fragility curves (e.g. Popescu *et al*. 2005). Figure (5.10a) presents several fragility curves corresponding to three values of Poisson's ratio (0.25; 0.3 and 0.35) and to three levels of damage [(i) minor damage for which $\delta v_{max}/b$=1.5x10^{-2}, (ii) medium damage for which $\delta v_{max}/b$=2.0x10^{-2} and (iii) major damage for which $\delta v_{max}/b$=2.5x10^{-2}] for the reference case (i.e. $L_{ln\,x}$=5 and $L_{ln\,y}$=0.5). In this figure, the footing pressure was normalized with respect to the mean value of the Young's modulus and the three damage levels were normalized with respect to the footing breadth. The curves of Figure (5.10a) can be employed to perform either an SLS probabilistic analysis or an SLS probabilistic design of strip footings. For the probabilistic analysis, this figure allows one to determine the probability of exceeding a tolerable vertical displacement corresponding to a given value of the applied footing pressure, to a given value of μ_E, to a given value of Poisson's ratio and to a given value of the prescribed damage level. Concerning the footing design, Figure (5.10a) can be employed to determine the footing pressure (and consequently the footing breadth b) for a given load, for a given μ_E value, for a given value of Poisson's ratio, for a prescribed damage level and for a target probability of exceeding this damage level. Figure (5.10a) was plotted in a semi-log scale in Figure (5.10b) to clearly identify the small P_e values at the distribution tail. As an application example of these curves, if μ_E=60MPa, ν=0.3 and a medium damage with a target P_e value of 10^{-3} is allowed, q_a/μ_E=0.00833. Consequently, the footing pressure is q_a=0.00833x60x10^3=500kN/m^2. Hence the probabilistic footing breadth required to support a given footing applied load P_a can be calculated as $b=P_a/q_a$.

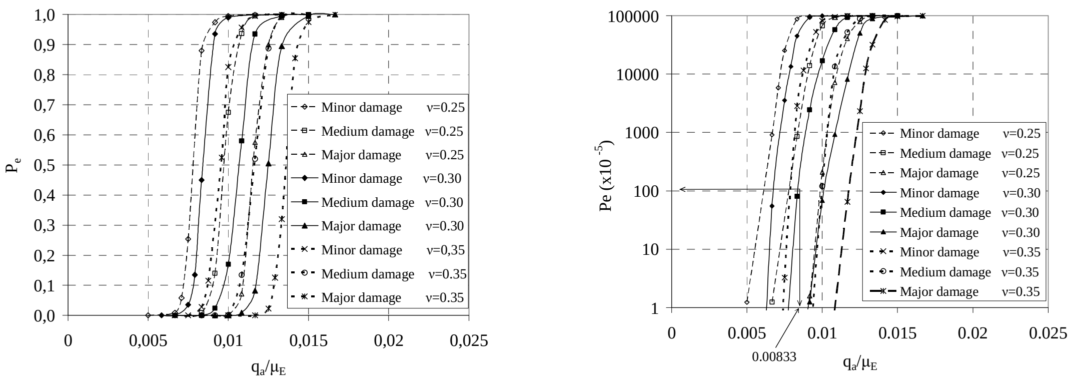

a. Normal scale **b.** Semi-log scale

Figure 5.10: Fragility curves for different values of ν and different damage levels

4. Conclusion

The probabilistic analysis of shallow foundations resting on a spatially varying soil was generally performed in literature using MCS methodology. The mean value and the standard deviation of the system response were extensively investigated. This was not the case for the failure probability because MCS methodology requires a large number of calls of the deterministic model to accurately calculate a small failure probability. This chapter fills this gap. It presents a probabilistic analysis at SLS of a strip footing resting on a soil with spatially varying Young's modulus using the subset simulation approach. The footing is subjected to a central vertical load. The vertical displacement of the footing center was used to represent the system response. The main findings of this chapter can be summarized as follows:

1- Validation of the results obtained by the SS approach

The probability P_e (probability of exceeding a tolerable vertical displacement) computed by the subset simulation approach was found very close to that computed by Monte Carlo Simulation methodology with a significant reduction in the number of calls of the deterministic model.

2 - Parametric study

a) In case of an isotropic random field, the probability P_e of exceeding a tolerable vertical displacement significantly increases with the increase in the autocorrelation length in the range of small to moderate values of the autocorrelation length. For large values of the autocorrelation length, P_e attains an asymptote. This asymptote was found too close to that of a homogeneous random soil (i.e. that corresponding to the case of a random variable). This clearly illustrates the benefit of considering the soil spatial variability in the analysis.

b) In case of an anisotropic random field, P_e presents a maximum value for a given ratio of the horizontal to the vertical autocorrelation length. For greater values of the horizontal and vertical autocorrelation lengths, the maximum value of P_e was found to be higher. When both the horizontal and the vertical autocorrelation lengths tend to infinity, one obtains the P_e value corresponding to the case of a random homogeneous soil. On the other hand, the numerical results have shown that P_e is more sensitive to the vertical autocorrelation length than the horizontal one.

d) The increase in the coefficient of variation of the Young's modulus was found to significantly increase the P_e value in both cases of isotropic and anisotropic random fields. The increase is greater than one order of magnitude for both cases of isotropic and anisotropic random fields when COV_E increases from 10% to 15%. This means that careful experimental investigations concerning the variability of this parameter are necessary to lead to reliable results.

CHAPTER 6

PROBABILISTIC ANALYSIS OF TWO NEIGHBOURING FOOTINGS RESTING ON A SPATIALLY VARYING SOIL USING AN IMPROVED SUBSET SIMULATION APPROACH

1. Introduction

In the previous chapter, the probabilistic analysis was performed using the subset simulation (SS) approach. Remember that in the first step of this approach, one should generate a given number of realisations of the uncertain parameters using the classical MCS technique. In the second step, one uses the Markov chain method based on Metropolis-Hastings (M-H) algorithm to generate realisations in the direction of the limit state surface (i.e. G=0). This step is repeated until reaching the limit state surface. It should be emphasized here that in case of a small failure probability, the limit state surface is located at a large distance from the mean value (i.e. the origin of the standard space of the uncertain parameters). Thus, the SS approach requires the repetition of the second step many times to reach the limit state surface. This increases the computation time and decreases the efficiency of the SS approach. To overcome this inconvenience, Defaux *et al*. (2010) proposed a more efficient method called "improved subset simulation (iSS)" approach. In this approach, the efficiency of the SS methodology is increased by replacing the first step of this method by a conditional simulation. In other words, instead of generating realisations directly around the origin by the classical MCS, the realisations are generated outside a hypersphere of a given radius. Consequently, the number of realisations required to reach the limit state surface is significantly reduced. Notice that Defaux *et al*. (2010) have employed the iSS to calculate the failure probability in the case where the uncertain parameters are modeled by random variables. In the present study, the iSS is employed in the case where the uncertain parameters are modeled by random fields.

This method is illustrated through the computation of the probability P_e of exceeding a tolerable differential settlement between two neighboring strip footings resting on a soil with a spatially varying Young's modulus. The footings are subjected to axial vertical loads with equal magnitude. The random field is discretized using the Karhunen-Loeve (K-L) expansion. The differential settlement between the two footings was used to represent the system response. The deterministic model used to compute the system response is based on numerical simulations using the commercial software FLAC^{3D}.

This chapter is organized as follows: the improved subset simulation (iSS) approach and its implementation in the case of random fields are first presented. This is followed by the probabilistic analysis of two neighboring strip footings resting on a soil with spatially varying Young's modulus. Then, a comparison between the results of the iSS approach and those of the classical SS approach is presented to illustrate the efficiency of the iSS approach with respect to the classical SS approach. Finally, a parametric study was performed to investigate the effect of the autocorrelation lengths on the P_e value in both cases of isotropic and anisotropic random fields. The chapter ends with a conclusion of the main findings.

2. Improved subset simulation (iSS) approach and its implementation in the case of random fields

Before the explanation of the iSS approach, it should be remembered that the failure probability by the classical SS approach is calculated as follows:

$$P(F) = P(F_1)\prod_{j=2}^{m} P(F_j | F_{j-1}) \tag{6.1}$$

where $P(F_1)$ is the failure probability corresponding to the first level of the SS approach, m is the number of levels required to reach the limit state surface and $P(F_j | F_{j-1})$ is an intermediate prescribed conditional failure probability.

The basic idea of the iSS approach is to replace the first step of the SS methodology (i.e. generating realisations directly around the origin by the classical MCS as shown in Figure 6.1) by a conditional simulation [Harbitz (1986) and Yonezawa *et al*. (1999)] in which the realisations are generated outside a hypersphere of a given radius R_h as shown in Figure (6.2). Based on this conditional simulation, the failure probability $P(F_1)$ corresponding to the first level is calculated as follows [Harbitz (1986) and Yonezawa *et al*. (1999)]:

$$P(F_1) = (1 - \chi_M(R_h^2))\frac{1}{N_s}\sum_{k=1}^{Ns} I_{F_1}(s_k) \tag{6.2}$$

where χ_n is the chi-square distribution with M degrees of freedom (M being the number of random variables) and $I_{F_1}(s_k)=1$ if $s_k \in F_1$ and $I_{F_1}(s_k)=0$ otherwise.

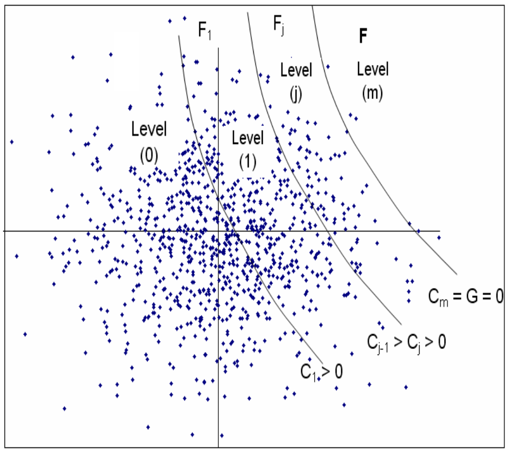

Figure 6.1: Nested failure domain

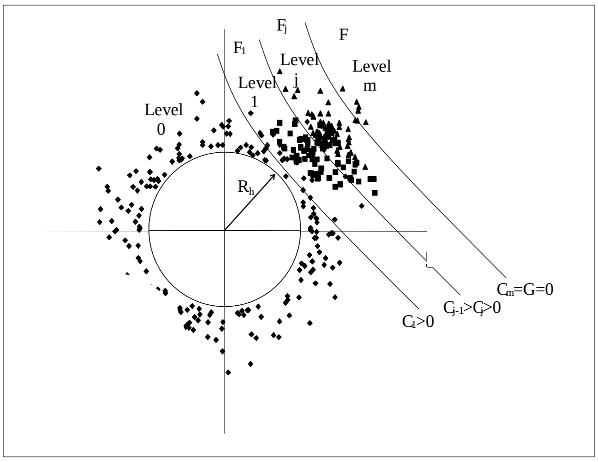

Figure 6.2: Samples generation outside a hypersphere of radius R_h

The advantage of using the conditional simulation is to generate realisations in the proximity of the limit state surface leading to a reduction in the number of realisations required to reach this surface. Notice finally that similar to the classical SS approach, the realisations of the remaining levels of the iSS approach are generated using the Markov chain method based on Metropolis-Hastings algorithm.

As mentioned before, this chapter aims at employing the iSS approach for the computation of the failure probability in the case of a spatially varying soil property. To achieve this purpose, a link between the iSS approach and the K-L expansion through the standard normal random variables is performed. This link is similar to the one described previously in chapter 5. The algorithm of the iSS approach proposed in this chapter for the case of a spatially varying soil property can be described as follows:

1. Generate a vector of M standard normal random variables $\{\xi_1, \ldots, \xi_i, \ldots, \xi_M\}$ by MCS methodology. This vector must satisfy the condition that its norm is larger than a prescribed radius R_h of a hypersphere centered at the origin of the standard space.
2. Substitute the vector $\{\xi_1, \ldots, \xi_i, \ldots, \xi_M\}$ in the K-L expansion to obtain the first realisation of the random field. Then, use the deterministic model to calculate the corresponding system response.
3. Repeat steps 1 and 2 until obtaining a prescribed number N_s of realisations and their corresponding system response values. Then, evaluate the corresponding values of the performance function to obtain the vector $G_0 = \{G_0^1, \ldots, G_0^k, \ldots, G_0^{Ns}\}$. Notice that the values of the performance function of the different realisations are arranged in an increasing order in the vector G_0. Notice also that the subscript '0' refers to the first level (level 0).
4. Evaluate the first failure threshold C_1 of the failure region F_1 as the $[(N_s \times \overline{p}_0)+1]^{th}$ value in the increasing list of elements of the vector G_0 where $\overline{p}_0$ is a prescribed value that represents the ratio between the number of realizations for which $G<C_1$ and the number of realizations N_s (i.e. the term $\frac{1}{N_s}\sum_{k=1}^{Ns} I_{F_1}(s_k)$ in Equation 6.2). Thus, among the N_s realisations, there are $[N_s \times \overline{p}_0]$ ones whose values of the performance function are less than C_1 (i.e. they are located in the failure region F_1).
5. Evaluate the conditional failure probability of the first level $P(F_1)$ using Equation (6.2).

6. Prescribe an intermediate constant conditional failure probability $P(F_j|F_{j-1})$ for all the remaining failure regions F_j where ($j=2, 3, \ldots, m$). Although the $P(F_j|F_{j-1})$ value can be arbitrary chosen, it is recommended to be chosen equal to the value of $\overline{p}_0$ used in step 4 to facilitate the implementation of the iSS approach. Notice that, for simplicity in notation, $P(F_j|F_{j-1})$ for j=2, 3, …, m will be referred to as p_0 in the remaining sections of this chapter.
7. The different vectors of random variables $\{\xi_1, \ldots, \xi_i, \ldots, \xi_M\}$ corresponding to the realisations that are located in the failure region F_1 (from step 4) are used as 'mother vectors' to generate additional $[(1-p_0)\text{x}N_s]$ vectors of random variables $\{\xi_1, \ldots, \xi_i, \ldots, \xi_M\}$ using the Markov chain method based on Metropolis-Hastings algorithm. These new vectors are substituted in the K-L expansion to obtain the corresponding random field realisations. Thus, one obtains the N_s realizations of level 1.
8. The values of the performance function corresponding to the realisations of level 1 are listed in an increasing order and are gathered in the vector of performance function values $G_1 = \{G_1^1, \ldots, G_1^k, \ldots, G_1^{Ns}\}$.
9. Evaluate the second failure threshold C_2 as the $[(N_s\text{x}p_0)+1]^{th}$ value in the increasing list of the vector G_1.
10. Repeat steps 7 and 8 to evaluate the failure thresholds $C_3, C_4, \ldots, C_m$ corresponding to the failure regions $F_3, F_4, \ldots, F_m$ by using each time the vectors of random variables $\{\xi_1, \ldots, \xi_i, \ldots, \xi_M\}$ corresponding to the realizations that are located in the failure region F_j as mother vectors to generate the additional vectors in this region. Notice that contrary to all other thresholds, the last threshold C_m is negative. Thus, C_m is set to zero and the conditional failure probability of the last level $[P(F_m/F_m\text{-}1)]$ is calculated as:

$$P(F_m | F_{m-1}) = \frac{1}{N_s} \sum_{k=1}^{Ns} I_{F_m}(s_k) \qquad (6.3)$$

where $I_{F_m} = 1$ if the performance function $G(s_k)$ is negative and $I_{F_m} = 0$ otherwise.

11. Finally, the failure probability $P(F)$ is evaluated according to Equation (6.1) in which $P(F_1)$ is calculated using Equation (6.2) and the failure probability of the last level is calculated using Equation (6.3).

Notice that similar to chapter 5, a normal PDF was used as a target probability density function P_t. However, a uniform PDF was chosen as a proposal probability density function P_p. The intermediate failure probability p_0 was chosen equal to 0.1. Also the modified Metropolis-Hastings algorithm proposed by Santoso *et al*. (2011) was used herein.

3. Probabilistic analysis of two neighboring strip footings

In the previous chapter, a probabilistic analysis at SLS of a single strip footing resting on a spatially varying soil was performed. In practice, footings are rarly isolated and interfere with each others depending on the spacing between them (Mabrouki *et al.* 2010). Thus, the case of two neighboring footings is considered in this chapter to illustrate the efficiency of the iSS approach. Two neighboring strip footings resting on a soil with a spatially varying Young's modulus and subjected to equal vertical loads were considered in the analysis. Indeed, due to the soil spatial variability, the two footings exhibit a differential settlement δ. The differential settlement δ was used to represent the system response. It is calculated as follows: $\delta = |\delta_1 - \delta_2|$ where δ_1 and δ_2 are the settlements (computed at the footing centers) of the two footings. The Young's modulus was modeled by a random field and it was assumed to follow a log-normal probability density function. Its mean value and coefficient of variation are respectively μ_E=60MPa and COV_E=15%. It was discretized using K-L expansion. The random field was assumed to follow an exponential covariance function. It was considered as a two-dimensional (2D) anisotropic random field with horizontal and vertical autocorrelation lengths denoted by $l_{ln\ x}$ and $l_{ln\ y}$ respectively. As mentioned in the preceding chapter, a ratio of $l_{ln\ x}$ to $l_{ln\ y}$ of 1 to 10 for these autocorrelation lengths is usually found in practice (Baecher and Christian 2003). Notice however that a wide range of values of the autocorrelation lengths was considered herein in order to explore some interesting features related to the autocorrelation lengths. The performance function used to calculate the probability P_e of exceeding a tolerable differential settlement is defined as follows:

$$G = \delta_{max} - \delta \qquad (6.4)$$

where δ_{max} is a prescribed tolerable differential settlement and δ is the computed differential settlement due to the soil spatial variability.

In the following subsections, the deterministic model used to calculate the differential settlement will be presented. Then, the validation of the iSS approach in the case of random fields will be performed by comparison of its results with those obtained by MCS methodology. Finally, the effect of the autocorrelation length on the P_e value in both cases of isotropic and anisotropic random fields will be presented and discussed.

3.1. Deterministic model

The deterministic model used to calculate the differential settlement δ is based on numerical simulations using FLAC^{3D}. For this computation, two footings (each of width b=2m) were considered in the analysis (Figure 6.3). Each footing is subjected to a central vertical load P_a=1000kN/m (i.e. a uniform vertical applied pressure q_a=500kN/m^2). The two footing centers are separated by a distance D=4m. This small distance was chosen in order to obtain a small soil domain that requires relatively small computation time. The small computation time helps to validate the results obtained by the iSS approach by comparison with those obtained by MCS methodology using a large number of calls of the deterministic model. An optimal non-uniform but symmetrical mesh composed of 1290 zones was employed. In order to accurately calculate the footings displacements, the mesh was refined near the edges of the footings where high stress gradient may occur. For the displacement boundary conditions, the bottom boundary was assumed to be fixed and the vertical boundaries were constrained in motion in the horizontal direction.

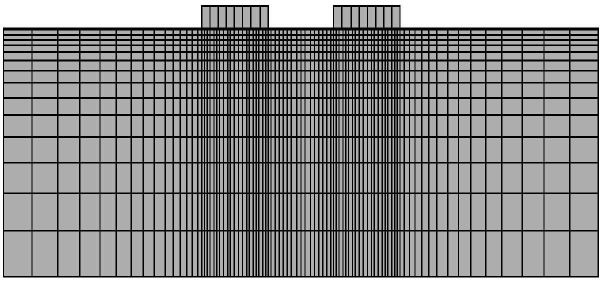

Figure 6.3. Soil domain and mesh used in the numerical simulations

Similar to the analysis performed in the preceding chapter, the soil behavior was modeled by a conventional elastic-perfectly plastic model based on Mohr-Coulomb failure criterion in order to take into account the possible plastification that may take place near the footing edges even under the service loads. The strip footings were modeled by a linear elastic model. They are connected to the soil *via* interface elements. The values of the different parameters of the soil, footings and interfaces are given in Table (6.1).

Table 6.1: Shear strength and elastic properties of soil, footing, and interface

Variable	Soil	Footing	Interface
c	20kPa	N/A	20kPa
φ	30^o	N/A	30^o
ψ=2/3 φ	20^o	N/A	20^o
E	60MPa	25GPa	N/A
ν	0.3	0.4	N/A
K_n	N/A	N/A	1GPa
K_s	N/A	N/A	1GPa

In order to calculate the differential settlement for a given random field realisation, (i) the coordinates of the center of each element of the mesh were calculated; then, the K-L was used to calculate the value of the Young's modulus at each element center, (ii) geostatic stresses were applied to the soil, (iii) the obtained displacements were set to zero in order to obtain the footing displacement due to only the footings applied loads and finally, (iv) the service loads were applied to the footings and the vertical displacements at the footings centers (δ_1 and δ_2) due to these loads are calculated. The differential settlement is calculated as the absolute difference between δ_1 and δ_2.

3.2. Validation of the iSS approach

This section presents a validation of the proposed iSS approach. Notice that for all the probabilistic analyses performed in this chapter, the tolerable differential settlement δ_{max} was assumed equal to 3.5x10^{-3}m. Notice also that the horizontal and vertical autocorrelation lengths $l_{ln\,x}$ and $l_{ln\,y}$ were normalized with respect to the distance D between the centers of the two footings (i.e. $L_{ln\,x}=l_{ln\,x}/D$ and $L_{ln\,y}=l_{ln\,y}/D$). The numerical results have shown that this assumption is valid when the ratio D/b is constant. Notice that contrary to the case of a single footing (chapter 5), the height of the soil domain was found to have no effect on the P_e value in this chapter. Notice finally that, the number of terms of K-L expansion used in this chapter is similar to that employed in chapter 5.

3.2.1. Selection of the optimal number N_s of realisations per level of iSS approach

In order to determine the optimal number of realisations N_s to be used per level, different values of N_s were considered. For each N_s value, the failure thresholds C_1, C_2, etc. were calculated and presented in Table (6.2) when the radius R_h of the hypersphere is equal to zero (i.e. for the classical SS approach). This table shows that the failure threshold value decreases with the successive levels until reaching a negative value at the last level. Table (6.3) presents the P_e values and the corresponding values of the coefficient of variation for the different number of realizations N_s. As expected, the coefficient of variation of P_e decreases with the increase in the number of realizations N_s.

Table 6.2: Evolution of the failure threshold with the different levels of the iSS approach and with the number of realisations N_s (R_h=0, $L_{ln\,x}$=2.5 and $L_{ln\,y}$=0.25)

Failure threshold C_j for each level j	Number of realisations N_s per level					
	200	400	600	800	1000	1200
C_1	0.00191	0.00199	0.00189	0.00204	0.00191	0.00195
C_2	0.00103	0.00099	0.00096	0.00110	0.00102	0.00103
C_3	0.00041	0.00032	0.00021	0.00037	0.00036	0.00034
C_4	- 0.00009	- 0.00051	-0.00036	- 0.00037	- 0.00039	- 0.00038

Table 6.3: Values of P_e and COV_{Pe} versus the number N_s of realizations per level

	Number of realisations N_s per level					
	200	400	600	800	1000	1200
P_e x(10^{-4})	1.85	3.48	4.63	2.36	3.65	3.67
COV_{Pe}	0.669	0.505	0.385	0.348	0.315	0.285

For each N_s value presented in Table (6.2), P_e corresponding to each level j was calculated by the iSS approach as follows:

$$P(F_j) = P(F_1) \times P(F_2 | F_1) \times ... \times P(F_j | F_{j-1}) \tag{6.5}$$

These P_e values were compared to those computed by the crude MCS methodology using a number N=30,000 realisations (Figure 6.4). Notice that at a given level j, the P_e value is calculated by MCS methodology as follows:

$$P(F_j) = \frac{1}{N} \sum_{k=1}^{N} I_F(G_k) \tag{6.6}$$

in which, G_k is the value of the performance function at the kth realization and I_F=1 if G_k<C_j and I_F=0 otherwise. The comparison has shown that for N_s≥1,000 realisations, the P_e value computed by the iSS approach at the different levels is very close to that computed by the crude MCS methodology (Figures 6.4e and 6.4f). Thus, N_s=1,000 realisations will be used in all the probabilistic analyses performed in this chapter. Notice that when N_s=1,000 realisations, the coefficient of variation of P_e by the iSS approach is COV_{Pe}=31.5%. A quasi similar value of COV (COV=31.3%) was obtained by MCS methodology but when using 30,000 realisations.

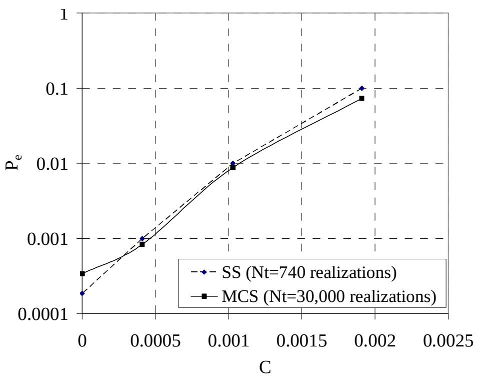

a. N_s=200 realisations per level

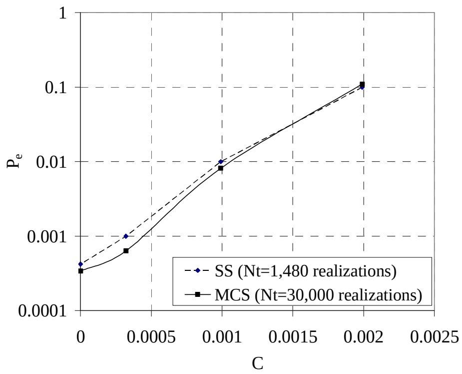

b. N_s=400 realisations per level

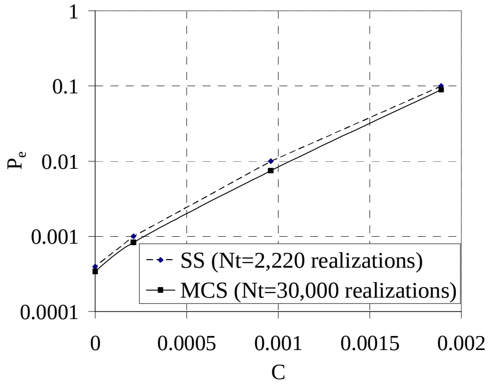

c. N_s=600 realisations per level

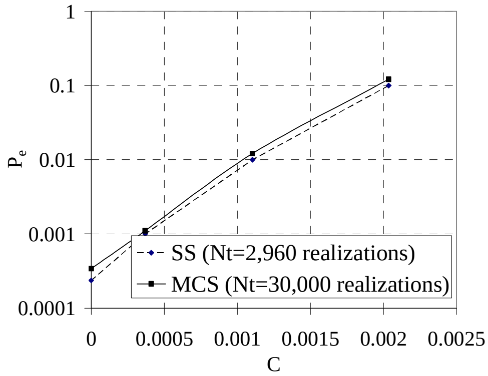

d. N_s=800 realisations per level

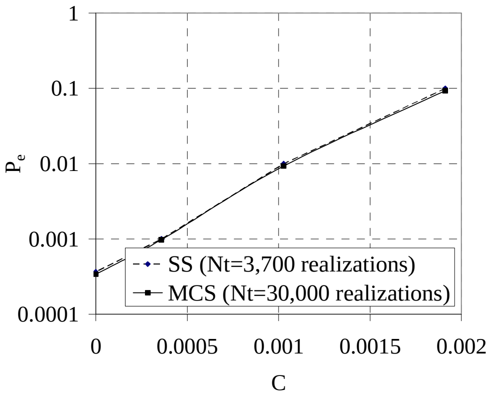

e. N_s=1000 realisations per level

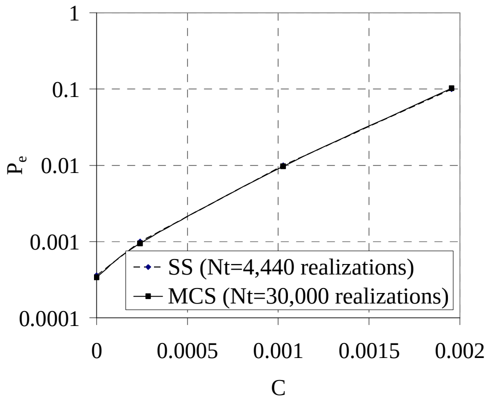

f. N_s=1200 realisations per level

Figure 6.4: Comparison between P_e computed by iSS and that computed by MCS methodology at each level of iSS (R_h=0, $L_{ln\,x}$=2.5 and $L_{ln\,y}$=0.25).

It should be mentioned here that although the computation time of the 30,000 realizations by MCS is significant (about 145 days), this number of realisations remains insufficient to assure an accurate P_e value with a small value of COV_{Pe}. As an alternative approach, one may determine the optimal N_s value (as explained in chapter 5) by successively increasing N_s and comparing the P_e values given by the iSS approach for each N_s value. The N_s value beyond which P_e converges (i.e. slightly varies with the increase of N_s) is the optimal one.

In the present analysis, it was found that P_e converges when N_s=1000 realizations. This is because the final P_e values (corresponding to C=0) are respectively equal to 3.65x10^{-4} and 3.61x10^{-4} for N_s=1000 and 1200 realizations. As a conclusion, this alternative procedure (which was proposed in chapter 5) seems to work well for the determination of the optimal N_s value.

3.2.2. Selection of the optimal radius R_h of the hypersphere

When R_h=0, four levels were required to reach the limit state surface G=0. This means that a total number of realisation N_t=1,000+(900x3)=3,700 realisations were required to calculate P_e with the iSS approach. Thus, for the same accuracy, the number of realisations (and consequently, the computation time) is reduced by 87.7% with respect to MCS when R_h=0 (i.e. when the classical SS is used). This number can again be reduced by increasing R_h (i.e. by using iSS). Table (6.4) shows that, when R_h increases, the total number of realisations decreases. When R_h=11.5, only two levels are required. Thus, the total number of realisations is N_t=1000+900=1,900 realisations. As a conclusion, the number of realisations (and consequently, the computation time) required by the SS approach could be reduced by 48.6% by employing the iSS approach.

Table 6.4: Effect of the radius of the hypersphere on the number of realizations required to calculate P_e ($L_{\ln x}$=2.5 and $L_{\ln y}$=0.25)

	MCS	R_h=0 (Classical SS)	iSS		
			R_h=10	R_h=11	R_h=11.5
P_e (x10^{-4})	3.40	3.65	3.58	3.36	3.45
Number of levels	-	4	3	3	2
number of realizations	30,000	3,700	2,800	2,800	1,900
computation time (minutes)	210,000	25,900	19,600	19,600	13,300

It is to be mentioned here that the radius R_h should be carefully chosen. If R_h is very small, the number of levels of the iSS approach will be equal to the number of levels of the classical SS approach and consequently the time cost will remain constant. On the other hand, if R_h is very large, the hypershpere might overlap with the failure region F leading to unsampled area in the failure region which leads to inaccurate value of the failure probability. This issue can be overcome (i) by calculating an approximate value of the failure probability using a simple and fast approach and then (ii) by computing the corresponding approximate value of the radius R_h to be used in the iSS approach. In this chapter, an approximate value $P_{e_{app}}$ of the probability of exceeding a tolerable differential settlement was calculated by the CSRSM using a small number of random variables and small PCE order [Huang *et al.* (2007) and Huang and Kou (2007)]:

It should be mentioned here that a high accuracy of the PCE is not necessary herein since an approximate $P_{e_{app}}$ value is sought. Thus, a small PCE order can be used. In this chapter, a second order PCE was used to approximate the system response. Concerning the number of standard normal random variables (number of terms in the K-L expansion), a small number was selected and the corresponding $P_{e_{app}}$ value was calculated. Then, this number was successively increased until $P_{e_{app}}$ converges to a constant value as shown in Table (6.5). This table indicates that $P_{e_{app}}$ converges to a value of 6.86x10^{-4} when the number of standard normal random variable is equal to 6. In this case, the number of collocation points is equal to 28 according to the concept of matrix invertibility by Sudret (2008).

Table 6.5: Effect of the number of standard normal random variables on $P_{e_{app}}$ value for the case where $L_{ln\,x}$=2.5 and $L_{ln\,y}$=0.25

Number of standard normal random variables M	$P_{e_{app}}$	Number of collocation points according to Sudret (2008)
3	0.00	10
4	8.63x10^{-5}	15
5	8.73x10^{-9}	21
6	6.46x10^{-4}	28
7	5.98x10^{-4}	36

After the determination of $P_{e_{app}}$, the corresponding approximate radius $R_{h\,app}$ of the hypershere can be determined. Notice that $R_{h\,app}$ represents the distance between the origin and the last failure threshold C_m. This means that only the first level of the iSS approach will likely be required to reach the last failure threshold. Thus, $P_{e_{app}}$ can be supposed equal to $P(F_1)$ and C_1=C_m=0. Consequently, one obtains:

$$P_{e_{app}} = P(F_1) = (1 - \chi_M(R_h^2))\frac{1}{N_s}\sum_{k=1}^{Ns} I_{F_1}(s_k) \tag{6.7}$$

where $I_{F_1}(s_k)=1$ if $G(s_k) \leq 0$ and $I_{F_1}(s_k)=0$ otherwise. Since the term $[\frac{1}{N_s}\sum_{k=1}^{Ns} I_{F_1}(s_k)]$ in Equation (6.7) is equal to $\overline{p}_0$ as mentioned before in section 2 (see step 4), Equation (6.7) can be rewritten as follows:

$$\chi_M(R_{h\,app}^{\;2}) = 1 - \frac{P_{e_{app}}}{\overline{p}_0} \tag{6.8}$$

from which:

$$R_{h\,app} = \sqrt{\chi_M^{-1}\left(1 - \frac{P_{e_{app}}}{\overline{p}_0}\right)} \tag{6.9}$$

in which $\chi_M^{-1}(.)$ is the inverse of the chi-square CDF. By using Equation (6.9), for the case studied herein where $\overline{p}_0 = 0.1$ and M=100, the approximate radius $R_{h\,app}$ corresponding to the approximate value of $P_{e_{app}} = 6.46x10^{-4}$ is equal to 11.77. After the determination of $R_{h\,app}$, the iSS approach can be used with R_h slightly smaller than $R_{h\,app}$ and M=100 terms to rigorously discretize the random field.

It should be emphasized here that in case where the uncertain parameters are modeled by random variables, $R_{h\,app}$ is equal to the reliability index β_{HL} since the standard normal random variables represent the uncertain physical parameters in the standard space of random variables. In such a case, both $R_{h\,app}$ and β_{HL} represent the minimal distance between the origin and the limit state surface. However, in the present case where the uncertain parameter (i.e. Young's modulus) is modeled by a random field, the standard normal random variables do not correspond to physical uncertain parameters. They are used in the K-L expansion to calculate the values of the uncertain parameters at each element of the soil domain. This means that the surface constructed using the standard normal random variables does not represent the limit state surface. In other words, there is no relation between $R_{h\,app}$ and β_{HL}.

3.3. Parametric study

This section aims at presenting a parametric study showing the effect of the autocorrelation lengths on the P_e value in both cases of isotropic and anisotropic random fields.

3.3.1. Effect of the autocorrelation length on P_e in the case of isotropic random field

Figure (6.5) shows the effect of the autocorrelation length on the P_e value in the case of an isotropic random field. This figure indicates that P_e presents a maximum value when $L_{ln\ x}$=$L_{ln\ y}$=1 (i.e. when the autocorrelation length is equal to the distance between the centers of the two footings).

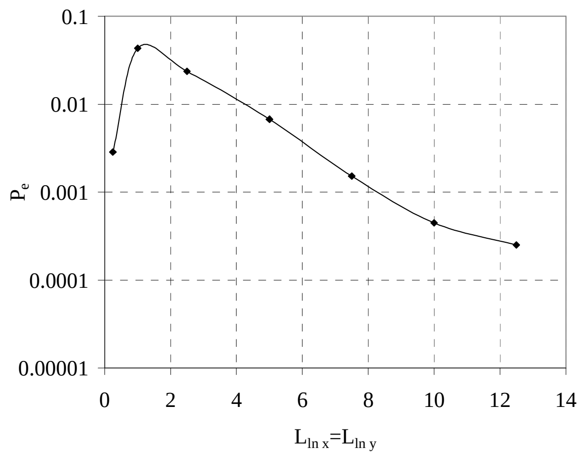

Figure 6.5: Effect of the autocorrelation length on P_e (isotropic random field)

This can be explained by the fact that when the autocorrelation length is very small, one obtains a highly heterogeneous soil in both the vertical and the horizontal directions with a great variety of high and small values of the Young's modulus beneath the footings (Figure 6.6a). In this case, the soil under the footings contains a mixture of stiff and soft soil zones. Due to the high rigidity of the footings, their movements are resisted by the numerous stiff soil zones in the soil mass; the numerous soft soil zones being of negligible effect on the footings displacements. This leads to small values of the footings displacements (i.e. to a small differential settlement) and thus, to a small value of P_e. On the other hand, when the autocorrelation length is large, the soil tends to be homogenous (Figure 6.6b). This means that the differential settlement tends to be very small (close to zero) which leads to a very small value of P_e. For the intermediate values of the autocorrelation length, there is a high probability that one footing rests on a stiff soil zone and the other on a relatively soft soil zone (Figure 6.6c). This leads to a high differential settlement and thus to a high P_e value. In this case, P_e presents a maximum.

a. $L_{ln\,x}=L_{ln\,y}=0.025$

b. $L_{ln\,x}=L_{ln\,y}=25$

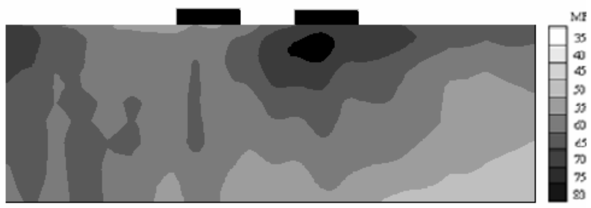

c. $L_{ln\,x}=L_{ln\,y}=1$

Figure 6.6: Grey-scale representation of the random field to show the effect of $L_{ln\,x}=L_{ln\,y}$ in case of isotropic random field

3.3.2. Effect of the autocorrelation lengths on P_e in the case of anisotropic random field

Figures (6.7) shows the effect of $L_{ln\,x}$ on P_e when $L_{ln\,y}$=0.25. This figure shows that P_e presents a maximum value when the autocorrelation length is equal to the distance between the two footings centers (i.e. when $L_{ln\,x}$=1). This observation can be explained as follows:

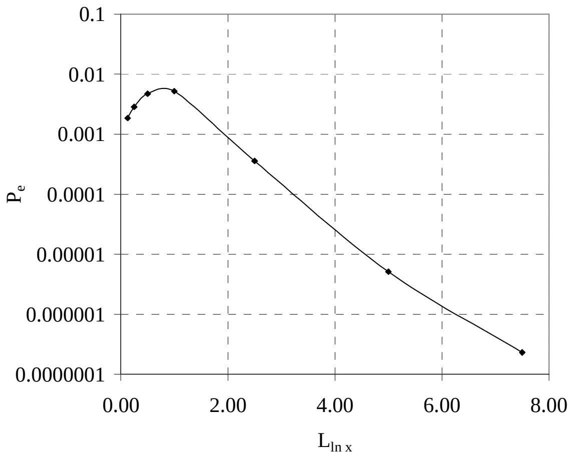

Figure 6.7: Effect of $L_{ln\,x}$ on P_e when $L_{ln\,y}$=0.25

For the very small values of $L_{ln\,x}$ compared to $L_{ln\,y}$, one obtains a vertical multilayer composed of thin sub-layers where each sub-layer may have a high or a small value of the Young's modulus (Figure 6.8a). The sub-layers with high values of the Young's modulus prevent the movements of both footings and thus lead to a small value of P_e.

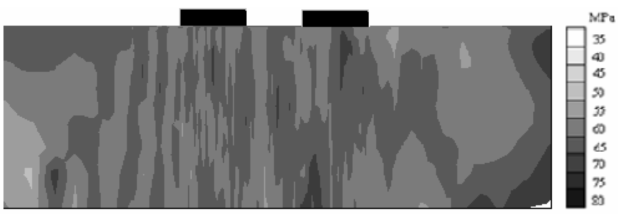

a. $L_{ln\,x}$=0.025 and $L_{ln\,y}$=0.25

b. $L_{ln\,x}$=25 and $L_{ln\,y}$=0.25

c. $L_{ln\,x}$=1 and $L_{ln\,y}$=0.25

Figure 6.8: Grey-scale representation of the random field to show the effect of $L_{ln\,x}$ in case of anisotropic random field

On the other hand, when $L_{ln\ x}$ is very large compared to $L_{ln\ y}$, one obtains a horizontal multilayer (i.e. the soil tends to the case of a one-dimensional vertical random field) for which each sub-layer may have a high or a small value of the Young's modulus (Figure 6.8b). This leads to the same displacement for both footings and thus to a very small value of P_e. Finally, for intermediate values of $L_{ln\ x}$, the horizontally extended stiff layers of Figure (6.8c) become less extended leading to a high probability that the footings rest on soil zones with different values of the Young's modulus. This leads to a greater differential settlement and consequently a greater value of P_e (Figure 6.8c).

The effect of $L_{ln\ y}$ is presented in Figure (6.9) when $L_{ln\ x}$=2.5. This figure also presents the P_e value corresponding to case of a one-dimensional horizontal random field with $L_{ln\ x}$=2.5. In this case, the soil was considered to be spatially varying only in the horizontal direction while it was considered to be homogeneous in the vertical direction. Figure (6.9) shows that the P_e value increases with the increase in $L_{ln\ y}$. This can be explained as follows: when $L_{ln\ y}$ is very small, the two footings rest on a horizontal multilayer composed of thin sub-layers where each sub-layer may have a high or a small value of the Young's modulus (Figure 6.10a). This means that δ_1 and δ_2 are almost equal. Thus, the differential settlement δ is very small which results in a small value of P_e.

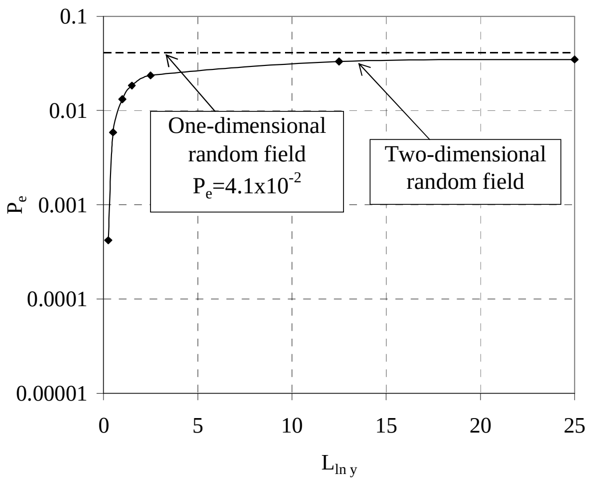

Figure 6.9: Effect of $L_{ln\ y}$ on P_e when $L_{ln\ x}$=2.5

On the other hand, when $L_{ln\,y}$ is very large, the soil tends to the case of a one-dimensional horizontal random field as shown in Figure (6.9). In this case, one obtains vertically extended stiff sub-layers adjacent to vertically extended soft sub-layers (Figure 6.10b). For the chosen value of $L_{ln\,x}$, there is a high probability that one footing rests on a vertical stiff layer and the other one rests on a vertical soft layer which leads to a high differential settlement and thus to a great value of P_e.

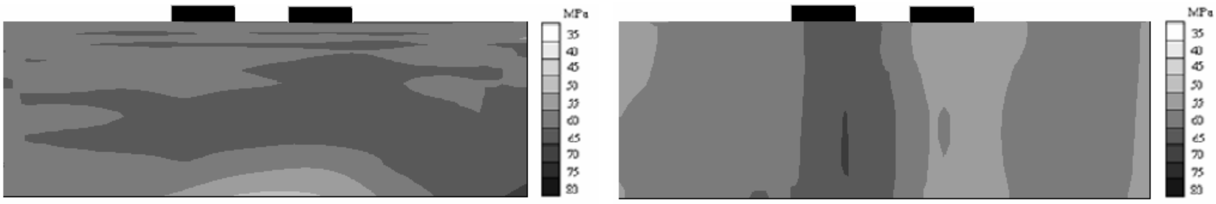

a. $L_{ln\,x}$=2.5 and $L_{ln\,y}$=0.025 **b.** $L_{ln\,x}$=2.5 and $L_{ln\,y}$=25

Figure 6.10: Grey-scale representation of the random field to show the effect of $L_{ln\,y}$ in case of anisotropic random field

4. Conclusion

This chapter presents an efficient method, called improved subset simulation (iSS), to perform a probabilistic analysis of geotechnical structures that involve spatial variability of the soil properties. This method is an improvement of the subset simulation approach presented in the previous chapter. It allows one to calculate the small failure probabilities using a reduced number of calls of the deterministic model. The iSS approach was illustrated through the probabilistic analysis at SLS of two neighboring strip footings resting on a soil with spatially varying Young's modulus. The differential settlement between the two footings was used to represent the system response. The probability P_e (i.e. the probability of exceeding a tolerable differential settlement) calculated by the improved subset simulation approach was found very close to that computed by Monte Carlo Simulation methodology or the classical subset simulation approach with a significant reduction in the number of calls of the deterministic model. The use of the iSS approach has reduced the number of calls of the deterministic model by about 50% with respect to the SS approach.

A parametric study to investigate the effect of the autocorrelation lengths on P_e in both cases of isotropic and anisotropic random fields has shown that:

1- In case of an isotropic random field, the probability P_e of exceeding a tolerable differential settlement presents a maximum value when the autocorrelation length is equal to the distance D that separates the two footings centers.

2- In case of an anisotropic random field, P_e significantly increases with the increase of the vertical autocorrelation length (for a given value of the horizontal autocorrelation length) and then, it attains an asymptote which corresponds to the case of a horizontal one-dimensional random field. On the other hand, for a given value of the vertical autocorrelation length, P_e presents a maximum when the horizontal autocorrelation length is equal to the distance D that separates the two footings centers.

GENERAL CONCLUSIONS

This thesis focuses on the probabilistic analysis of shallow foundations. Two types of probabilistic analyses were performed. Part I of this thesis presents a simplified probabilistic analysis in which the uncertain parameters were modeled by random variables characterized by their probability density functions (PDFs). However, Part II of this thesis presents an advanced probabilistic analysis in which the soil uncertain parameters were modeled by random fields characterized not only by their PDFs but also by their autocorrelation functions.

1 – Part (I): Simplified probabilistic analysis

Part I consists of three chapters (chapters 2, 3 and 4). In chapters 2 and 3, a circular footing resting on a (c, φ) soil and subjected to an inclined load was considered in the analysis. Both ULS and SLS were studied. In chapter 2, the response surface method (RSM) was used and only the soil uncertainties were considered in the analysis. However, in chapter 3, the collocation-based stochastic response surface method (CSRSM) was employed and both the soil and loading uncertainties were considered in the analysis. The system response used at ULS was the safety factor F defined with respect to the soil shear strength parameters (c and $tan\varphi$). For the SLS, two system responses were used. These are the footing vertical and horizontal displacements. Two failure modes (soil punching and footing sliding) were considered in the ULS analysis. Also, two modes of unsatisfactory performance (exceeding a vertical and horizontal footing displacement) were considered in the SLS analysis. The numerical results of chapters 2 and 3 have shown that:

a. The safety factor F defined with respect to the soil shear strength parameters c and $tan\varphi$ considers the combined effect of both failure modes (soil punching and footing sliding) at ULS. This safety factor provides a unique and rigorous safety level of the soil-footing system. The use of this factor has the advantage of seeking the most predominant mode of failure using a deterministic approach.

b. A global sensitivity analysis using the PCE-based Sobol indices has shown that the vertical load component *V* has a negligible weight in the variability of the safety factor and it can be considered as deterministic in the ULS analysis. On the other hand, the global sensitivity analysis in the SLS has shown that (i) the variability of the footing horizontal displacement is mainly due to the horizontal load component *H* and (ii) the variability of the footing vertical displacement is mainly due to the Young's modulus and the vertical load component; the Young's modulus being of larger weight.

c. When considering only the uncertainties of the soil parameters, both the deterministic and the probabilistic analyses at ULS have shown that there are several optimal loading configurations in the interaction diagram. These configurations correspond to a unique optimal load inclination and they subdivide the interaction diagram into two zones of predominance where either soil punching or footing sliding is predominant. The optimal loading configurations are situated on the line joining the origin and the extremum of the interaction diagram. Finally, the optimal load inclination was found to be independent of the uncertainties of the soil parameters.

d. Although the deterministic approach was able to determine the zones of predominance of sliding and punching when considering only the soil uncertainties, it was not able to determine these zones when considering the uncertainties of the load components. The probabilistic approach was necessary in this case.

e. The uncertainty of the horizontal load component *H* was found to slightly extend the zone of sliding predominance in the interaction diagram with respect to that obtained by the deterministic approach. This means that contrary to the variability of the soil properties, the variability of the load components affects the optimal load configurations.

f. The safety factor F was found to exhibit more variability for the load configurations corresponding to the zone of sliding predominance.

g. The optimal loading configurations obtained at SLS are similar to those obtained at ULS. These configurations are those for which neither vertical nor horizontal movement is predominant.

h. The footing vertical displacement was found to exhibit larger variability for the load configurations corresponding to the zone of predominance of the vertical soil movement. However, the footing horizontal displacement was found to exhibit larger variability for the loading configurations corresponding to the zone of predominance of the horizontal soil movement.

In chapter 4, the subset simulation approach was combined with the CSRSM to obtain additional probabilistic outputs of the SS calculation without additional calls of the deterministic model. A strip footing resting on a (c, φ) soil and subjected to a vertical load was considered in the analysis. Only a ULS analysis was performed in this chapter. The system response was the ultimate bearing capacity. The numerical results of this chapter have shown that the combination between the subset simulation approach and the CSRSM provides several advantages. In addition to the failure probability, it provides the PDF of the system response and the corresponding statistical moments with no additional time cost. Also, it allows one to perform a global sensitivity analysis using the PCE-based Sobol indices. Moreover, it allows the computation of the failure probability for different thresholds of the system response using a single subset simulation computation.

As it may be seen for Part I, the new contributions of chapters 2 and 3 do not involve the development of new probabilistic methods. Instead, an extensive probabilistic analysis of circular foundations subjected to inclined loads was undertaken in these chapters. This type of loading which induces both soil punching and footing sliding was not considered before in the framework of the probabilistic analysis. Furthermore, the present probabilistic analysis has confirmed the superiority of the CSRSM with respect to the RSM regarding the number of calls of the deterministic model and the number of the probabilistic outputs. On the other hand, chapter 4 has provided an extension of the SS approach. This extension allows one to obtain additional probabilistic outputs with respect to the classical SS approach with no additional time cost.

2 – Part (II): Advanced probabilistic analysis

Part II consists of two chapters (chapters 5 and 6). In chapter 5, the subset simulation approach was used to perform a probabilistic analysis at SLS of a single strip footing resting on a soil with a spatially varying Young’s modulus and subjected to a vertical load. The system response was the vertical displacement at the footing center. However, in chapter 6, a more efficient approach called “improved subset simulation (iSS)” approach was employed. The efficiency of the iSS approach was illustrated through the probabilistic analysis at SLS of two neighboring strip footings resting on a soil with a spatially varying Young’s modulus and subjected to equal vertical loads. In this case, the system response was the differential settlement between the two footings. The aim of both chapters (5 and 6) is to develop computationally-efficient probabilistic methods that can consider the soil spatial variability. Indeed, the existing probabilistic methods are very time-consuming since they are based on MCS methodology. Furthermore, they do not provide the failure probability; only the statistical moments of the system response are provided because of the great number of calls of the deterministic model required in that case.

The probabilistic numerical results of chapter 5 have shown that:

- Compared to the MCS methodology, the use of the subset simulation approach has significantly reduced the number of realisations required to calculate the probability P_e of exceeding a tolerable vertical displacement.
- A parametric study has shown that, in case of isotropic random fields, P_e increases with the increase of the autocorrelation length. For large values of the autocorrelation length, P_e attains an asymptote. This asymptote was found to be too close to the P_e value of a homogeneous soil (i.e. that corresponding to the case of a random variable). This illustrates the benefit of considering the soil spatial variability in the design of geotechnical structures.
- In case of anisotropic random fields, the parametric study has shown that P_e presents a maximum value for a given ratio of the horizontal to vertical autocorrelation lengths.
- The increase in the coefficient of variation of the Young's modulus significantly increases the P_e value.

The probabilistic numerical results of chapter 6 have shown that:

- The number of realisations required by the subset simulation approach to calculate the probability P_e of exceeding a tolerable differential settlement was reduced by half when employing the improved subset simulation approach.
- A parametric study has shown that, in case of isotropic random fields, P_e presents a maximum value when the autocorrelation length is equal to the distance between the centers of the two footings.
- In case of anisotropic random fields, for a given value of the vertical autocorrelation length, P_e presents a maximum when the horizontal autocorrelation length is equal to the distance between the centers of the two footings. However, for a given value of

the horizontal autocorrelation length, P_e increases with the increase in the vertical autocorrelation length and then it attains an asymptote corresponding to the case of a one-dimensional horizontal random field.

Ongoing research topics may involve the following items:

1- Applying the subset simulation or the improved subset simulation approach in the case of a multilayer soil medium (e.g. soft over stiff soil or stiff over soft soil) that exhibit spatial variability.

2- Extending the present subset simulation approach (involving soil spatial variability) to the geotechnical problems that include more than one failure mode (multiple performance functions). This approach is called “parallel subset simulation” and it was developed in literature in the case where the uncertain parameters are modelled by random variables.

3- Combining the subset simulation approach with the Polynomial Chaos Expansion (PCE) in case of random fields to obtain the PDF of the system response with no additional time cost. Notice however that contrary to chapter 4, this combination is not straightforward herein because of the proliferation of the number of PCE coefficients as a result of the great number of random variables in this case. The Sparse Polynomial Chaos Expansion may be used to solve this issue.

REFERENCES

1. Ahmed, A. Soubra, A.-H. (2011). "Subset simulation and its application to a spatially random soil." *Geotechnical Risk Assessment and Management, GeoRisk 2011, ASCE,* Atlanta, Georgia: 209-216.

2. Ahmed, A., Soubra, A.-H. (2012a). "Extension of subset simulation approach for uncertainty propagation and global sensitivity analysis." *Assessment and Management of Risk for Engineered Systems and Geohazards*, **6(3):** 162-176.

3. Ahmed, A., Soubra, A.-H. (2012b). "Probabilistic analysis of strip footings resting on a spatially random soil using subset simulation approach." *Assessment and Management of Risk for Engineered Systems and Geohazards,* **6(3):** 188-201.

4. Ahmed, A., Soubra, A.-H., (2012c). "Improved subset simulation for the SLS analysis of two neighboring strip footings resting on a spatially random soil." *State of the arte and practice in geotechnical engineering, GeoCongress 2012, ASCE,* Oakland, California: 2826-2836.

5. Anderson, O.D. (1976). "Time series analysis and forecasting: The box-Jenkins approach." *Butterworths*, London, 182p.

6. Ang, A. H-S, and Tang, W.H. (1975). "Probability concepts in engineering planning and design", *Vol. 1: Basic principles. John Wiley & Sons,* New York.

7. Au, S.K., and Beck, J.L. (2001). "Estimation of small failure probabilities in high dimensions by subset simulation." *Probabilistic Engineering Mechanics*, **16:** 263-277.

8. Au, S.K., and Beck, J.L. (2003). "Subset simulation and its application to seismic risk based on dynamic analysis." *Journal of Engineering Mechanics, ASCE,* **129(8):** 901-917.

9. Au, S.K., Cao, Z.J., and Wang, Y. (2010). "Implementing advanced Monte Carlo Simulation under spreadsheet environment." *Structural Safety*, **32(5):** 281-292.

10. Au, S.K., Ching, J., and Beck, J.L. (2007). "Application of subset simulation methods to reliability benchmark problems." *Structural Safety*, **29:** 183-193.

11. Babu, S.G.L., Srivastava, A., and Murthy D.S.N. (2006). "Reliability analysis of the bearing capacity of a shallow foundation resting on cohesive soil." *Canadian Geotechnical Journal*, **43:** 217-223.

12. Baecher, G.B., and Christian, J.T. (2003). "Reliability and statistics in geotechnical engineering." *John Wiley & Sons Ltd, The Atrium, Southern Gate, Chichewter, West Sussex PO19 8SQ, England, ASBN 0-471-49833-5.* 205-242.

13. Baecher, G.B., Marr, W.A., Lin, J.S., and Consla, J. (1983). "Critical parameters of mine tailings embankments." *Denver, CO, U.S.,* Bureau of Mines.

14. Bauer, J. and Pula, W. (2000). "Reliability with respect to settlement limit-states of shallow foundations on linearly-deformable subsoil." *Computers and Geotechnics,* **26:** 281-308.

15. Berveiller, M., Sudret, B., and Lemaire, M. (2006). "Stochastic finite element: a non intrusive approach by regression." *Revue Eurpéenne de Mécanique Numérique,* **15(1-2-3):** 8-92.

16. Bhattacharya, G., Jana, D., Ojha, S., and Chakraborty, S. (2003). "Direct search for minimum reliability index of earth slopes." *Computers and Geotechnics,* **30:** 455-462.

17. Blatman, G., Sudret, B. (2010). "An adaptive algorithm to build up sparse polynomial chaos expansions for stochastic finite element analysis." *Probabilistic Engineering Mechanics*, **25:** 183–97.

18. Box, G.E.P., and Jenkins, G.M. (1970). "Time series analysis: forecasting and control." *Holden-Day,* San Fransisco, 553 p.

19. Brenner, C., and Bucher, C. (1995). "A contribution to the SFE-based reliability assessment of non linear structures under dynamic loading." *Probabilistic Engineering Mechanics,* **10(4):** 265-273.

20. Cherubini, C. (2000), "Reliability evaluation of shallow foundation bearing capacity on c', φ' soils." *Canadian Geotechnical Journal*, **37:** 264-269.

21. Cherubini, C., Giasi, I., and Rethati, L. (1993). "The coefficient of variation of some geotechnical parameters." *Probabilistic Methods in Geotechnical Engineering.* Edited by Li, K.S., and Lo, S-C.R., A.A. Balkema, Rotterdam, 179-183.

22. Cho, S.E., (2010). "Probabilistic Assessment of slope stability that considers the spatial variability of soil properties." *Journal of Geotechnical and Geoenvironmental Engineering, ASCE,* **136(7):** 975-984.

23. Cho, S.E., and Park, H.C. (2010). "Effect of spatial variability of cross-correlated soil properties on bearing capacity of strip footing." *International Journal for Numerical and Analytical Methods in Geomechanics,* **34:** 1-26.

24. Chowdhury, R.N., and Xu, D.W. (1993). "Rational polynomial technique in slope-reliability analysis." *Journal of Geotechnical Engineering, ASCE*, **119(12):** 1910-1928.

25. Chowdhury, R.N., and Xu, D.W. (1995). "Geotechnical system reliability of slopes." *Reliability Engineering and System Safety,* **47:** 141-151.

26. Christian, J.T., Ladd, C., and Baecher, G. (1994). "Reliability applied to slope stability analysis." *Journal of Geotechnical Engineering, ASCE,* **120(12):** 2180-2207.

27. Das, P.K., and Zheng, Y. (2000). "Cumulative formation of response surface and its use in reliability analysis." *Probabilistic Engineering Mechanics,* **15:** 309-315.

28. Davis, J.C. (1986). "Statistics and data analysis in geology." *2nd ed., John Wiley and Sons,* New York, 646p.

29. Defaux, G., Meister, E., and Pendola, M. (2010). "Mécanique probabiliste et intégrité des cuves des réacteurs nucléaires." *JFMS'10,* Toulouse.

30. Deodatis, G., (1990). "Bounds on response variability of stochastic finite element systems." *Journal of Engineering Mechanics, ASCE,* **116(3):** 565-585.

31. Deodatis, G., (1991). "The weighted integral method, I : stochastic stiffness matrix." *Journal of Engineering Mechanics, ASCE,* **117(8):** 1851-1864.

32. Der Kiureghian, A., and Ke, J.-B. (1988). "The stochastic finite element method in structural reliability." *Probabilistic Engineering Mechanics,* **3(2):** 83-91.

33. Duncan, J.M. (2000). "Factors of safety and reliability in geotechnical engineering." *Journal of Geotechnical and Geoenvironmental Engineering, ASCE,* **126(4):** 307-316.

34. Duprat, F., Sellier, A., and Lacarrière, L. (2004). "Evaluation probabiliste du risque de corrosion par carbonatation." *Revue Française de Génie Civil,* **8(8):** 975-997.

35. Ejezie, S., and Harrop-Williams, K. (1984). "Probabilistic characterization of Nigerian soils." *In Probabilistic Characterization of Soil Properties, Bridge Between Theory and Practice, ASCE,* 140-156.

36. El-Ramly, H., Morgenstern, N.R., and Cruden, D.M. (2003). "Probabilistic stability analysis of a tailings dyke on presheared clay-shale." *Canadian Geotechnical Journal,* **40:** 192-208.

37. Fenton, G.A., and Griffiths, D.V. (2002), "Probabilistic foundation settlement on spatially random soil." *Journal of Geotechnical and Geoenvironmental Engineering, ASCE,* **128(5):** 381-390.

38. Fenton, G.A., and Griffiths, D.V. (2003). "Bearing capacity prediction of spatially random c-φ soils." *Canadian Geotechnical Journal,* **40:** 54-65.

39. Fenton, G.A., and Griffiths, D.V. (2005). "Three-dimensional probabilistic foundation settlement." *Journal of Geotechnical and Geoenvironmental Engineering, ASCE*, **131(2):** 232-239.

40. Fenton, G.A., Zhou, H., Jaksa, M.B., and Griffiths, D.V. (2003). "Reliability analysis of a strip footing designed against settlement." *Applications of statistics and probability in civil engineering, Der Kiureghian, Madanat & Pestana (eds) © 2003 Millpress, Rotterdam,* ISBN 90 5966 004 8.

41. Fredlund, D.G., and Dahlman, A.E. (1972). "Statistical geotechnical properties of glacial lake Edmonton sediments." *In Statistics and Probability in Civil Engineering,* Hong Kong University Press.

42. Ghanem, R., and Spanos, P. (1991). "Stochastic finite elements – A spectral approach." *Springer,* New York.

43. Griffiths, D.V., and Fenton, G.A. (2001). "Bearing capacity of spatially random soil. The undrained clay Prandtl problem revisited." *Géotechnique,* **51(4):** 351-359.

44. Griffiths, D.V., Fenton, G.A., and Manoharan N. (2006). “Undrained bearing capacity of tow-strip footings on spatially random soil.” *International journal of geomechanics, ASCE,* **6(6):** 421-427.

45. Griffiths, D.V., Fenton, G.A., and Manoharan, N. (2002). “Bearing capacity of rough rigid strip footing on cohesive soil: Probabilistic study.” *Journal of Geotechnical and Geoenvironmental Engineering, ASCE*, **128(9):** 743-755.

46. Haldar, A., Mahadevan, S. (2000). “Probability, reliability and statistical methods in engineering design.” *John wiley and Sons, Inc.*, New Yourk.

47. Harr, M.E. (1987). “Reliability-based design in civil engineering.” *McGraw-Hill Book Company,* New York, 290p.

48. Hasofer, A.M., and Lind, N.C. (1974), “Exact and invariant second-moment code format.” *Journal of Engineering Mechanics, ASCE,* **100(1):** 111-121.

49. Hassan, A., and Wolff, T. (1999). “Search algorithm for minimum reliability index of earth slopes.” *Journal of Geotechnical and Geoenvironmental Engineering, ASCE,* **125(4):** 301-308.

50. Honjo, Y. (2008). “Monte Carlo Simulation in reliability analysis.” *In: Phoon, K.K., ed.* Reliability-based design in Geotechnical Engineering: Computations and applications. *Taylor & Francis*: 169-171.

51. Houmadi, Y., Ahmed, A., Soubra, A.-H. (2012). “Probabilistic analysis of a one-dimensional soil consolidation problem.” *Assessment and Management of Risk for Engineered Systems and Geohazards*, **6 (1):** 36-49.

52. Huang, S., and Kou, X. (2007). “An extended stochastic response surface method for random field probles.” *Acta Mechanica Sinica*, **23:** 445-450.

53. Huang, S., Liang, B., and Phoon, K.K. (2009). "Geotechnical probabilistic analysis by collocation-based stochastic response surface method: An EXCEL add-in implementation." *Assessment and Management of Risk for Engineered Systems and Geohazards*, **3(2):** 75-86.

54. Huang, S., Mahadervan, S., and Rebba, R. (2007). “Collocation-based stochastic finite element analysis for random field problems.” *Probabilistic Engineering mechanics,* **22:** 194-205.

55. Isukapalli, S.S. (1999). “Uncertainty analysis of transport-transformation models.” *Ph.D thesis,* the state university of New Jersey.

56. Isukapalli, S.S., Roy, A., and Georgopoulos, P.G. (1998). “Stochastic response surface methods (SRSMs) for uncertainty propagation: Application to environmental and biological systems.” *Risk Analysis*, **18(3):** 357-363.

57. Jaksa, M.B. (1995). “The influence of spatial variability on the geotechnical design properties of a stiff, overconsolidated clay.” *Ph.D. Thesis*, Faculty of Engineering, University of Adelaide.

58. Jaksa, M.B. (1995). “The influence of spatial variability on the geotechnical design properties of a stiff, overconsolitated clay.” *Ph.D thesis,* University of Adelaide, Australia.

59. Kim, S.-H., and Na, S.-W. (1997). “Response surface method using vector projected sampling points.” *Structural Safety,* **19(1):** 3-19.

60. Kulhawy, F.H. (1992). “On evaluation of statistic soil properties.” *In stability and performance of slopes and embankments II (GSP31), ASCE, Edited by seed, R.B. and Boulanger,* R.W., New York, 95-115.

61. Lacasse, S., and Nadim, F. (1996). “Uncertainties in characterizing soil properties.” *Uncertainty in the Geologic Environment, ASCE,* Madison, 49-75.

62. Lee, I.K., White, W., and Ingles, O.G. (1983). “Geotechnical Engineering.” *Pitman,* London, England.

63. Li, C.-C. and Der Kiureghian, A. (1993). “Optimal discretization of random fields.” *Journal of Engineering Mechanics*, **119(6):** 1136-1154.

64. Li, D., Chen, Y., Lu, W., Zhou, C. (2011). “Stochastic response surface method for reliability analysis of rock slopes involving correlated non-normal variables.” *Computers. and Geotechnics,* **38(1):** 58-68.

65. Liang, R.Y., Nusier, O.K., and Malkawi, A.H. (1999). “A reliability based approach for evaluating the slope stability of embankment dams.” *Engineering Geology,* **54:** 271-285.

66. Liu, W.-K., Belytschko, T., and Mani, A. (1986a). “Probabilistic finite elements for non linear structural dynamics.” *Computer Methods in Applied Mechanics and Engineering,* **56:** 61-86.

67. Liu, W.-K., Belytschko, T., and Mani, A. (1986b), “Random field finite elements.” *International Journal for Numerical Methods in Engineering,* **23(10):** 1831-1845.

68. Low, B.K. and Phoon, K.K. (2002), “Practical first-order reliability computations using spreadsheet.” *Proc Probabilistics in Geotechnics, Technical and Economic Risk Estimation, Graz,* 15-19: 39-46.

69. Low, B.K. and Tang, W.H. (1997). “Probabilistic slope analysis using Janbu’s generalized procedure of slices.” *Computers and Geotechnics,* **21(2):** 121-142.

70. Low, B.K., Gilbert, R.B., and Wright, S.G. (1998). "Slope reliability analysis using generalized method of slices." *Journal of Geotechnical and Geoenvironmental Engineering, ASCE,* **124(4):** 350-362.

71. Lumb, P. (1966). “The variability of natural soils.” *Canadian Geotechnical Journal,* **3:** 74-97.

72. Lumb, P. (1970). “Safety factors and the probability distribution of soil strength.” *Canadian Geotechnical Journal,* **7:** 225-242.

73. Lumb, P. (1972). "Precision and accuracy of soil tests." *In Statistics and Probability in Civil Engineering*, Hong Kong University Press.

74. Mabrouki, A., Benmeddour, D., Frank, R., and Mellas, M. (2010). "Numerical study of the bearing capacity for two interfering strip footings on sands." *Computers and Geotechnics*, **37:** 431-439.

75. Malkawi, A.H., Hassan, W., and Abdulla, F. (2000). "Uncertainty and reliability analysis applied to slope stability." *Structural Safety*, **22:** 161-187.

76. Mao, N. (2011). "Analyse des fondations superficielles filantes soumises à un chargement centré." *Ph.D thesis*, university of Nantes, France.

77. Mao, N., Al-Bittar, T., and Soubra, A.-H. (2012). "Probabilistic and design of strip foundations resting on rocks obeying Hoek-Brown failure criterion." *International Journal of Rock Mechanics and Mining Sciences*, **49:** 45–58.

78. Melchers, R.E. (1999). "Structural Reliability: Analysis and Prediction." *Ellis Horwood Ltd.*, Chichester, U. K., 437p.

79. Mollon, G., Dias, D. and Soubra A-H. (2009), "Probabilistic analysis of circular tunnels in homogeneous soils using response surface methodology." *Journal of Geotechnical and Geoenvironmental Engineering, ASCE*, **135(9):** 1314-1325.

80. Mollon, G., Dias, D., and Soubra, A.-H. (2011). "Probabilistic analysis of pressurized tunnels against face stability using collocation-based stochastic response surface method." *Journal of Geotechnical and Geoenvironmental Engineering, ASCE*, **137(4):** 385-397.

81. Morse, R.K. (1972). "The importance of proper soil units for statistical analysis." *In Statistics and Probability in Civil Engineering*, Hong Kong University Press.

82. Neves, R.A., Chateauneuf, A., Venturini, W.S., Lemaire, M. (2006). "Reliability analysis of reinforced concrete grids with nonlinear material behavior." *Reliability Engineering and System Safety*, **91:** 735–744.

83. Neves, R.A., Mohamed-Chateauneuf, A., Venturini, W.S. (2008). "Component and system reliability analysis of nonlinear reinforced concrete grids with multiple failure modes." *Structural Safety*, **30:** 183–199.

84. Nour, A., Slimani, A. and Laouami N. (2002). "Foundation settlement statistics via finite element analysis." *Computers and Geotechnics*, **29:** 641–672.

85. Phoon, K.K. and Kulhawy, F.H. (1996). "On quantifying inherent soil variability." *Geotechnical Earthquake Engineering and Soil Dynamics, ASCE, Geotechnical Special Publication*, 75, 326-340.

86. Phoon, K.K., and Huang, S.P. (2007). "Geotechnical probabilistic analysis using collocation-based stochastic response surface method." *Applications of statistics and probability in civil engineering* – Kanda, *Takada & Furuta (eds)*, Tokyo.

87. Phoon, K.K., and Kulhawy, F.H., (1999). “Evaluation of geotechnical property variability.” *Canadian Geotechnical Journal,* **36:** 625-639.

88. Phoon, K.K., Kulhawy, F.H., and Grigoriu, M.D. (1995). “Reliability-based design of foundations for transmission line structures.” *Rpt. TR-105000, Electric Power Research Inst., Palo Alto (CA)*, 380p.

89. Popescu, R., Deodatis, G., and Nobahar, A. (2005). “Effect of random heterogeneity of soil properties on bearing capacity.” *Probabilistic Engineering Mechanics,* 20: 324-341.

90. Przewlocki, J. (2005). “A stochastic approach to the problem of bearing capacity by the method of characteristics.” *Computers and Geotechnics,* **32:** 370-376.

91. Pula, W., et Shahrour, I. (2003). "Influence of vertical and horizontal variability of soil strength on the reliability of shallow foundations." *International Symposium on shallow foundations, FONDSUP*, 423-432.

92. Riahi, H., Bressolette, Ph., Chateauneuf, A., Bouraoui, Ch., and Fathallah, R. (2011). “Reliability analysis and inspection updating by stochastic response surface of fatigue cracks in mixed mode.” *Engineering Structures,* **33:** 3392–3401.

93. Santoso, A.M., Phoon, K.K., and Quek, S.T. (2011). “Modified Metropolis-Hastings algorithm with reduced chain-correlation for efficient subset simulation.” *Probabilistic Engineering Mechanics,* **26(2):** 331-341.

94. Schuëller, G.I., Pradlwarter, H.J., and Koutsourelakis, P.S. (2004). “A critical appraisal of reliability estimation procedures for high dimentions.” *Probabilistic Engineering Mechanics*, **19:** 463-474.

95. Sivakumar B.G.L., and Amit, S. (2007), “Reliabilty analysis of allowable pressure on shallow foundation using response surface method.” *Computers and Geotechnics*, **34:** 187-194.

96. Sobol, I.M. (2001). “Global sensitivity indices for nonlinear mathematical models and their Monte Carlo estimates.” *Mathmatics and Computers in Simulation,* **55:** 271-280.

97. Soubra, A.-H and Mao, N. (2012). “Probabilistic analysis of obliquely loaded strip foundations using Polynomials Chaos Expansion methodology.” *Soils and Foundations*, in press.

98. Soubra, A.-H. (1999). “Upper-bound solution for bearing capacity of foundations.” *Journal of Geotechnical and Geoenvironmental Engineering, ASCE,* **125(1):** 59-68.

99. Soubra, A.-H., Youssef Abdel Massih, D., Kalfa, M. (2008). “Bearing capacity of foundations resting on a spatially random soil.” *GeoCongress 2008, ASCE,* GSP N° 178, New Orleans, Louisiana, USA, 66-73.

100. Soubra, A-H., Youssef Abdel Massih, D.S. (2010), “Probabilistic analysis and design at the ultimate limit state of obliquely loaded strip footings.” *Géotechnique*, **60(4):** 275-285.

101. Spanos, P.D., and Ghanem, R. (1989). “Stochastic finite element expansion for random media.” *Journal of Engineering Mechanics, ASCE,* **115(5):** 1035-1053.

102. Srivastava, A., and Sivakumar B.G.L. (2009), “Effect of soil variability on the bearing capacity of clay and in slope stability problems.” *Engineering Geology*, **108**: 142-152.

103. Sudret, B. (2008). “Global sensitivity analysis using polynomial chaos expansion.” *Reliability Engineering and System Safety*, **93:** 964-979.

104. Sudret, B., and Berveiller, M. (2008). “Stochastic finite element methods in geotechnical engineering.” *In: Phoon, K.K., ed. Reliability-Based design in Geotechnical Engineering: Computations and applications. Taylor & Francis*: 260-296.

105. Sudret, B., and Der Kiureghian, A. (2000). “Stochastic finite element methods and reliability: A State-of-the-Art Report.” *Report No. UCB/SEMM-2000/08 Structural Engineering, Mechanics and Materials Department of Civil & Environmental Engineering, University of California,* Berkeley.

106. Sudret, B., Berveiller, M., and Lemaire, M. (2006). “A stochastic finite element procedure for moment and reliability analysis.” *Eur. J. Comput. Mech.,* **15 (7-8):** 825–866.

107. Tandjiria, V., Teh, C.I., and Low, B.K. (2000). “Reliability analysis of laterally loaded piles using response surface methods.” *Structural Safety,* **22:** 335-355.

108. Vanmarcke, E.H. (1977). “Probabilistic modeling of soil profiles.” *Journal of the Geotechnical Engineering Division, ASCE,* **103(11):** 1227-1246.

109. Vanmarcke, E.H. (1983). “Random fields: Analysis and synthesis.” M.I.T, *Press,* Cambridge, Mass., 382p.

110. Webster, M., Tatang, M., and McRae, G. (1996). “Application of the probabilistic collocation method for an uncertainty analysis of a simple ocean model.” *Reports series no. 4,* MIT.

111. Wolff, T.H. (1985). “Analysis and design of embankment dam slopes: A probabilistic approach." *Ph.D thesis*, Purdue University, Lafayette, Ind.

112. Wolff, T.H. (1996). “Probabilistic slope stability in theory and practice.” *Uncertainty in Geological Environment, Madison, WI, ASCE,* 419-433.

113. Xiu, D., and Karniadakis, G.E. (2002). “The Wiener-Askey polynomial chaos for stochastic differential equations.” *SIAM J. on Scientific Computing,* **24(2):** 619-44.

114. Youssef Abdel Massih, D. (2007). “Analyse du comportement des fondations superficielles filantes par des approches fiabilistes.” *Ph.D thesis*, university of Nantes, France.

115. Youssef Abdel Massih, D., and Soubra, A.-H. (2008). "Reliability-based analysis of strip footings using response surface methodology." *International Journal of Geomechanics,* **8(2):** 134-143.

116. Youssef Abdel Massih, D.S., Soubra, A.-H., and Low, B.K. (2008). "Reliability-based analysis and design of strip footings against bearing capacity failure." *Journal of Geotechnical and Geoenvironmental Engineering, ASCE,* **134(7):** 917-928.

117. Yuceman, M.S., Tang, W.H. and Ang, A.H.S. (1973). "A probabilistic study of safety and design of earth slopes." *Civil Engineering Studies, Structural Research Series 402,* University of Illinois, Urbana.

118. Zevgolis, I.E., and Bourdeau, P.L. (2010). "Probabilistic analysis of retaining walls." *Computers and Geotchnics,* **37(3):** 359-373.

119. Zhang, J. and Ellingwood, B. (1994). "Orthogonal series expansion of random fields in reliability analysis." *Journal of Engineering Mechanics, ASCE,* **120(12):** 2660-2677.

120. Zimbone, S.M., Vickers, A., Morgan, R.P.C., and Vella, P. (1996). "Field *investigations* of different techniques for measuring surface soil shear strength*."* *Soil Technology,* **9:** 101-111.

APPENDIX A

EIGENVALUES AND EIGENFUNCTIONS FOR THE EXPONENTIAL COVARIANCE FUNCTION

Let *E(X, θ)* be a Guassian random field where *X* denotes the spatial coordinates and *θ* indicates the nature of the random field. If μ is the mean value of this random field, it can be approximated by the K-L expansion as follows (Spanos and Ghanem 1989 and Ghanem and Spanos 1991):

$$E(X,\theta) \approx \mu + \sum_{i=1}^{M} \sqrt{\lambda_i}\phi_i(X)\xi_i(\theta) \tag{A.1}$$

where M is the size of the series expansion, λ_i and ϕ_i are the eigenvalues and eigenfunctions of the covariance function $C(X_1, X_2)$, and $\xi_i(\theta)$ is a vector of standard uncorrelated random variables. In the present thesis, an exponential covariance function was used. For a 2D Guassian random field, this function is given as follows:

$$C[(x_1, y_1),(x_2, y_2)] = \sigma^2 \exp\left(-\frac{|x_1 - x_2|}{l_x} - \frac{|y_1 - y_2|}{l_y} \right) \tag{A.2}$$

in which, σ is the standard deviation of the random field, l_x and l_y are respectively the horizontal and the vertical autocorrelation lengths and (x_1, y_1) and (x_2, y_2) are the coordinates of two points in the space. For the exponential covariance function, Ghanem and Spanos (1991) provided an analytical solution for the eigenvalues and eigenfunctions.

For a one-dimensional horizontal random field generated in the interval $[-a_x, a_x]$, the eigenvalues can be calculated as follows:

$$\lambda_i^{(x)} = \frac{2c}{\omega_i^2 + c^2} \tag{A.3}$$

where

$$c = \frac{1}{l_x} \tag{A.4}$$

and

$$\begin{cases} c - \omega_i \tan(\omega_i a_x) = 0 & for\, i\, odd \\ \quad and \\ \omega_i + c \tan(\omega_i a_x) = 0 & for\, i\, even \end{cases} \tag{A.5}$$

The eigenfunctions are calculated as follows:

$$\phi_i^x(x) = \frac{\cos(\omega_i x)}{\sqrt{a_x + \frac{\sin(2\omega_i a_x)}{2\omega_i}}} \qquad for\ i\ odd \tag{A.6}$$

$$\phi_i^x(x) = \frac{\sin(\omega_i x)}{\sqrt{a_x + \frac{\sin(2\omega_i a_x)}{2\omega_i}}} \qquad for\ i\ even \tag{A.7}$$

For a one-dimensional vertical random field generated in the interval $\lfloor -a_y, a_y \rfloor$, the eigenvalues and eigenfunctions are calculated using the same equations after replacing the horizontal coordinate (x), the horizontal half width (a_x) of the domain and the horizontal autocorrelation length (l_x) respectively by the vertical coordinate (y), the vertical half depth (a_y) of the domain and the vertical autocorrelation length (l_y):

In case of a two-dimensional random field, the eigenvalues and eigenfunctions are calculated as the product of the eigenvalues and eigenfunctions of the one-dimensional random field as follows:

$$\lambda_i = \lambda_{i1}^{(x)} \lambda_{i2}^{(y)} \tag{A.8}$$

$$\phi_i(x, y) = \phi_{i1}^{(x)}(x)\phi_{i2}^{(y)}(y) \tag{A.9}$$

APPENDIX B

DESCRIPTION OF THE SOFTWARE FLAC^{3D}

1. Introduction

FLAC^{3D} (Fast Lagrangian Analysis of Continua) is a computer code which allows one to perform three dimensional (3D) numerical simulations. It should be mentioned that FLAC^{3D} allows the application of stresses (stress control method) or velocities (displacement control method) on the geotechnical system. The application of stresses or velocities creates unbalanced forces in this system. The solution of a given problem in FLAC^{3D} is obtained by damping these forces to reduce them to very small values compared to the initail ones. The stresses and strains are calculated at several time intervals (called cycles) until a steady state of static equilibrium or a steady state of plastic flow is achieved in the soil mass.

It should be mentioned here that the programming language FISH in FLAC^{3D} allows one to create functions that claculates the stresses, displacements, rotations, etc. at any point in the soil mass.

The following sections present the methods of computaion of some system responses using FLAC^{3D}.

2. Computaion of the ultimate load of a vertically loaded footing

For the computation of the ultimate footing load using FLAC^{3D}, the displacement control method was used. In this method, a small vertical velocity (10^{-6}/timestep in this thesis) is applied to the lower nodes of the footing and then, several cycles are run until reaching a steady state of plastic flow. The steady state of plastic flow is assumed to be reached when the two following conditions are satisfied:

- The load becomes constant with the increase in the number of cycles. In other words, increasing the number of cycles no longer changes the footing load (see Figure B.1).
- The unbalanced forces tend to a very small value (10^{-5} in this thesis) as shown in Figure (B.2).

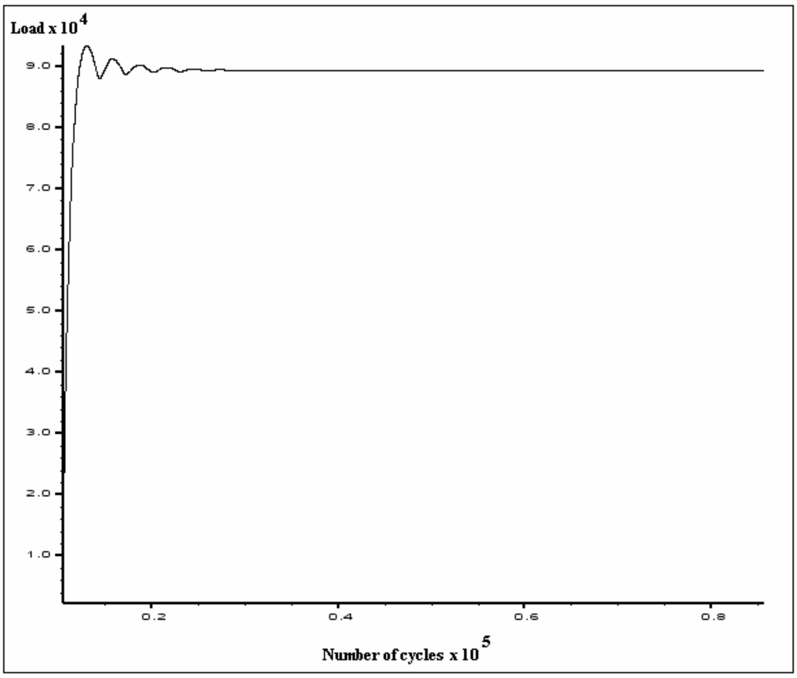

Figure B.1: Load versus the number of cycles

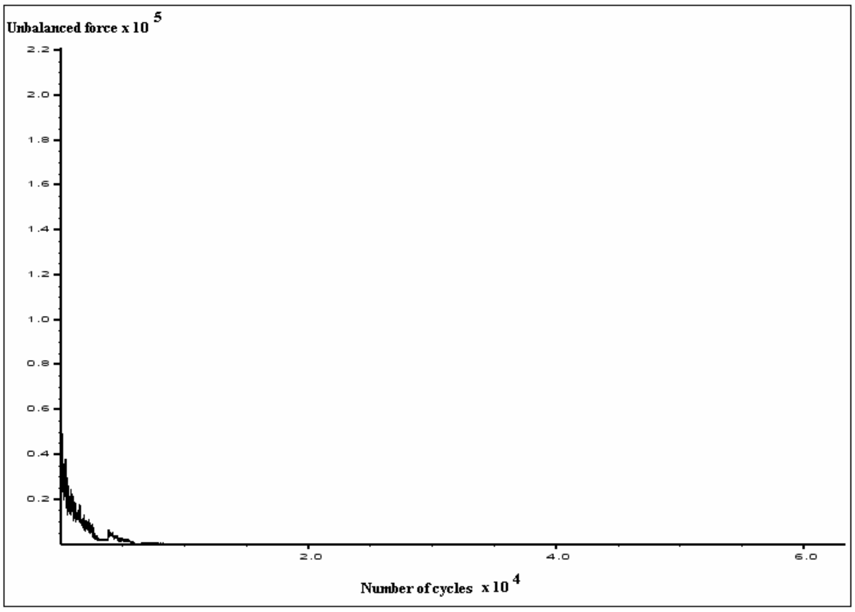

Figure B.2: Unbalanced forces versus the number of cycles

At each cycle, the footing load is obtained by using a FISH function that computes the summation of stresses of all elements of the soil-footing interface. The value of the footing load when reaching the steady state of plastic flow is the ultimate failure load of the footing.

3. Computation of the vertical and horizontal displacements of an obliquely loaded footing

In order to calculate the vertical and horizontal displacements of an obliquely loaded footing, the load components *V* and *H* are applied at the footing base. Then, cycles are run until reaching a steady state of static equilibrium in the soil mass. The steady state of static equilibrium is assumed to be reached when the two following conditions are achieved:

- The displacement tends to a constant value with the increase in the number of cycles. In other words, the increase in the number of cycles no longer changes the displacement (see Figure B.3).
- The unbalanced forces tend to a very small value (10^{-6} in this thesis).

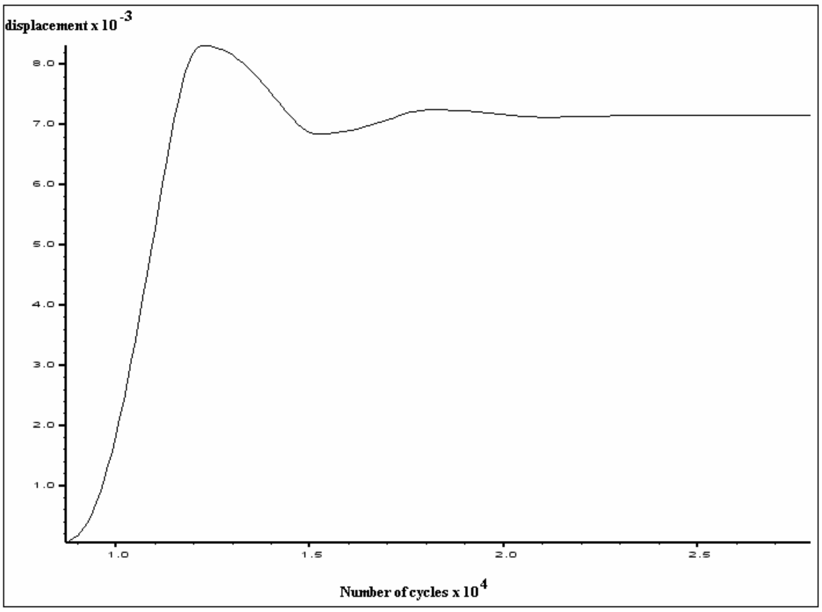

Figure B.3: displacement versus the number of cycles

APPENDIX C

SYSTEM FAILURE PROBABILITY EQUATIONS

For a geotechnical problem involving two failure modes (soil punching and footing sliding as an example), the system failure probability $P_{f_{sys}}$ of the two failure modes is calculated as follows:

$$P_{f_{sys}} = P_f(P \cup S) = P_f(P) + P_f(S) - P_f(P \cap S) \quad \text{(C.1)}$$

where $P_f(P \cap S)$ is the failure probability of the intersection of the two failure modes, $P_f(P)$ et $P_f(S)$ are respectively the failure probability due to soil punching and footing sliding. The failure probability of the intersection of the two failure modes is calculated as follows:

$$max[P(A), P(B)] \leq P_f(P \cap S) \leq P(A) + P(B) \quad \text{(C.2)}$$

where:

$$P(A) = \Phi(-\beta_P)\Phi\left(-\frac{\beta_S - \rho_{PS}\beta_P}{\sqrt{1-\rho_{PS}^2}}\right) \quad \text{(C.3)}$$

$$P(B) = \Phi(-\beta_S)\Phi\left(-\frac{\beta_P - \rho_{PS}\beta_S}{\sqrt{1-\rho_{PS}^2}}\right) \quad \text{(C.4)}$$

in which $\Phi(.)$ is CDF of the standard normal variables, β is the reliability index and ρ_{PS} is the coefficient of correlation between the two failure modes. It is calculated using the following equation:

$$\rho_{PS} = \langle \alpha_P \rangle \{\alpha_S\} \quad \text{(C.5)}$$

where α_P and α_S are the respectively the vectors of sensitivity indices of the soil punching and the footing sliding. These vectors are calculated as follows:

$$\alpha_P = \frac{u_P^*}{\beta} \tag{C.6}$$

$$\alpha_S = \frac{u_S^*}{\beta} \tag{C.7}$$

where u_P^* and u_S^* are respectively the vectors of the standard normal random variables at the design point. Notice here that Equation (C.2) is used when $\rho_{PS} > 0$. In cases where $\rho_{PS} < 0$, $P_f(P \cap S)$ is given by:

$$0 \leq P_f(P \cap S) \leq min[P(A), P(B)] \tag{C.8}$$

Notice that the lower bounds in Equations (C.2 and C.8) should be considered to obtain the most critical value of the system failure probability.

APPENDIX D

HERMITE POLYNOMIALS

1. One-dimensional Hermite polynomials

The one-dimensional Hermite polynomials of orders 0, 1, 2, 3, …, p+1 are given by:

$$\begin{aligned}
&\phi_0(\xi) = 1 \\
&\phi_1(\xi) = \xi \\
&\phi_2(\xi) = \xi^2 - 1 \\
&\phi_3(\xi) = \xi^3 - 3\xi \\
&\phi_{p+1}(\xi) = \xi\,\phi_p(\xi) - p\phi_{p-1}(\xi)
\end{aligned} \tag{D.1}$$

where ξ is a standard normal random variable.

2. Multidimensional Hermite polynomials

The multidimensional Hermite polynomial Ψ_i of order p is given by:

$$\psi^{(p)}(\xi_1,\ \ldots,\ \xi_n) = (-1)^p e^{0,5\zeta^T\zeta} \frac{\partial^p}{\partial\xi_1 \ldots \partial\xi_n} e^{0,5\zeta^T\zeta} \tag{D.2}$$

in which ζ is a vector of n standard normal random variables $\{\xi_i\}_{i=1,2,\ldots,n}$. The multidimensional Hermite polynomials are the product of one-dimensional Hermite polynomials of order less than or equal to p. As an example, for a problem with n=3 random variables and a PCE of order p=4, there are $P = \frac{(3+4)!}{3!4!} = 35$ terms in the PCE as shown in Table (C.1). This table shows the different Ψ_i terms and their corresponding orders. It also provides the values of $E(\Psi_i^2)$ for the different terms of the PCE.

Table C.1: Hermite polynomials Ψ_i for 3 random variables and their variance $E(\Psi_i^2)$

i	Coefficient a_i	order p	Ψ_i	$E\left(\Psi_i^2\right)$
0	a_0	0	1	1
1	a_1	1	ξ_1	1
2	a_2	1	ξ_2	1
3	a_3	1	ξ_3	1
4	a_{11}	2	$\xi_1^2 - 1$	2
5	a_{12}	2	$\xi_1\xi_2$	1
6	a_{13}	2	$\xi_1\xi_3$	1
7	a_{22}	2	$\xi_2^2 - 1$	2
8	a_{23}	2	$\xi_2\xi_3$	1
9	a_{33}	2	$\xi_3^2 - 1$	2
10	a_{111}	3	$\xi_1^3 - 3\xi_1$	6
11	a_{112}	3	$\xi_1^2\xi_2 - \xi_2$	2
12	a_{113}	3	$\xi_1^2\xi_3 - \xi_3$	2
13	a_{122}	3	$\xi_1\xi_2^2 - \xi_1$	2
14	a_{123}	3	$\xi_1\xi_2\xi_3$	1
15	a_{133}	3	$\xi_1\xi_3^2 - \xi_1$	2
16	a_{222}	3	$\xi_2^3 - 3\xi_2$	6
17	a_{223}	3	$\xi_2^2\xi_3 - \xi_3$	2
18	a_{233}	3	$\xi_2\xi_3^2 - \xi_2$	2
19	a_{333}	3	$\xi_3^3 - 3\xi_3$	6
20	a_{1111}	4	$\xi_1^4 - 6\xi_1^2 + 3$	24
21	a_{1112}	4	$\xi_1^3\xi_2 - 3\xi_1\xi_2$	6
22	a_{1113}	4	$\xi_1^3\xi_3 - 3\xi_1\xi_3$	6
23	a_{1122}	4	$\xi_1^2\xi_2^2 - \xi_2^2 - \xi_1^2 + 1$	4
24	a_{1123}	4	$\xi_1^2\xi_2\xi_3 - \xi_2\xi_3$	2
25	a_{1133}	4	$\xi_1^2\xi_3^2 - \xi_3^2 - \xi_1^2 + 1$	4
26	a_{1222}	4	$\xi_1\xi_2^3 - 3\xi_1\xi_2$	6
27	a_{1223}	4	$\xi_1\xi_2^2\xi_3 - \xi_1\xi_3$	2
28	a_{1233}	4	$\xi_1\xi_2\xi_3^2 - \xi_1\xi_2$	2
29	a_{1333}	4	$\xi_1\xi_3^3 - 3\xi_1\xi_3$	6
30	a_{2222}	4	$\xi_2^4 - 6\xi_2^2 + 3$	24
31	a_{2223}	4	$\xi_2^3\xi_3 - 3\xi_2\xi_3$	6
32	a_{2233}	4	$\xi_2^2\xi_3^2 - \xi_3^2 - \xi_2^2 + 1$	4
33	a_{2333}	4	$\xi_2\xi_3^3 - 3\xi_2\xi_3$	6
34	a_{3333}	4	$\xi_3^4 - 6\xi_3^2 + 3$	24

APPENDIX E

PCE-BASED SOBOL INDICES

Sobol indices of each input random variable or a combination of random variables are calculated using the PCE coefficients. The basic idea is to re-arrange the terms of the PCE so that each term contains only one random variable or combination of random variables. For example, for a PCE of order 4 with three random variables, the system response Γ can be written as follows:

$$\begin{aligned}
\Gamma &= a_0 + a_1\xi_1 + a_2\xi_2 + a_3\xi_3 + a_{11}\left(\xi_1^2 - 1\right) + a_{12}\xi_1\xi_2 + a_{13}\xi_1\xi_3 + a_{22}\left(\xi_2^2 - 1\right) + a_{23}\xi_2\xi_3 + a_{33}\left(\xi_3^2 - 1\right) \\
&\dots + a_{111}\left(\xi_1^3 - 3\xi_1\right) + a_{112}\left(\xi_1^2\xi_2 - \xi_2\right) + a_{113}\left(\xi_1^2\xi_3 - \xi_3\right) + a_{122}\left(\xi_1\xi_2^2 - \xi_1\right) + a_{123}\xi_1\xi_2\xi_3 + a_{133}\left(\xi_1\xi_3^2 - \xi_1\right) \\
&\dots + a_{222}\left(\xi_2^3 - 3\xi_2\right) + a_{223}\left(\xi_2^2\xi_3 - \xi_3\right) + a_{233}\left(\xi_2\xi_3^2 - \xi_2\right) + a_{333}\left(\xi_3^3 - 3\xi_3\right) \\
&\dots + a_{1111}\left(\xi_1^4 - 6\xi_1^2 + 3\right) + a_{1112}\left(\xi_1^3\xi_2 - 3\xi_1\xi_2\right) + a_{1113}\left(\xi_1^3\xi_3 - 3\xi_1\xi_3\right) + a_{1122}\left(\xi_1^2\xi_2^2 - \xi_2^2 - \xi_1^2 + 1\right) \\
&\dots + a_{1123}\left(\xi_1^2\xi_2\xi_3 - \xi_2\xi_3\right) + a_{1133}\left(\xi_1^2\xi_3^2 - \xi_3^2 - \xi_1^2 + 1\right) + a_{1222}\left(\xi_1\xi_2^3 - 3\xi_1\xi_2\right) + a_{1223}\left(\xi_1\xi_2^2\xi_3 - \xi_1\xi_3\right) \\
&\dots + a_{1233}\left(\xi_1\xi_2\xi_3^2 - \xi_1\xi_2\right) + a_{1333}\left(\xi_1\xi_3^3 - 3\xi_1\xi_3\right) + a_{2222}\left(\xi_2^4 - 6\xi_2^2 + 3\right) + a_{2223}\left(\xi_2^3\xi_3 - 3\xi_2\xi_3\right) \\
&\dots + a_{2233}\left(\xi_2^2\xi_3^2 - \xi_3^2 - \xi_2^2 + 1\right) + a_{2333}\left(\xi_2\xi_3^3 - 3\xi_2\xi_3\right) + a_{3333}\left(\xi_3^4 - 6\xi_3^2 + 3\right)
\end{aligned} \tag{E.1}$$

The PCE terms in Equation (E.1) can ber e-arranged in groups where each group contains one random variable or a combination of random variables as follows:

$$\begin{aligned}
\Gamma &= \left[a_0\right] + \left[a_1\xi_1 + a_{11}\left(\xi_1^2 - 1\right) + a_{111}\left(\xi_1^3 - 3\xi_1\right) + a_{1111}\left(\xi_1^4 - 6\xi_1^2 + 3\right)\right] \\
&\dots + \left[a_2\xi_2 + a_{22}\left(\xi_2^2 - 1\right) + a_{222}\left(\xi_2^3 - 3\xi_2\right) + a_{2222}\left(\xi_2^4 - 6\xi_2^2 + 3\right)\right] \\
&\dots + \left[a_3\xi_3 + a_{33}\left(\xi_3^2 - 1\right) + a_{333}\left(\xi_3^3 - 3\xi_3\right) + a_{3333}\left(\xi_3^4 - 6\xi_3^2 + 3\right)\right] \\
&\dots + \left[\begin{array}{l} a_{12}\xi_1\xi_2 + a_{112}\left(\xi_1^2\xi_2 - \xi_2\right) + a_{122}\left(\xi_1\xi_2^2 - \xi_1\right) + a_{1112}\left(\xi_1^3\xi_2 - 3\xi_1\xi_2\right) \\ + a_{1122}\left(\xi_1^2\xi_2^2 - \xi_2^2 - \xi_1^2 + 1\right) + a_{1222}\left(\xi_1\xi_2^3 - 3\xi_1\xi_2\right) \end{array}\right] \\
&\dots + \left[\begin{array}{l} a_{13}\xi_1\xi_3 + a_{113}\left(\xi_1^2\xi_3 - \xi_3\right) + a_{133}\left(\xi_1\xi_3^2 - \xi_1\right) + a_{1113}\left(\xi_1^3\xi_3 - 3\xi_1\xi_3\right) \\ + a_{1133}\left(\xi_1^2\xi_3^2 - \xi_3^2 - \xi_1^2 + 1\right) + a_{1333}\left(\xi_1\xi_3^3 - 3\xi_1\xi_3\right) \end{array}\right] \\
&\dots + \left[\begin{array}{l} a_{23}\xi_2\xi_3 + a_{223}\left(\xi_2^2\xi_3 - \xi_3\right) + a_{233}\left(\xi_2\xi_3^2 - \xi_2\right) + a_{2223}\left(\xi_2^3\xi_3 - 3\xi_2\xi_3\right) \\ + a_{2233}\left(\xi_2^2\xi_3^2 - \xi_3^2 - \xi_2^2 + 1\right) + a_{2333}\left(\xi_2\xi_3^3 - 3\xi_2\xi_3\right) \end{array}\right] \\
&\dots + \left[\begin{array}{l} a_{123}\xi_1\xi_2\xi_3 + a_{1123}\left(\xi_1^2\xi_2\xi_3 - \xi_2\xi_3\right) + a_{1223}\left(\xi_1\xi_2^2\xi_3 - \xi_1\xi_3\right) \\ + a_{1233}\left(\xi_1\xi_2\xi_3^2 - \xi_1\xi_2\right) \end{array}\right]
\end{aligned} \tag{E.2}$$

The PCE in Equation (E.2) consists of 8 groups corresponding respectively to:

(1)
$(\xi_1),\ (\xi_2),\ (\xi_3)$ *First order terms*
$(\xi_1,\xi_2),\ (\xi_1,\xi_3),\ (\xi_2,\xi_3)$ *Second order terms*
(ξ_1,ξ_2,ξ_3) *Third order terms*

The first order terms provide the contribution of each random variable individually in the variability of the system response. However, the second order terms provide the contribution of the combinations of two random variables and the third order terms provide the contribution of the combinations of three random variables. The Sobol index corresponding to each one of these terms is calculated as follows:

$$SU_\alpha = \frac{\sum a_\alpha . E(\psi_\alpha^2)}{\sigma^2} \tag{E.3}$$

where σ^2 is the variance of the system response calculated using the PCE coefficients. It is given by:

$$\sigma^2 = \mathrm{var}\left(\sum_{i=1}^{P-1} a_i\,.\psi_i\right) = \sum_{i=1}^{P-1} a_i^2 . E(\psi_i^2) \tag{E.4}$$

in which $E(\psi_i{}^2)$ is the variance of the multidimensional Hermite plynomial ψ_i. It is given by Sudret *et al.* (2006) as follows:

$$E(\psi_i{}^2) = i_1!.i_2!...i_n! \tag{E.5}$$

The values of $E(\psi_i{}^2)$ corresponding to the different ψ_i terms are given in Table (C.1).

APPENDIX F

METROPOLIS-HASTINGS ALGORITHM

The Metropolis–Hastings algorithm is a Markov chain Monte Carlo (MCMC) method. It is used to generate a sequence of new realizations from existing realizations (that follow a target PDF called 'P_t'). Refer to Figure (F.1) and let $s_k \in F_j$ be a current realization which follows a target PDF 'P_t'. Using a proposal PDF 'P_p', a next realization $s_{k+1} \in F_j$ that follows the target PDF 'P_t' can be simulated from the current realization s_k as follows:

a. A candidate realization $\hat{s}$ is generated using the proposal PDF (P_p). The candidate realization $\hat{s}$ is centered at the current realization s_k.

b. Using the deterministic model, evaluate the value of the performance function $G(\hat{s})$ corresponding to the candidate realization $\hat{s}$. If $G(\hat{s})<C_j$ (i.e. $\hat{s}$ is located in the failure region F_j), set $s_{k+1}= \hat{s}$; otherwise, reject $\hat{s}$ and set $s_{k+1}=s_k$ (i.e. the current realization s_k is repeated).

c. If $G(\hat{s})<C_j$ in the preceding step, calculate the ratio $r_1=P_t(\hat{s})/P_t(s_k)$ and the ratio $r_2=P_p(s_k|\hat{s})/P_p(\hat{s}|s_k)$, then compute the value $r=r_1r_2$.

d. If $r\geq1$ (i.e. $\hat{s}$ is distributed according to the P_t), one continues to retain the realization s_{k+1} obtained in step b; otherwise, reject $\hat{s}$ and set $s_{k+1}=s_k$ (i.e. the current realization s_k is repeated).

Notice that in step b, if the candidate realization $\hat{s}$ does not satisfy the condition $G(\hat{s})<C_j$, it is rejected and the current realization s_k is repeated. Also in step d, if the candidate realization $\hat{s}$ does not satisfy the condition $r\geq1$ (i.e. $\hat{s}$ is not distributed according to the P_t), it is rejected and the current realization s_k is repeated. The presence of several repeated realizations is not desired as it leads to high probability that the chain of realizations remains in the current state. This means that there is high probability that the next failure threshold C_{j+1} is equal to the current failure threshold C_j. This decreases the efficiency of

the subset simulation approach. To overcome this inconvenience, Santoso *et al*. (2011) proposed to modify the classical M-H algorithm as follows:

a. A candidate realization ŝ is generated using the proposal PDF (P_p). The candidate realization ŝ is centered at the current realization s_k.

b. Calculate the ratio $r_1=P_t(\hat{s})/P_t(s_k)$ and the ratio $r_2=P_p(s_k|\hat{s})/P_p(\hat{s}|s_k)$, then compute the value $r=r_1r_2$.

c. If $r\geq 1$, set $s_{k+1}=\hat{s}$; otherwise, another candidate realization is generated. Candidate realizations are generated randomly until the condition $r\geq 1$ is satisfied.

d. Using the deterministic model, evaluate the value of the performance function $G(s_{k+1})$ of the candidate realization that satisfies the condition $r\geq 1$. If $G(s_{k+1})<C_j$ (i.e. s_{k+1} is located in the failure region F_j), one continues to retain the realization s_{k+1} obtained in step c; otherwise, reject ŝ and set $s_{k+1}=s_k$ (i.e. the current realization s_k is repeated).

These modifications reduce the repeated realizations and allow one to avoid the computation of the system response of the rejected realizations. This becomes of great importance when the time cost for the computation of the system response is expensive (i.e. for the finite element or finite difference models).

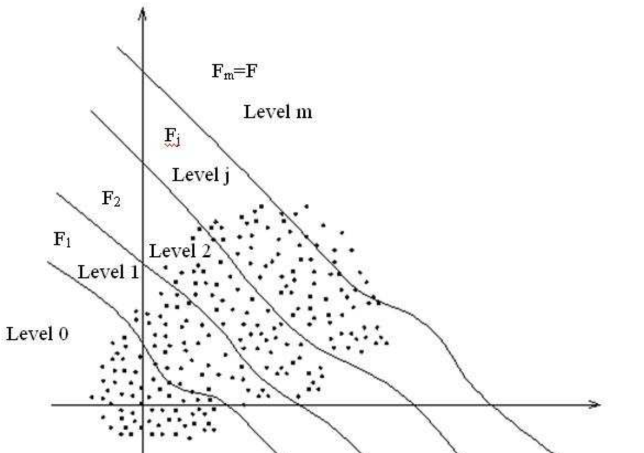

Figure F.1: Nested Failure domain